SOLID STATE LIGHT SOURCE BASED ANALYTICAL MEASUREMENT SYSTEMS FOR ATMOSPHERIC PARTICLES

by

SHILPA RASHINKAR

Presented to the Faculty of the Graduate School of
The University of Texas at Arlington in Partial Fulfillment
of the Requirements
for the Degree of

MASTER OF SCIENCE IN CHEMISTRY

THE UNIVERSITY OF TEXAS AT ARLINGTON
December 2011

ACKNOWLEDGEMENTS

I would like to thank my thesis advisor, Prof. Purnendu K. Dasgupta, for his years of continued guidance, and assistance with my thesis work. He is a respectable scientist and a very good mentor who allowed me to develop my approach and explore my interests. Each and every tryst with him has added value in me as a researcher and a person, in general.

I would also like to acknowledge the efforts of my thesis committee members and thank them for their time, support and valuable guidance: Dr. Peter Kroll and Dr. Kevin Schug.

I am also thankful to the members of Dasgupta Research Group that I had the pleasure of working with: Dr. Shin-ichi Ohira, Dr. Jason Dyke, Dr. Chao Lu, Dr. Abul Azad, Dr. Mrinal Sengupta, Dr. Martina Kroll, Dr. Qingyang Li and others. I also appreciate financial support from the Department of Chemistry and Biochemistry of the University of Texas at Arlington. I am grateful to the present and past staff members of Chemistry department, viz., Ms. Deborah Cooke, Ms. Ruth Handley, Ms. Autumn Patridge, Mr. Jim Garner, Ms. Jill Howard and Dr. Brian Edwards for their help and guidance.

I would also like to thank my father Murlidhar Rashinkar, my mother Pramila Rashinkar, my in-laws, my brothers, friends and Kajori Dasgupta for their unconditional love, support and encouragement. I believe I owe deepest thanks to everyone in my entire family who have always supported me.

This thesis could not have been accomplished without Santosh Mishra, my husband, who is always with me no matter how dubious my decisions were. He always gives me warm encouragement and love in every situation and I would like to dedicate my thesis to him and my son Sushrut.

October 24, 2011

ABSTRACT

SOLID SOURCE LIGHT SOURCE BASED ANALYTICAL
MEASUREMENT SYSTEMS
FOR ATMOSPHERIC
PARTICLES

Shilpa Rashinkar, M.S.

The University of Texas at Arlington, 2011

Supervising Professor: Purnendu K. Dasgupta

Solid-state light sources such as light-emitting diodes, use a ‘solid’ semiconductor block instead of a conventional heated filament or discharge source. Such light sources are preferred in analytical instrumentation because of various environmental benefits, cost benefits and most importantly performance benefits due to their characteristic features. This thesis deals with the fabrication of solid-state light source based analytical instrumentation for measuring size distribution and spectral absorption characteristics of ambient aerosol particles and provides insights into the behavior of aerosol organic carbon concentrations determined in a continuous and automated manner.

Various analytical instruments are commercially available for either measuring the particle size or optical absorption of ambient aerosols, but not both. Also, the instruments available for determining the optical absorption of particles do so only at one or two wavelengths. This thesis describes a unique instrument that uses an array of eleven light-emitting diodes ranging in wavelength from ultraviolet to near-infrared that are alternately turned on as the light

source and a 512-element photodiode array as the detector, the latter providing information on where spatially particles are deposited, This “particle spectrometer” provides semi-quantitative information about size and optical absorption of aerosol particles sampled by the device.

Additionally I report on the efficiency of various particle collection systems for collecting fine and ultrafine particulate matter that can operate continuously. This will contribute to the development of analytical instrumentation capable of collecting atmospheric aerosol and analyzing its organic carbon content in a continuous and automated fashion.

TABLE OF CONTENTS

LIST OF ILLUSTRATIONS

LIST OF TABLES

Table Page

CHAPTER 1

INTRODUCTION

1.1 Solid-state light sources

Solid-state light sources typically rely on an electrically polarized solid semiconductor diode emitting light rather than gas filled or evacuated enclosures containing a heated filament or discharge source as with traditional incandescent light bulbs and fluorescent lamps.[1] Such sources can be made with inorganic semiconductors or semiconductors made from organic polymers.[2] Control of spectral power distribution, spatial distribution, color temperature, temporal modulation, and polarization properties make these sources attractive in various applications.[3] In lighting applications, the huge potential benefits of solid-state light sources, in particular reduction of energy consumption, decrease in dependence on foreign oil, reduction of greenhouse gases (CO_2) and acid rain–causing SO_2 emissions, and decrease of mercury pollution have been discussed.[3] Solid state lighting could cut the consumption of electricity used for lighting in half.[4] These sources can also be turned on and off at high speeds and this aspect can be of much analytical value. A light-emitting diode (LED) based on inorganic III-V semiconductors is by far the most common solid state light source in use today.[2]

Quantitative chemical analysis has been dominated by spectrochemical measurements. LED sources have been used in analytical instruments for more than three decades.[5] Dasgupta et al. have extensively described low cost and robust LED based sensors and detectors. LED-based applications include: absorbance detectors, fluorescence detectors, spectroelectrochemical detectors, and multipurpose detectors for nephelometry, clinical photometric analysis, optical immunoassays, blood sedimentation sensing, hemoglobin measurement, flow rate sensing, etc.[6] Dasgupta et al. have used in particular LED-excited Liquid Core Waveguide (LCW) - based fluorescence detectors for on-site measurement of trace atmospheric gases like hydrogen peroxide[7] and formaldehyde.[8]

1.2 Aerosols and carbonaceous aerosols

A suspension of fine solid particles or liquid droplets in a gas is called as aerosol.[9] Aerosol particulate matter can either be primary (i.e., directly emitted into the atmosphere) or secondary (i.e., formed by chemical reactions in the atmosphere from gaseous precursors).[10] The composition of atmospheric aerosol depends on its source, which could range from wind-blown mineral dust (from the earth's crust) to sea spray aerosol (containing salts and organic compounds).[11] Ammonium, nitrate and sulfate are prevalent in ambient atmospheric particles.[12] Carbonaceous materials like near-elemental sub-graphitic carbon ("soot") and organic compounds also contribute substantially.[13] Carbon present in atmospheric aerosols can be categorized into inorganic carbon (IC), organic carbon (OC), and elemental carbon (EC).[14] Inorganic carbon (IC) is crustal carbon and is usually non-reactive and non-toxic. Organic carbon (OC) forms the bulk (50-90%) of the "soot" mass.[15] The terms elemental carbon (EC) (also called as black carbon (BC) or graphitic carbon (GC) or "light absorbing carbon") and "soot" are often used interchangeably (despite not being synonymous) and is generally so characterized based on the measurement technique.[16] Highly light-absorbing carbon is often characterized by the optical term, BC, while elemental form of carbon is represented by the term EC. The thermally refractory property of carbon is related to its graphitic structure and hence the term GC applied to nonvolatilized carbon that remains after pyrolysis. In practice, EC, some IC and some OC combine to comprise BC.[16]

1.3 Sources of aerosols & sizes of aerosol particles

Atmospheric particulate matter is either formed by gas-to-particle conversion or are emitted directly by a variety of natural and anthropogenic sources. Windblown dust, which contributes to atmospheric aerosol loading, is a primary source. Biogenic aerosols, such as pollen, are also considered to be primary aerosols. Their size ranges from few tenths of μm to tens of μm and include (but are not limited to) fungi, microbes, plant debris and humic matter.[17] Major anthropogenic sources of carbonaceous aerosols include industrial combustion sources, power generation, residential heating, biomass burning and traffic/vehicular emissions.[17] There is

concern that some engineered nanoparticles (including metal oxides, carbon based nanotubes and fullerenes, dendrimers, nanotubes, nanowires and quantum dots) may contribute to the primary aerosol if their use increases dramatically; the toxicity of such nanoparticles are of concern.[18]

The behavior of atmospheric particulate matter can be characterized based on its shape, size and density.[9] The mean diameter of aerosol particles varies from 0.001 to 100 μm.[9] The size of atmospheric particulate matter is generally represented by aerodynamic diameter, which is defined as the diameter of a unit density (1 g/cm^3) sphere that has the same settling velocity (the velocity at which the drag force exhibited by particle equals the gravitational force acting on the particle) as that of the particle under consideration.[19] PM_{10}, $PM_{2.5}$, PM_1 and $PM_{0.1}$ are the designations assigned to particles having their aerodynamic diameters less than 10 micrometers (μm), 2.5 μm, 1 μm and 0.1 μm, respectively.[9] Particles with aerodynamic diameter between 10 to 2.5 μm are called "inhalable coarse" particles while those with diameters less than 2.5 μm are called as "inhalable fine" particles.[20] Particles labeled as "ultrafine particles" or UFPs are those having aerodynamic diameter less than 0.1 μm diameter.[21]

UFPs have very high concentration (10,000-30,000/cm^3) in cities.[22] Because of their small size, UFPs have very high surface areas (10^5 times more than "coarse" particles and 100-1000 times more than that of "fine" particles per unit mass).[23] Fine particles can travel to and be deposited in the deep lung. Although many reactive soluble gases like SO_2 are typically removed efficiently by the upper respiratory tract, when sorbed on fine particles, they can be efficiently delivered to the deep lung. Thus, because of the significant surface area they represent, particulate matter plays an important role atmospheric chemistry and environmental health.

1.4 Health and environmental effect of particles

Particulate matter plays a vital role in health and environmental effects that depend on their size, shape, structure, composition, impurities, solubility, charge, agglomeration and attached functional groups.[19] Inhalable coarse particles are generally removed in the nose and throat while inhalable fine and ultrafine particles, owing to their small size, traverse the

nasopharyngeal and tracheobronchial regions before deposition in the alveolar region of the lungs and may ultimately be transported into the blood stream.[24] Many studies have indicated that health problems, especially respiratory problems, can be correlated to particulate pollution.[25] Recent studies have indicated that $PM_{2.5}$ particles lead to reduced lung function, vascular inflammation, asthma, bronchitis, atherosclerosis (hardening of arteries), Alzheimer, some types of cancer, greater incidence of heart attacks and other cardiovascular problems.[26,27] The same PM_{10} and finer particles affect the environment adversely. They impair visibility,[28] increase acidity of lakes and streams,[29] cause damage to crops and forests,[30] soil and stones and reduce ecological diversity.[20]

1.5 Particle/ BC/OC measurement techniques

Various instruments have been used for particle size measurement as well as qualitative measurement of Black Carbon, Elemental Carbon and Organic Carbon.

Some of the currently available instrumentation for aerosol particle size determination are: electrostatic classifier (which determines electric mobility based size of the particle), aerodynamic particle sizer, impactor, time-of-flight particle counter, condensation particle counter, quartz crystal microbalance and optical particle counters.[31] These and other commercial aerosol samplers (like cyclones; Lundgren and Battelle impactors, cascade impactors[32,33,34]) suffer from one or more of the following limitations. These include particle loss, particle bounceoff or reentrainment, fine particle leakage and limited number of stages or size fractions.[35,36,37] Prodi *et al.* developed an inertial spectrometer sampler which alleviated several aforementioned issues and separated the particles (as a function of particle inertia) according to their size.[38]

Commercially available BC/OC measurement instruments can be classified depending on whether they use filters for sample collection prior to measurement. Photoacoustic spectroscopy can measure particle loading with good time resolution and excellent limit-of-detection does not use filters; it utilizes the principle of strong absorption of light by BC particles.[39] But photoacoustic spectroscopy is sensitive to variations in relative humidity, temperature and gaseous NO_2.[37] Optical and thermal methods are used for the measurement of BC/OC collected on glass fiber

filters. The filter is heated in the presence of low levels of oxygen, this converts BC/OC to CO_2, which is then measured downstream. (The carbon is often sub-classified depending on the temperature at which is vaporized or converted to CO_2). Principles of reflectance, transmittance or back scattering measurement methods are commonly used for the measurement of BC on the filter.[38] Hansen *et al.* pioneered the usage of an *Aethalometer*, for real time measurement of aerosol particles (at 530 nm) (which improved the speed of analysis and decreasing the cost of analysis per sample).[38] Optical measurements using a single wavelength may not be sufficient for correct evaluation of different colored particles present in the atmosphere.[37] Commercially available Aethalometer models (AE22 and AE31 from Magee Scientific Inc.) provide better results for the monitoring of particles at two or more wavelengths (as compared to single wavelength monitoring).[39,40]

1.6 Thesis overview

The primary objective of this thesis work was to improve and develop solid-state light source based optical measurement systems for atmospheric particles. This was accomplished by studying, modifying, characterizing and then implementing various parameters in a particle spectrometer of our design. The device is solid state light source based and uses multiple wavelengths and particles are deposited along the length of a filter depending on their size. The spectrometer can be utilized to generate both qualitative and quantitative information regarding the nature of atmospheric particulate matter (optical absorption, particle size distribution) and their concentration.

In a related but independent effort, I studied the efficiency of an atmospheric particle collection system designed to measure the amount of ambient aerosol organic carbon and also interpreted observed data in terms of air parcel back trajectories.

Chapter 2 provides the details of my primary work on the use of solid-state light sources for the development of analytical instrumentation (a UV-Vis-IR particle spectrometer), for the measurement of optical size as well as particle size of atmospheric aerosol. The device consisted of an 11-element LED array fixed above a quartz fiber filter tape and a 512-element photodiode

array (PDA) fixed below the filter tape. Particulate matter was collected on the quartz fiber filter tape through a nozzle placed above one end of the filter tape with a long rectangular active area. The effect of the distance of the nozzle tip from the surface of the quartz filter was studied; this plays a critical role in the distribution of the particles along the filter. The distance of LED array from the quartz filter tape was also studied; this controls adequate light distribution across the length of the filter tape. Each LED of a different wavelength was turned on individually for a time and the transmitted light was measured by the PDA. We characterized the spatial distribution of the deposited particles as a function of wavelength. The fraction of absorbance in the plateau region versus the peak region of the spectrum was used as an index of particle size. This chapter also provides the details of the measurement of color as well as the aerodynamic size of the particles collected on the quartz filter tape.

Atmospheric carbonaceous aerosol has unique chemical complexity due to uncertainties in its sources and properties. Carbonaceous aerosols consist of variety of oligomers and polymeric matter from multiple sources. Chapter 3 of this thesis describes the development of a fully automated measurement system for ambient aerosol organic carbon, capable of unattended operation over extended periods; this work was done in conjunction with my research colleague, Dr. Chao Lu; the majority of the credit for the work discussed in this Chapter 3 goes to Dr. Lu. I contributed specifically towards determining the efficiency of collecting particulate matter in different sizes by different types of particle collection. The commercial particle counter used for this work used a laser source for counting the particles. Ambient aerosol collection in this portion of the work was studied at very high flow rates so as to allow the measurement of 'ultra-fine' particles (their number concentration is high but mass concentration still remains low); these are believed to contain significant amounts of black carbon (BC).

Overall, the work described here has contributed to the overall goal of the laboratory towards the development of affordable novel powerful analytical instrumentation of importance to atmospheric measurements and specifically the utilization of solid-state light sources and detectors for such efforts. Chapter 4 presents conclusions and future directions of research based

on this work. The work presented in Chapter 3 has already been published while work presented in chapter 2 is being submitted for publication.

CHAPTER 2

MULTIWAVELENGTH SIZE DISCRIMINATING PARTICLE SPECTROMETER: A NEW TOOL FOR CHARACTERIZING ATMOSPHERIC PARTICULATE MATTER

2.1 Introduction

2.1.1 Aerosols

The particle size distribution of aerosols in the atmosphere spans over five orders of magnitude (from 0.001 to 100 micrometer) and these particles play a very important role in atmospheric chemistry as well as impacting the environment. [9] The effects may be direct or indirect, physical, chemical, or physiological.[1]

Aerosols strongly absorb the radiation from the sun over a broad wavelength range reducing the total light reaching the surface of the earth thus reducing the local surface temperature.[9] Other consequence of these aerosols, especially those containing black carbon, is that they heat up the air affecting the vertical temperature profile, evaporation, cause latent heat fluxes, affect atmospheric stability and the strength of convection. [39] Aerosols, which contain Black Carbon (BC, fraction of carbonaceous aerosol which absorbs 'visible spectrum' light and hence decreases the light intensity passing through it) and Elemental Carbon (EC) or soot (which is non-volatile and non-reactive carbon), are the most prominent polluting particulate and are found in the exhaust following incomplete combustion of any carbonaceous fuel.[41,42] Black carbon comprises a significant portion of the atmospheric aerosol. The major sources of aerosol BC can be grouped into three broad categories: combustion of fuels for the generation of energy, biomass burning for agricultural purposes, and naturally occurring forest fires.

2.1.2 Heath effects of aerosols

Airborne particulate matter (PM) has been associated with numerous respiratory ailments like asthma, infezema, etc.[43] The annual number of deaths from air pollution is greater than that of the people died from Chernobyl accident.[44] The aerodynamic diameter of an aerosol particle

(the diameter of the unit density (1 g/cm^3) sphere that has the same settling velocity as that of the particle) governs the location in the respiratory tract where the particle is likely to be deposited.[43,45] Fine particles of mass median aerodynamic diameter <2.5 μm ($PM_{2.5}$), essentially consisting of combustion related particles and photochemical particles (commonly produced by photoinduced reactions to form sulfates, nitrates and ammonium salts), are trapped in peripheral airways and alveoli leading to adverse respiratory conditions.[43,46] Aerosols also act as a vector for adsorbed gaseous pollutants. Different aerosol particles have different spectral properties and their color ranges from colorless NaCl crystals to red-brown crustal dust, to black diesel soot.[47,48]

2.1.3 Qualitative and quantitative measurements of aerosols

A variety of instruments are commercially available for particle size measurement or for the qualitative measurement of Black Carbon, Elemental Carbon and Organic Carbon (which is the volatile and/or reactive carbon in heated air stream).[31]

Currently available instrumentation for particle size determination use different approaches to provide specific types of particle size for the same particle. For instance, electric mobility size determination of a particle by electrostatic classifier utilizes particle shape and size; aerodynamic size determined by aerodynamic particle sizer and impactor utilizes particle shape, size and density; optical size determination by light scattering principle utilizes shape, size and particle refractive index.[11] These sizes determined by different techniques can be different from geometric size (or Stokes size) essentially determined using a gamma camera.[32]

Various commercial aerosol samplers (cyclones; cascade, virtual, lundgren, and battelle impactors; PIXE(3,1) analyzer; etc.) have been developed;[31,33] but suffer from various limitations. These consisted of but are not limited to: limited number of stages leading to wide size range or poor particle size discrimination, limited number of collectible size fractions, particle loss, particle bounce off or reentrainment, and fine particle cross leakage.[34,35,36] In addition, some samplers suffer from lengthy sample preparation steps. Prodi et al. addressed these limitations and developed an inertial spectrometer sampler (based on PIXE) which consisted of a channel with a rectangular cross-section and a 90 degree bend for separating the particles (as a function of

particle inertia) according to their size and thereby alleviating many of the issues that plague other samplers.[36]

The methods for determination of BC can be classified into two categories: those in which the sample is concentrated on a filter and those measured directly. In the non-filter category, photo acoustic spectroscopy is the dominant technique and is based on the strong absorption of light (in a broad wavelength range) by the BC particles.[39] This method has good time resolution, low limit-of-detection and is capable of providing real time data; but is sensitive to effects from relative humidity, temperature and NO_2.[47,37] For the samples concentrated onto glass fiber filters, thermal and optical measurements are made of the BC particles. Then, because BC is chemically and thermally stable, the filter can be washed with solvent or heated at relatively low temperatures to remove any volatile organic carbons (VOCs) adsorbed on the BC particles. BC is then converted to CO_2 due to heat and is collected downstream on the adsorber and measured.[37] Reflectance, transmittance and back scattering measurement methods have been used for the measurement of BC on the filter.[38] Although the filter method approach is time consuming and needs complicated and expensive instrumentation, it is still the standard reference method for all other techniques.[38,49]

It was nearly three decades ago that Hansen et. al. advocated the use of an aethalometer, which measures the optical absorption of aerosol particles at 530 nm, for real time analysis (which improved the speed of analysis and decreasing the cost of analysis per sample).[38] Earlier, optical absorption was performed at one wavelength and then was extrapolated to other wavelengths using power-law relationship.[49] Optical measurements using a single wavelength may not be sufficient for correct evaluation of different colored particles present in the atmosphere.[37] Commercially available aethalometer models (from Magee Scientific Inc.) viz., AE22 and AE 31 utilize two wavelengths (370 and 950 nm) and seven wavelengths (370, 470, 520, 590, 660, 880 and 950 nm) respectively for studying aerosol. The AE 31 model measures C_{soot} in the near IR region and derives C_{brown} from near UV region after subtraction of C_{soot} absorption component.[40,49]

All the methods mentioned above either measured the atmospheric BC concentration or provided information about the particle size. In this paper, we described a new particle spectrometer design, which can not only measure the particulate matter in the atmosphere, but also provide the particle size information and their absorbance spectra from 275 nm to 850 nm range. The instrument presented here uses an LED array in the latest version and the instrument itself is robust, inexpensive, efficient, stable and provides very reliable results.

2.2 Experimental

2.2.1 *Design*

A typical particle spectrometer samples ambient aerosol on a filter tape and measures the optical extinction (with a time resolution of 5 minutes), typically at a fixed wavelength. In this work, we have developed a size selective, multiple wavelength particle spectrometer that has an 11-element LED array ranging from 375-850 nm and a 512 element photodiode array (TSL208R, TAOS) (Figure 2.1). The particle spectrometer consists of lower and upper sections (as shown in Appendix A.1); the lower section (8.20 cm x 2.59 cm x 1.49cm) contains a 512- photodiode array while the upper section (8.23 cm x 2.59 cm x 4.39 cm) consists of eleven LEDs and the sample inlet as shown in Figure 2.1. The LED wavelength sequence from left to right is 375 nm, 410 nm, 440 nm, 470 nm, 500 nm, 525 nm, 570 nm, 595 nm, 620 nm, 660 nm and 850 nm. A quartz fiber filter (Pall, Q250F, 25 mm wide) is placed between the two sections of the device. Aerosols or particulate matter are collected on this quartz fiber filter. The air sample is introduced through a nozzle (0.94 mm diameter). The distance from the surface of the quartz filter to the nozzle is 20 mm. This distance plays a critical role in the particle distribution along the filter. The nozzle is located above pixel #150 of the photodiode array. The last 20 pixels are blocked by the filter holder and the information on these pixels are not used. A stainless steel tube (HTX 11-36, Hypo tube type 304 s/s, 2.4 mm id) is connected in the bottom portion of the device for aspiration of the air, the amount of which is being controlled by a mass flow controller device, connected to a vacuum pump (Appendix Figure A.2). A water trap was connected between the particle spectrometer and the mass flow calibrator so as to avoid moisture reaching the pump. A flow rate

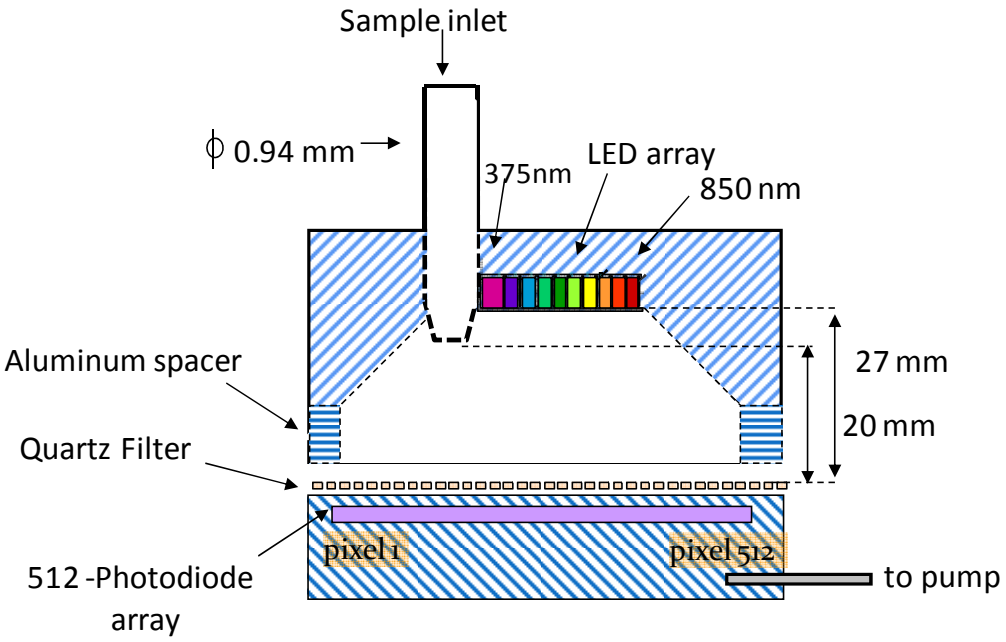

Figure 2.1 Schematic cartoon of the particle spectrometer (not to scale)

of 4 SLPM determined to be optimum based on previous experiments was used. The operating software for sequential lighting up the individual LED elements of the LED array is written in-house (using SoftWIRE, a graphical programming extension of Microsoft Visual Studio.NET); each LED is programmed to light up sequentially for 4 seconds.

2.2.2 *Experimental set up*

The spatial distribution pattern of dyed NaCl particles of different sizes were studied using a commercial vibrating orifice aerosol generator (VOAG, model 3450, TSI).[50] Various particle sizes of four different dyed NaCl particles were generated using different concentrations of dye-containing NaCl solutions (dyes being used were Eriochrome Red B, Malachite Green, Methylene Blue and Metanil Yellow) and allowed to deposit on quartz filter, at the same time particles were counted by a laser particle counter (METONE, Model A2212, P/N 2080446) (Appendix Figure A.2).

In order to get good sensitivity from the particle spectrometer, we optimized parameters like distance between LED and filter, distance between nozzle and filter and effect of sample flow rate while generating monodisperse same size particles. Also, color and size distribution study was performed by generating monodisperse aerosols containing four different dyes viz., Eriochrome Red B, Methylene Blue, Malachite Green and Metanil Yellow in different sizes with a VOAG. The color distributions of these dye particles, obtained from the particle spectrometer, were compared with the absorbance spectra of the respective dye solutions obtained by standard solution phase spectrophotometry (Agilent 8452A) to show the correlation in data obtained from particle spectrometer and spectrophotometer. To demonstrate the dual use of particle spectrometer for measurement of particle size as well as particle color, different sized and different color (dyed) NaCl particles were allowed to deposit sequentially on the same quartz filter strip and the results were compared with those taken individually on separate filter strips.

2.3 Results and discussion

In general, large size particles, having greater mass greater and hence greater inertia, deposit closer to the nozzle while the small size particles tend to disperse and deposit more evenly across the area of the filter. This leads to higher absorbance close to pixel number 160 (located below the nozzle/air inlet) while the absorbance plateaus out at pixel numbers farther away from the air inlet (as shown in Figure 2.2). The particle distribution is analyzed using linear photodetector sensor (512 element photodiode array), and the particle size information is interpreted. This principle of particle size determination was first used in inertial spectrometer (INSPE) and other particle samplers.[34,36] In inertial spectrometer, the aerosol stream is directed through a nozzle with a sharp 90 degree bend into a horizontal channel and through the filter on the floor of this channel. Around this aerosol-directing nozzle, a clear air stream is also introduced which shields the aerosol stream. Large particles deposit on filter near the bend because of high inertia, whereas smaller particles are carried further along the channel before depositing. The INSPE has the advantage of continuous particle size separation along its channel. However, The INSPE needs a clear air shielding flow around the aerosol inlet nozzle, this makes the device more complex and the shielding flow will also affect the particle separation. In our particle spectrometer, there is no clear air shielding flow, and the sample channel does not have a narrow 90 degree bend (as in INSPE), and the particle separation was achieved by the drag due to the vacuum flow from the sampling pump, (instead of the clear air flow in INSPE). The particle will distribute symmetrically in particle spectrometer if a circular filter and big chamber is used. But the photodiode array used in particle spectrometer is 0.5 mm X 7 cm in dimension and in order to increase the sensitivity, the sample area was restricted to 2 mm X 10 cm.

2.3.1 Selection of filter for particle deposition

Various filters were tested for use in the particle spectrometer. Particles deposited on the polymer filters have a very high chance to be relocated by the draft produced by the sampling, and taking an accurate absorbance measurement was more difficult due to increased noise. The glass fiber filter provided the best results. Particles penetrate and lodge inside the matrix of the

glass fiber filter. Because the glass fibers are optically clear, the absorbance can be measured easily and accurately.

2.3.2 Distance between LED and filter

The distance between LED and filter is an important parameter to be optimized to achieve high and uniform light intensity across the sample area. If the LED array is positioned closer to the filter tape, then the area immediately below LED is illuminated brightly but uniform light illumination across the filter tape is not obtained. If the LED array is placed far from the filter tape, then uniform illumination is achieved but with poor intensity. Different distances between the LED and filter tape were tried and 2.7 cm was selected as the optimum distance among 0.9 cm, 1.4 cm, 1.9 cm. 2.7 cm, 3.2 cm and 3.7 cm (as shown in Appendix Figures A.3 and A.4 for 850 nm). The blank response was subtracted from the sample response lowering the variation of LED intensity of LEDs closer to nozzle and further away from nozzle. Light distribution for all the LEDs range from 375 nm – 850 nm as shown in Appendix Figures A.5.

2.3.3 Distance between nozzle and filter

The distance between the lower end of the nozzle (for air sample inlet) to the filter tape affects the particle distribution pattern for a given sampling flow rate. This parameter was optimized by repeated analysis of VOAG generated identically sized particles (0.73 µm) at 3 SLPM for different nozzle-to-filter distance viz., 1 cm, 2cm and 3 cm, as shown in Appendix Figure A.6. When the nozzle is placed close to the filter (say 1 cm), even the smallest particles fail to travel any reasonable distance (nozzle tip location corresponds to pixel number 150), while as the nozzle-to-filter distance increases, particles travel a greater distance before lodging in the filter. Hence the optimum distance between the nozzle and filter was selected as 2 cm, keeping all other parameters constant.

2.3.4 Effect of sample flow rate on the particle distribution over the filter

With nozzle parameters kept constant, sample flow rate affects the particle distribution pattern, as aerosol velocity and inertia (both functions of sample flow rate) determines the deposition of particles along the quartz filter. The effect of the sampling flow rate (1, 2, 3 and 5

SLPM) on particle distribution is shown in Appendix Figure A.7 where identically sized particles (0.73 µm) were generated using VOAG instrument and allowed to deposit on filter tape. As the flow rate increases due to changes in inertia, the particles do not travel the lateral distance across the filter and instead impact directly below the nozzle. A tunable range is achievable by simply altering the flow rate. However, there is a limitation on the sampling flow rate as when it is too large, then particles deposited right under the nozzle can be relocated due to the force and surface of quartz filter tape can be destroyed, adversely affecting the measurement. Based on the experimental study, 4 SLPM was selected as the optimum flow rate.

2.3.5 Particle color distribution study

The dye solution spectra (Appendix Figure A.8) obtained by spectrophotometer, was compared with the dye particle absorption spectra (Appendix Figure A.9), obtained by the particle spectrometer. In the case of the particle spectrometer spectra, the absorbance of dye particles vs. the wavelength of each LED were plotted for 0.01 mM concentrations of Methylene Blue (MB), Malachite Green (MG), Metanil Yellow (MY) and Eriochrome Red B (ERB). Similarly, for the spectrophotometric spectra, absorbance of dye solution vs. wavelength were plotted for 0.01 mM concentrations of Methylene Blue, Malachite Green, Metanil Yellow and Eriochrome Red B. It should be noted that the apparent color of a solid dye particle does not always match its color in solution phase. Hence, the particle spectrometer indicates an absorbance pattern for the dye aerosol particles similar to that of the solution phase (Figure A.8 and A.9); but, show slightly different absorbance pattern (high absorbance values) at low wavelengths (for Malachite Green and Metanil Yellow).

2.3.6 Particle size distribution study

Smaller particles tend to follow the flow streamlines and deposit uniformly along the quartz filter tape whereas larger particles tend to deposit close to the nozzle position in the particle spectrometer. The quantitative behavior depends on the nozzle exit velocity (governed by flow rate and nozzle terminal diameter) and the nozzle-to-filter distance. Thus different sized particles exhibit different distribution patterns on the filter strip. In order to depict the distribution

patterns in detail, data presented is normalized (maximum absorbance, regardless of particle size at the nozzle position and all absorbance is divided by this maximum). Dye particle size can be increased via nucleation by increasing the sodium chloride concentration in the dye solution mixture fed to the vibrating orifice aerosol generator (VOAG). Figure 2.2 shows the absorbance spectra of 0.01 mM Eriochrome Red B dye particles of different sizes (0.37 µm, 0.40 µm, 0.80 µm and 1.21 µm). While all particles have the absorbance maximum at the nozzle position, the drop-off is much sharper for larger particle size. Larger particles show a rapid decrease in absorbance further from the nozzle.

Particle concentration can be measured by measuring the absorbance on relevant pixels (from Pixels#150 to Pixels #500), and to take the average of those 350 pixels, this average absorbance is proportional to the BC concentration in this period. Two methods were used to calculate the particle size.

In the first method, the average absorbance registered in the 10 pixels right beneath the nozzle were calculated and taken as the max absorbance value A_{max}, the A/A_{max} % was calculated and plotted for each pix (as show in Appendix Figure A.10), it has been seen that different particles have different distribution patterns. The A/A_{max} % from pixels # 300 to 400 is seen to be constant within each particle size, but changed with varying particle size. We take the average of A/A_{max} % from pixel 300 to 400 as the measurement of the particle size. Results are shown in Appendix Figure A.11. The best fitting equation is: $y = 98.415e^{-1.342\,x}$, R^2 =0.9997; where y is the average of A/A_{max} % from pixel 300 to 400, and x is the particle size in µm. This method will be referred to as "Method A".

In the second method, the absorbance average is calculated from pixel # 150 to 500 ($A_{average}$), and the ratio of $A/A_{average}$ is then plotted. The plot of different particle sizes is shown in Appendix Figure A.12. The average of the ratio from pixel # 150 to 160 was taken as a measure of the particle size, the best fit plot is shown in Appendix Figure A.13; the equation is $y = 0.848 + 1.498\,x + 0.494\,x^2$. Both methods were used to calculate the particle size in atmosphere BC measurement, and the results will be discussed in a later section. This method is referred to as "Method B".

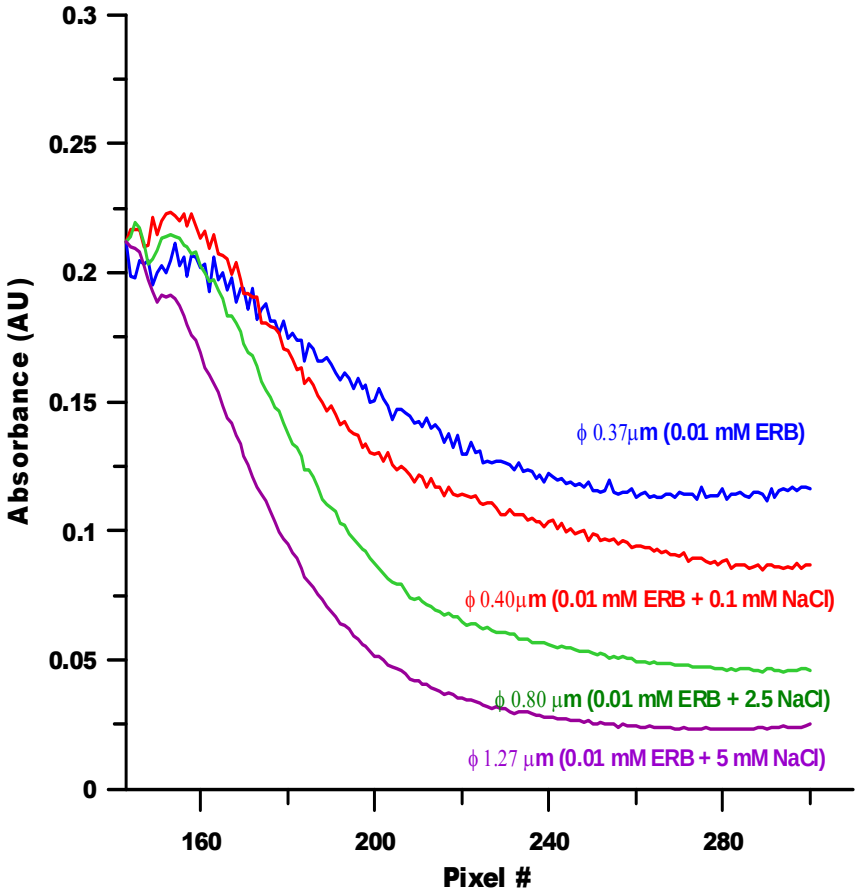

Figure 2.2 Percentage of maximum absorbance of different size of Eriochrome Red B dyed NaCl particles vs pixel number. This plot shows higher absorbance at pixel number 160 (located below the air inlet) which plateaus out at higher pixel numbers (indicating even distribution of small size particles). The slopes of the curves are characteristic of different sized particles indicating that the particle spectrometer can distinguish between different sizes of similar colored particles.

2.3.7 Particle size and color distribution study

Four different colored dye particles of different particle sizes viz., Malachite Green (0.37 µm), Methylene Blue (0.40 µm), Eriochrome Red B (0.80 µm) and Metanil Yellow (1.21 µm) were generated and allowed to deposit on a single quartz filter tape. Absorbance values of these dyes were studied at the wavelength of their maximum absorption, and particle distribution patterns were observed (Appendix Figure A.14). It is seen that even for a complex mixture of four different colored dye particles of different particle sizes, the data is easily discriminated on the basis of their size and color using this instrument. (Appendix Figure A.15). For simplicity, the additive property of two differently colored aerosol particles of two different particle sizes was verified using Microsoft Excel Solver™ software and is discussed henceforth. The experimental data was obtained for two different sizes and colors of dye particles (i) deposited on two separate filter tapes, and (ii) deposited sequentially on the same filter. The absorbance data obtained from these two cases were tested for mathematical linear combination additivity for each pixel at each wavelength i.e. whether sum total absorbance achieved for case (i) can be added linearly to obtain the absorbance for that of case (ii). For example, absorbance of two different dye particles viz., Malachite green (0.24 µm aerodynamic diameter) and Methylene blue (0.33 µm aerodynamic diameter) if deposited individually on two separate filters, after applying suitable multiplication factor (K) should add to absorbance of that obtained by these two dyes depositing on the same filter.

The following equation was used to determine the multiplication factors K_{MG} (for Malachite Green) and K_{MB} (for Methylene Blue) for the absorbance additivity property of the particle spectrometer.

$S_{MG+MB} = K_{MG}*A_{MG} + K_{MB}*A_{MB}$

S_{MG+MB} = Sum of absorbance of two dye particles, Malachite Green and Methylene Blue, on same filter for 410 - 660 nm wavelengths.

A_{MG} = Sum of absorbance values of (0.01 mM Malachite Green, 0.24 µm dia.) for 410 - 660 nm on one filter

A_{MB} = Sum of absorbance values of (0.01 mM Methylene Blue, 0.33 μm dia.) for 410 - 660 nm on another filter.

Solver yielded the absorbance multiplication factors K_{MG} and K_{MB} values to be 1.025 and 1.255 respectively. Note that even if aerosol generation is carried out for identical lengths of time in different runs, the exact concentration of the aerosol generated varies. These multiplication factors help in determining the individual contribution of aerosol constituents.

Also, particle distribution pattern obtained by dyes sequentially added on quartz filter, falls in to the standard deviation of distribution pattern obtained by dyes individually added on quartz filter (Appendix Figure A.16).

2.3.8 On-site measurement of ambient air BC concentration and particle size

Particle spectrometer was tested by sampling ambient air at different locations in Lubbock (latitude: 33.578, longitude: -101.855) in the state of Texas. A commercial aethalometer, connected in tandem to particle spectrometer, was also used for the analysis. Four different locations were chosen for the study, one was the city bus downtown station, where the diesel fueled city buses passed every 30 to 60 min; the second location was a baseball field located ~ 1 miles west of the west loop 289, which is located between TX 82 and Spur 327, there were also some road construction activities near the sampling site. The third site was adjacent to the Science Spectum Museum and OMNI theater building, which is located on the south of south loop 289. We tried to monitor the loop traffic but the sampling site was located ~ 30 meters upwind. The wind direction and speed had a substantial effect on the BC concentration as measured by the two instruments. The fourth site was the third floor of the Chemistry building at the TTU campus, both instruments were collecting ambient air sample through the window of the lab of the Chemistry building. A six-channel laser particle counter was also used to sample the ambient air and the particle counted from each channel was recorded. Here we only list the Lubbock city bus station site results and Chemistry building site results. The results of baseball field and Science Spectrum Museum building sites results were affected by the wind speed and its direction. The commercial aethalometer and the particle spectrometer described in this paper

had very good agreement in measuring the BC concentration at all sites. At Lubbock city bus station, a large spike in concentration coincided with the bus arrival and was registered by both instruments. The BC concentration varied from 300 to 10000 ng/m^3, and both instruments gave identical response (Appendix Figure A.17). TTU Chemistry building (used as one of the sampling site) was located in the center of the campus and was distant from any major road traffic. As seen from Appendix Figure A.18, the BC concentration at this site was very low and varied between 200 to 300 ng/m^3. Several spikes registered by both instruments were most likely due to the arrival or departure of some cars at the parking lots near the Chemistry building. As seen from Appendix Figure A.18, a substantial event happened at around 9 AM (on October 4, 2005) as a truck idled at the loading dock of the Chemistry building to unload/load supplies. The window through which the ambient air was sampled was just located above the loading dock.

As described previously, the true merit of the particle spectrometer is its ability to not only calculate the total BC concentration but to also provide data regarding the particle size. Sampling was carried out for 8 hours at the previously listed locations. Both methods A and B were applied for determining average particle size. At the city bus station it was 0.14 and 0.21 μm, at Science Spectum Museum and OMNI theater building, it was 0.36 and 0.40 μm, and at the baseball field it was 0.33 and 0.33 μm using methods A and B respectively. It was observed that the average particle size measured at the city bus station was significantly smaller than the other two sites. Assuming the BC present in the ambient air is largely produced by automotive exhaust, a reasonable supposition for the reduced particle size observed at the bus station could be correlated to the fact that high combustion temperature (of the bus's diesel engines) resulted in small size BC (as compared to relatively larger size of emitted particle from gasoline engines).[51] Further evidence for this hypothesis was supplied by the truck 'idling' event at the TTU Chemistry building near the sampling site. During the 20 minute period in which the truck idled below the window, the measured average particle size was only 0.13 and 0.22 μm using method A and method B respectively, compared to the 24 hour average of 0.28 and 0.34 μm when calculated with methods A and B respectively. That means that the freshly emitted particles by diesel engine

are smaller than the older particles emitted by the gasoline engine. The increase in particle size with time could be attributed to nucleation process. The 0.1 - 0.2 μm and 0.2 - 0.3 μm channel particle counter data and the average particle size data collected from the six channel laser particle counter are listed in Appendix Figure A.19. Comparison of the average particle size determined using the particle counter and particle spectrometer was difficult, because many particles had poor absorption efficiency to be measured by the particle spectrometer. During the truck idling event, however, BC may be assumed to be the dominant species. The average particle size measured by the particle counter and our particle spectrometer agree very well, especially when method A is used. For both instruments the particle size was found to be below 0.2 μm.

2.3.9 Measurements of organic carbon at 375 nm

Absorbance measurements of atmospheric particles, collected on the quartz filter in the particle spectrophotometer, were carried out by the LED array light source. Counting of particles was simultaneously performed either by a handheld airborne particle counter (P/N Handheld 2016) or by a benchtop particle counter (METONE P/N A2212). After comparing all absorbance measurements, it was found that the absorption from the 375 nm LED produced fortuitously anomalous results (Appendix Figure A.20). Instead of the continuum as seen among the other LED absorption measurements, a second absorption peak was seen for 375 nm. Because this anomaly was clearly not due to standard particle absorption, a glass fiber filter (Pall Corporation P/N Q250F) was installed before the particle spectrophotometer instrument and atmospheric air sampling was carried out as before. All particles were captured by the filter allowing only vapors to pass as was indicated by the absence of the large particle peak at pixel # 150. The abnormal peak corresponding to 375 nm still persisted indicating the collection of vapors present in the atmosphere (Appendix Figure A.21). Wood smoke was also analyzed and it is clear the response from the 375 nm LED is from some vapor phase material. A thorough study comparing generated particles of different size and atmospheric particles collected on the filter will be carried out in future work.[52]

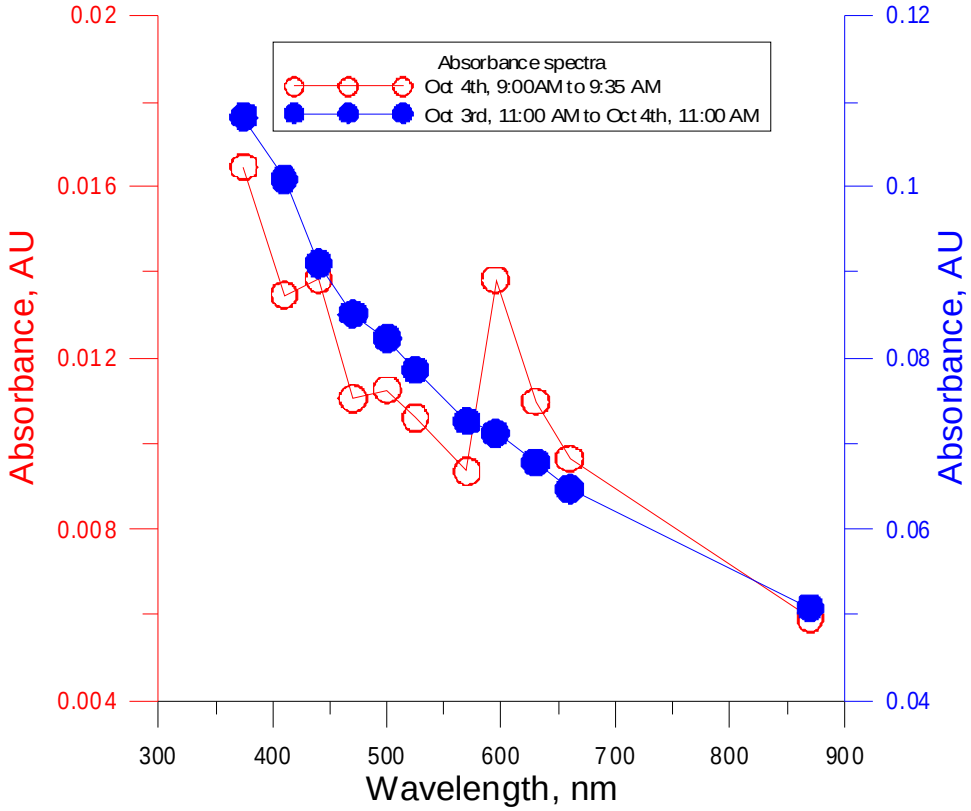

Figure 2.3 Absorbance spectra of particles collected on 3rd October and 4th October 2005.

2.3.10 The absorption spectra of BC at different location

The particle spectrometer has been successfully applied for the field study and the anomaly in the data could be easily correlated to the events happening during the sampling period at the site. From the sampling site experiments as well as the lab study experiments, it has been established that the particles collected had higher absorbance at shorter wavelengths as opposed to the longer wavelengths. At all three sampling sites, with the exception of TTU Chemistry building, an absorbance peak was observed at 600 nm. However, during the trucking idling event from 9:00-9:30 AM, a similar absorbance peak occurs at 600 nm (Figure 2.3). Hence, engine exhaust particles have a unique absorbance at 600 nm. This conforms the absorbance of pure diesel soot at 660 nm.[26]

2.4 Conclusions

The new particle spectrometer design described is simple, inexpensive, and measures the BC concentration in the atmosphere and is in good agreement with commercially available instruments. In addition it can provide very important information such as particle size and absorbance spectra of colored particulate matter. Also, it can measure the vapor content of the air sample and could help in humidity measurements. This unique characteristic makes it possible for this newly designed particle spectrometer to differentiate the source and the type of the BC or colored particles in the atmosphere.

CHAPTER 3

SEMI-CONTINUOUS AUTOMATED MEASUREMENT OF ORGANIC CARBON IN ATMOSPHERIC AEROSOL SAMPLES

3.1 Introduction

The characterization and measurement of atmospheric carbonaceous aerosols have long been of interest. Shah et al.[53] examined 1300 urban and rural US samples and found carbon to account for ~13% of the total suspended particle mass. About 67% of the carbon may be organic, mostly combustion-derived. In the 1980's, ~40% of the $\leq$2.1 μm particle mass in Los Angeles was reportedly carbonaceous;[54] others reported ~49% of the mass of summertime 0.15-0.45 μm particles to be organic.[55] In atmospheric fine particles, carbon is the most abundant element.[56]

Carbon in atmospheric aerosols is broadly classified into: inorganic carbonate (IC) (primarily crustal and not particularly reactive/toxic), organic carbon (OC), and elemental carbon (EC). EC has interchangeably been called soot, black carbon (BC) or graphitic carbon (GC) but increasingly distinctions are being made.[57] BC is an optical term, denoting highly light-absorbing carbon. EC is a chemical term referring to the element; a thermally refractory substance with graphitic structure. In practice, BC is a mixture of EC, some OC and some inorganic material: BC is a major contributor to visibility degradation.

Prather et al. recently reviewed atmospheric aerosol analysis, focusing on organic aerosol characterization.[58] While particle mass spectrometry is the most powerful technique to look at specific compounds in aerosols, with the exception of recently developed thermal desorption gas chromatography-mass spectrometry techniques,[59] accurate quantitation is impossible by these approaches and high MW low volatility compounds are difficult to measure regardless. The broad review by McMurry is now dated but there have been few fundamental

advances in real time aerosol carbon analyzers since.[37] Virtually all-extant EC/OC analyzers are based on thermal methods relying on selective pyrolysis of different carbon forms. Tanner et al. review the prior literature and present an early method.[60] Turpin et al. devised the first "on-line" version of the thermal/optical (T/O) method.[61,62] The sample, collected on a quartz filer, is heated in a helium stream while the optical absorbance of the filter is monitored. The evolved gases are oxidized (e.g., by passage through heated MnO_2) to CO_2 that can be detected by nondispersive infrared spectrometry[62] (see www.sunlab.com for a commercial instrument[63]) or coulometric titration.[64] Early practice was dominated by flame ionization detection after converting CO_2 to CH_4, as in the NIOSH standard method to determine carbon concentration in diesel particulate matter.[65] In the NIOSH approach, the sample collected on a quartz filter is heated stepwise. By ~500 ℃, any OC is either volatilized or charred; the loss of optical transmittance can correct for (uncertainties are discussed in ref. [66]) this pyrolytically generated carbon that contributes to the EC measured in the last step. The sample is further heated to 850℃ to decompose IC to CO_2. The purge gas is next switched to O_2 in He and EC is combusted to CO_2. The possible parametric variations are infinite; Chow and Watson in particular have devoted decades to arrive at a protocol that will yield equivalent results in different laboratories.[57,58] The distinction between EC and OC is operationally defined; the ratio can differ by an order of magnitude in different protocols.[57,58,65] Organic vapors adsorb on quartz filters and numerous solutions have been advocated;[67] the multitude of the proposed approaches suggests that none is ideal. To minimize filter artifacts, an impactor based commercial instrument was developed.[68,69]

Compared to atmospheric aerosol OC, the measurement of aqueous OC (dissolved/total organic carbon DOC/TOC), the latter includes suspended material; the definition of "dissolved" being operational[70]) is substantially better developed and in wide use.[71] A typical measurement involves chemical oxidation, e.g., by persulfate, which is often thermally or UV assisted. The evolved CO_2 is quantified in a number of ways;[72] we have ourselves described a capacitance sensor coupled to an asymmetric membrane that can be used to sense CO_2 in such applications.[73]

Persulfate is capable of oxidizing not only DOC but also suspended carbonaceous material. EPA method 415.2 (also method 5310C[74]) can determine carbon in particles up to 200 µm diameter. Atmospheric measurements are concerned with far smaller particles. It is known that UV-assisted persulfate treatment will oxidize even difficult to oxidize humic acids;[75] like substances in atmospheric aerosols have recently become of interest.[76] There is no explicit extant information if EC is oxidized by persulfate under typically used conditions. Literature on regeneration of activated carbon adsorbents by persulfate treatment.[76] obviously suggests oxidation of the adsorbate but not the sorbent carbon. For soil or sedimentary carbon, distinctions between "soot", "hard" and "soft" carbon by measuring total carbon by oxidation at 1020 ℃ after various types of pretreatment have be en made; the definitions are operational and arbitrary.[77] One such pretreatment involves persulfate incubation at 120 °C for 2 h; it is clear that some carbon remains. Any other similar definition of BC/EC is also operational and has been much discussed.[78] Efforts have been made to use the T/O approach to also distinguish between "char" and "soot".[79]

More sensitive and faster aerosol EC and OC measurements are needed; few new approaches have appeared. Thermal cycling of T/O-based instruments require a minimum cycle time. For a 30 min sample, current commercial instruments specify an LOD of 500 ng/m^3 (www.sunlab.com). Monitoring light absorbing BC involves no chemistry and is straightforward; see Chow et al.[57,58] for a recent review. The factor used to convert light extinction to BC mass concentration is empirical but is generally derived from extensive experience. Nevertheless, such instruments provide high temporal resolution BC profiles. A faster and more sensitive OC measuring technique can be a complement to such BC measurements. Here, we describe such an instrument; it relies on a cyclone operated with a 50% cutoff ~<100 nm, with water in the collector cup. The collected sample slurry is periodically transferred to a reactor where the OC is oxidized to CO_2, quantified by conductivity change of serial LiOH-filled membrane sensors. A small sampling time and impaction on water is chosen to avoid filter artifacts.[80,81]

3.2 Principles

3.2.1 Measurement strategies

For high purity process water applications, sensitive TOC analyzers with LODs as good as 50 pg C/mL are presently available. It may therefore seem that the combination of a continuous flow particle collector (see e.g., a relevant review[82]) and a continuous TOC analyzer may provide an attractive solution. The problem with this approach is atmospheric CO_2. With a Henry's law constant of 3.4×10^{-2} M/atm and a CO_2 concentration of ~4×10^{-4} atm, saturation with atmospheric CO_2 will pose a background >150 ng C/mL that will vary depending on temperature, presence of other gases that affect pH and any changes in CO_2 concentration. Quantitative removal of the CO_2 by a denuder while transmitting fine particles will be difficult to achieve at high flow rates and the problem may simply morph into the difficulty of quantitatively reproducing the extent of the CO_2 removal.

For discrete sampling, because of rapid saturation with atmospheric CO_2, dissolved CO_2 concentration does not change with the sampling duration. But the collected amount of particulate carbon increases continuously with the sampling duration. Sampling for a finite duration therefore solves the CO_2 problem and the amounts collected are such that it hardly requires the ultimate in detection capabilities.

3.2.2 Choice of the CO_2 absorber and sensing strategy

We previously compared photometric and conductometric approaches for the measurement of gaseous CO_2 after absorption in an aqueous acceptor in a membrane based collector. These measurements were conducted by detectors separate from the collectors. Conductometry based measurement was judged to be superior.[83]

While membrane collectors with integrated long path optical detectors have since been reported; [84,85] we elected to stay with conductometry. The choice of the best absorber for absorbing and conductometrically measuring CO_2 is not intuitive. There can be three basic choices: (a) pure water, (b) a weak base of intermediate basicity such as Tris,[83] and (c) a strong base. The theoretical conductometric behavior for pure water, 5 mM Tris, and 5 mM LiOH are

shown compared to each other in Figure 3.1. If we consider a target LOD of 50 ng C in our reactor volume of ~5 mL, this corresponds to ~1 µM C. At the 1-5 µM C level, a LiOH absorber provides ~2-3x as much signal as the water absorber while the signal from the Tris absorber is still negative. In fact even at much higher C levels the LiOH based sensor still outperforms the Tris-based sensor although a positive signal is now observed with Tris. Because the background conductance of water is far less than that of LiOH, S/N can however, be better for water than for LiOH. If pure water is consistently available and one can make a differential measurement before and after the CO_2 absorption, water will provide the best LOD.[86] Unfortunately, the exact sensitivity and calibration with water is dependent on the initial purity of the water (i.e., the level of CO_2 it already has, details can be gleaned from the data for the water absorber in the Appendix Figure B.2). While the availability of high purity water as absorber is not an issue in monitoring high purity water TOC levels,[86] it is different for a field instrument. We chose therefore to use a strong base solution as an absorber, where the sensitivity/calibration is independent of prior absorption of any CO_2. For lower background conductance, LiOH was chosen over NaOH or KOH.

3.3 Experimental section

3.3.1 Reagents

Potassium persulfate ($K_2S_2O_8$, anhydrous, 99.99%, Aldrich), sulfuric acid (UHP semiconductor grade, Fisher), O_2 and N_2 gases (UHP grade, Matheson) and LiOH (monohydrate, Aldrich) were obtained as indicated. Working LiOH solutions (5 mM and 150 mM) were prepared from a stock and protected from CO_2 by a soda-lime vent cartridge (SL, see Figure 3.2). Water (>18 MΩ•cm and TOC <1 ppb) was supplied by a Milli-Q gradient water system. Activated carbon (Norit A, Baker), graphite powder (www.pocostore.com), buckminsterfullerene (99.8% C-60, balance C-70, 100% soluble in dichloromethane, www.sesres.com) and carbon black (type N231, www.sidrich.com, Appendix Table B.1 has characterization data) were obtained as indicated. Hexane soot was collected by burning *n*-hexane in an alcohol lamp and collecting the

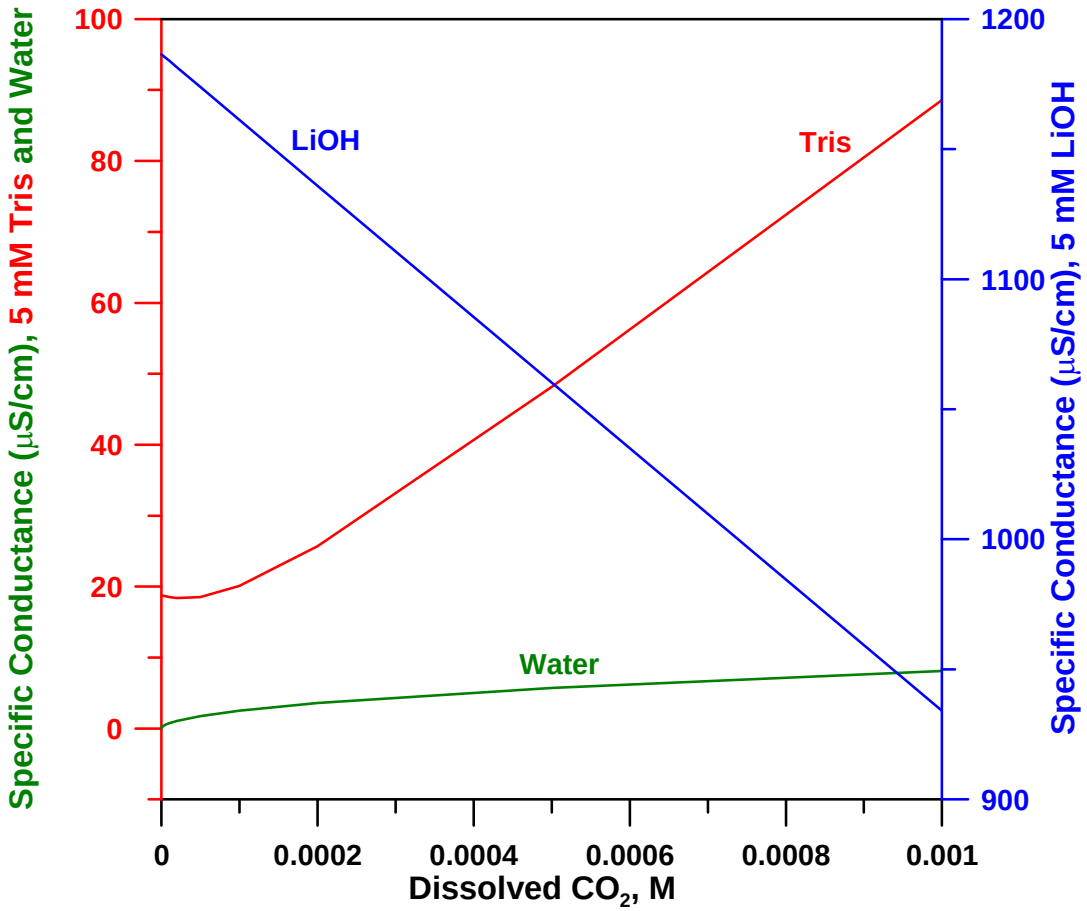

Figure 3.1 Comparison of conductivities of pure water, 5 mM Tris, and 5 mM LiOH as they absorb different amounts of CO_2. Response over a more extended concentration range is given in Appendix B.

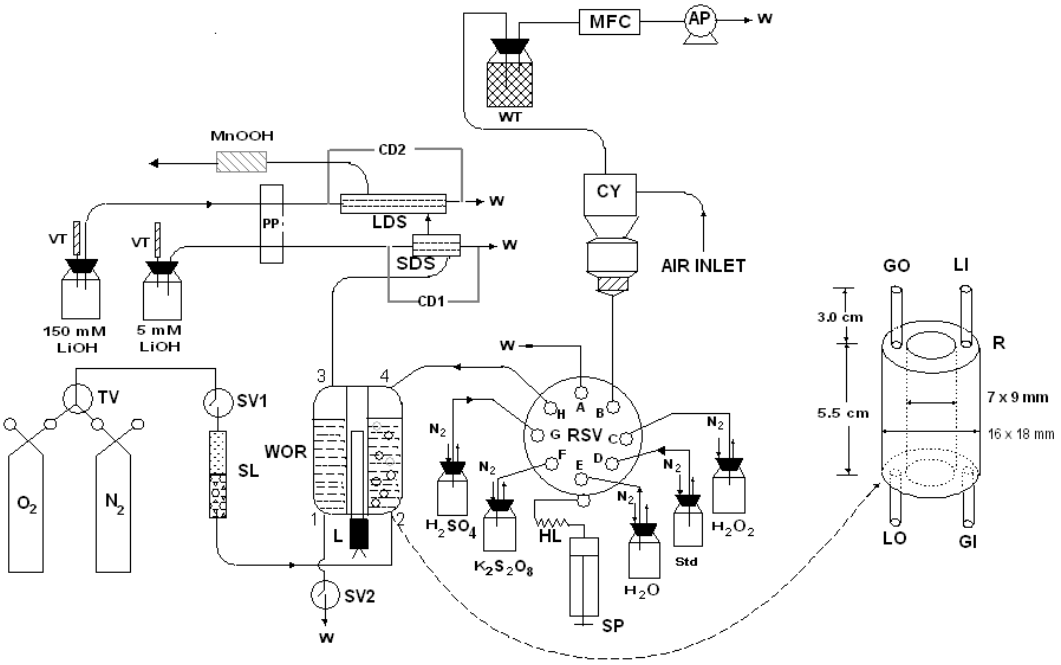

Figure 3.2 System Schematic. TV: 3-way solenoid valve, SV1,2: On/off solenoid valves, SL: soda-lime, VT: vent trap, filled with soda-lime, W: waste, L: UV lamp; WOR: wet oxidation reactor (details on right panel; GI/GO: Gas inlet/outlet, LI/LO: Liquid inlet/outlet); SP: Syringe pump; HL: holding loop; RSV: rotary selector valve; PP: Peristaltic pump;MnOOH: Carulite activated Mn oxide ozone destruction catalyst; LDS, SDS: Long and Short diffusion scrubber sensors; CD1,2: Conductivity detectors; CY: Cyclone; WT: water trap; MFC: Mass flow controller; AP: Air pump

soot on the surface of an inverted watch glass that was periodically scraped off.[87] All other chemicals were of reagent grade and used without purification.

3.3.2 System description

The system is schematically shown in Figure 3.2. A syringe pump (SP, 48 Ksteps, P/N 54022), modified with a horizontal offset adapter[88] and equipped with a 8-port rotary selector valve (RSV, P/N 24520) and a 5-mL zero dead volume glass syringe (P/N 24691, all from www.kloehn.com) were used for liquid manipulations. The adapter allows a 5.2 mL volume holding loop (HL, 11SW PTFE tubing, www.zeusinc.com) between SP and RSV. Using HL to hold the collected sample is important: if fine particles are taken into the syringe, the plunger eventually seizes. The wet oxidation reactor (WOR), shown in the right inset was fabricated in-house from quartz; the dimensions are given in the figure. The fused quartz UV lamp (L, Analamp 81-1025-01, Ozone-producing, 2.5-cm long, powered by a P/N 90-0001-01 supply, www.bhkinc.com) transmits the 185-nm line. The lamp is put in the donut hole of the WOR, using Al foil shim to hold it in place. Al-foil on the WOR exterior serves as reflector and prevents operator exposure. Subsequent to these studies we learned that wrapping a poly(tetrafluoro(ethylene) (PTFE) tape around the WOR is more effective as a reflector.[89] This arrangement has since been adopted but requires that the WOR be put in an enclosure to prevent operator UV exposure and the enclosure be fan-cooled. All data reported here were obtained with the Al-foil covered reactor. Connections to the quartz inlet/outlet tubes were made with stainless steel tubes inserted into them with low expansion ceramic adhesive (940LE, www.Cotronix.com) making the seal. Initial experiments showed that any carbonaceous material, including fluorocarbon polymers, if exposed to the UV irradiation, contributes to an increased CO_2 background.

The particle collector is a miniature cyclone collector (CY, URG2000, specified 50% cutoff (D_{50}) is 2.5 μm @ 3 L/min, www.urgcorp.com). We operated this device at a sampling rate of 28 standard liters per minute (SLPM, ~30.5 L/min at laboratory pressure and temperature) with a resulting measured D_{50} ~< 0.1 µm. The air pump (AP, Bendix 4-13408) provided aspiration with

controlled sampling rate (MFC, www.aalborg.com). A glass wool filled water trap (WT) before the MFC protected against water ingress into the MFC. As supplied, CY has a removable cap at the bottom where the particles are deposited. A replacement aluminum cap with a 10-32 threaded aperture in the slightly conical bottom presently substituted the standard cap. A short length of stainless steel tubing (1.6 mm o.d., 1 mm i.d.) connects CY bottom to RSV (port B). At the beginning of each sampling period, 3.8 mL water was introduced to CY. At the end of the sampling period, this solution is withdrawn by SP into HL.

As discussed further below, much as the T/O approach can use a number of steps to differentiate between OC classes, similar steps of increasing oxidative vigor can be applied here. But as in the T/O system, typical use will likely involve a single total OC value. This abbreviated single step protocol is described here.

With the collected sample still in HL, RSV was switched sequentially to ports G and F and 0.5 mL each of 0.5 M H_2SO_4 and 0.1 M $K_2S_2O_8$ were aspirated into HL. L is now turned on and the HL content is delivered directly into the WOR through port H. (We experimented with a syringe equipped with a gas flushing port but carryover between cycles was found to be <5% with standard syringes.)

Now the instrument proceeds in parallel to (a) prepare CY for the next sample and (b) proceed with analysis in the WOR. For a, CY bottom is first washed. Water (3.8 mL, port E) is aspirated into HL, delivered (port B) into CY, aspirated back and delivered to waste (port A). Water (3.8 mL) is aspirated again and delivered to CY; it is now ready to commence sampling. From the time air sampling is stopped (and liquid withdrawal from CY started), a total of 20 min elapses before air sampling begins again. As presently configured, the instrument works on a 60% sampling duty cycle, with a 50 min cycle time.

Just prior to beginning the analytical step (b above) in the WOR, the CO_2 sensors (*vide infra*) are refilled. A peristaltic pump (Model RP-1, Dynamax, USA, 125 µL/min) turns on for 6 min and refreshes the LiOH solutions in the sensors. Since the sensor operation takes place in a stopped flow mode, a pump is not essential; gravity or pneumatic pressure induced flow, turned

on/off by a solenoid valve, can be used.[84] A peristaltic pump was used here for convenience. Immediately as liquid flow was stopped, solenoid valve 1 (SV1) was turned on and oxygen (selected by three–way valve TV) started bubbling through port 2 of the WOR; a mass flow controller *(*www.brooksinstrument.com*),* not shown in Figure 3.2, placed just before WOR port 2 controlled the gas flow rate to 10 standard cubic centimeters per minute (sccm). Bubbling oxygen serves to keep the reactor contents mixed, well-oxygenated and purges CO_2 from it. The intense UV irradiation not only initiates the decomposition of persulfate, it also forms ozone in the reactor solution. All help oxidize OC to CO_2.

The evolved CO_2 passes over two serial miniature diffusion scrubbers[90] configured as conductivity-based CO_2 sensors. These are short lengths of porous polypropylene membrane tubes with terminating stainless steel liquid inlet/outlet tubes, all incorporated in a PTFE jacket, a schematic appears in Appendix Figure B.1(Miniature diffusion scrubber sensors: M, gas permeable membrane tube; J, jacket tube; T, tee; SST, stainless steel tube; LI, liquid inlet; LO, liquid outlet; GI, gas inlet; GO, gas outlet. In essence these are short lengths of porous hydrophobic polypropylene membrane tubes (Accurel PP Q3/2, 0.2 µm pore size, 70% porosity, 0.6 mm I.D. ×1.0 mm O.D, www.membrana.com) that have stainless steel liquid inlet/outlet tubes (LI/LO) SST (0.44 mm i.d. × 0.64 mm o.d.; HTX-23, www.smallparts.com) inserted to a depth of 15 mm in to the porous tube, M. Tube M was incorporated in a PTFE jacket J (3 mm i.d. 9SW PTFE tubing, Zeus) terminated at each end with tees, T, ($^1/_{16}$ in. barbed nylon tees, AP0406TBEN, www.arkplas.com) that provide for gas inlet/outlet (GI/GO). SST entrance end of the tees were sealed with metal filled epoxy). The short-diffusion scrubber-detector (SDS) and the long-diffusion scrubber-detector (LDS) have active membrane lengths of 4 and 20 mm, respectively. Gas flow enters the SDS and then the LDS; the gaseous effluent from the LDS is vented through an activated Mn oxide catalyst bed (Carulite 200, www.caruschem.com) that destroys ozone. The DS stainless steel tube ends serve both as solution ports and electrodes for conductivity detection. We variously used (a) in-house built detection electronics,[91] (b) a single detector time shared between the two sensors and (c) two independent commercial detectors

(model CDM-I, www.Dionex.com). All of the ambient data here is based on the LDS/CDM-I combination. The liquid and gas flows are countercurrent. While the gas flows serially, the liquid absorbers flow independently through each scrubber. Al foil was wrapped around both the scrubbers to protect them from stray UV light and then covered with foam thermal insulation. A short length of nickel tubing (0.5/0.8 mm i.d./o.d., CTNI-200, www.smallparts.com) connects WOR port 3 to the SDS gas inlet. Each liquid outlet was connected by a 0.5 m long capillary tube (0.30 mm i.d. 30SW PTFE, Zeus), that provides some back-pressure to liquid flow and prevent bubble formation.

Except as already stated, PTFE tubing (0.66/1.6 mm i.d./o.d., wrapped with Al-tape to prevent CO_2 intrusion) or PEEK tubing (0.5/1.6 mm i.d./o.d.) was used. Automated operations for the UV lamp, the pumps and the solenoid valves were programmed by an independent timer. The syringe pump is triggered by the timer; pump operations are stored in its own memory. The pump has 3 digital I/O ports and can itself handle all the timer-controlled devices if used with a demultiplexer.

CO_2 evolution data registered by the sensors are acquired for 20 min; the oxidation was perceptibly complete in all cases by 15 min. At the end of the analysis cycle, the lamp turns off, solenoid valve 2 (SV2) opens and WOR contents drain to waste through port 1 aided by the gas flow through port 2. SV2 shuts off, the syringe aspirates 5 mL water, delivers to the WOR that is now drained again. We used a 30 min sampling period, the analysis cycle is necessarily shorter. We incorporated a second WOR wash step (there is time to wash yet another time, if desired). Both SV1 (gas) and SV2 (drain) are now shut off.

3.4 Results and discussion

3.4.1 Sensor saturation and absorber concentration

Slow liquid phase diffusion poses additional considerations for membrane-based sensors operated in a stopped-flow mode. The solution layer near the membrane saturates rapidly with CO_2; the device departs from the predicted theoretical conductance long before the capacity of the whole liquid to absorb the gas is exhausted.[84,92] The efficiency of porous membrane DS's for

collecting CO_2 acutely depends on the pH of the absorber.[82] Sensor saturation due to absorber exhaustion is encountered both for the SDS and the LDS but the LDS, with a much higher LiOH concentration has a much higher upper determination limit (UDL); detailed results can be seen in Appendix Figure B.3.

The high absorber concentration permitting a high UDL unfortunately also mean a high background conductance, increased noise and a poor LOD. To ameliorate this problem we used the SDS filled with low concentration LiOH (5 mM) placed ahead of the LDS (filled with 150 mM LiOH). The short sensor saturated far more rapidly but provided linear response in the 0-16 µM C range and an LOD ~140 ng C (*vide infra*). Since the SDS removed so little of the CO_2 influx, it was possible to have a serial detection arrangement[93] with independent absorber liquids that allowed both a low LOD and a high UDL.

3.4.2 Choice of an analysis protocol

Initially we attempted a stepwise oxidation protocol that involved (a) adding acid and bubbling N_2 to measure IC, (b) turning on the UV source, (c) bubbling oxygen with UV on (ozone is formed), (d) adding H_2O_2 (O_3 + H_2O_2 + UV is often referred to as the advanced oxidation process in wastewater treatment[94]), and (e) adding persulfate, with a finite time interval at each step before the next addition. We also experimented with adding an aliquot of TiO_2 suspension between c and d but it was difficult to remove all the TiO_2 from the WOR in subsequent cycles. This approach mimics in a fashion the stepwise protocol in the T/O approach to measuring aerosol carbon. Any combination of these steps are possible (e.g., Appendix Figure B.4 shows the results of a protocol incorporating a, b+c, and e). In performing ambient measurements at our location, we quickly noted that relative to variations in the measured OC levels, IC levels (based on observed levels, this is largely from CO_2 and not particulate carbonate) were relatively low and invariant. We therefore used a simplified approach where the sample is directly oxidized by UV-persulfate in the presence of O_2/(O_3) and a "blank" is only periodically obtained by interposing a fiber filter in-line (Pallflex 7202, Tissuquartz) and subtracting this blank value from all results to obtain OC values. Admittedly, this abbreviated approach may not be applicable when aerosol

OC levels are low or aerosol carbonate concentration /pCO_2 is large and varies with time. Nevertheless, we believe that the condition that OC>>IC and IC ~ constant is met for the majority of situations. Even in those cases that this condition is not met, IC influence can be minimized by using dilute H_2SO_4, rather than water, as the cyclone collection medium. In addition, we noted that even when we use a single oxidation step, the rate of CO_2 formation still provides information on the ease of oxidation of the collected OC.

3.4.3 Collection: Effective particle size cutoff

The virtue of a filter for collecting an air sample is the ability to reliably collect very fine particles. We have previously developed analyzers where a pair of filters that were alternately sampled and washed/dried formed the heart of the collection system.[95] This system sought to analyze water soluble aerosol components; the likelihood that fine insoluble carbonaceous particles can be quantitatively retrieved from such a filter is essentially zero. Conventional impactors do not usually work well with a water surface for collection,[96] but remarkable success have been achieved with wetted wall cyclones in collecting larger particles, e.g., bacteria/spores at very high flow rates.[97] It is well known that the particle size cutoff (referred typically in terms of the 50% cutoff, D_{50}) for any cyclone collector shifts to lower values as the sampling rate is increased.[98] We explored the reduction in D_{50} when a cyclone is operated at a sampling rate much beyond the design flow rate. Further, we put water in the collector bottom to ascertain how much of it will actually evaporate during operation. The rate of this evaporation was monitored by measuring the humidity of the cyclone inlet and exit air. It is important to note that the rate of water evaporation is also a measure of the degree to which vapor phase compounds (including organic vapors) in the sample air interact with the collector water since the water-air interaction must be bidirectional. This experiment therefore also indicates the potential of the water medium for the undesirable collection of water-soluble volatile organic compounds (VOC's).

Of several cyclones tested, the URG2000 (D_{50} 2.5 µm at 3 L/min) appeared very efficient in collecting small particles when operated at ~10x the design flow rate. The penetration of particles from laboratory air or a Collison nebulizer through the cyclone was determined (Figure

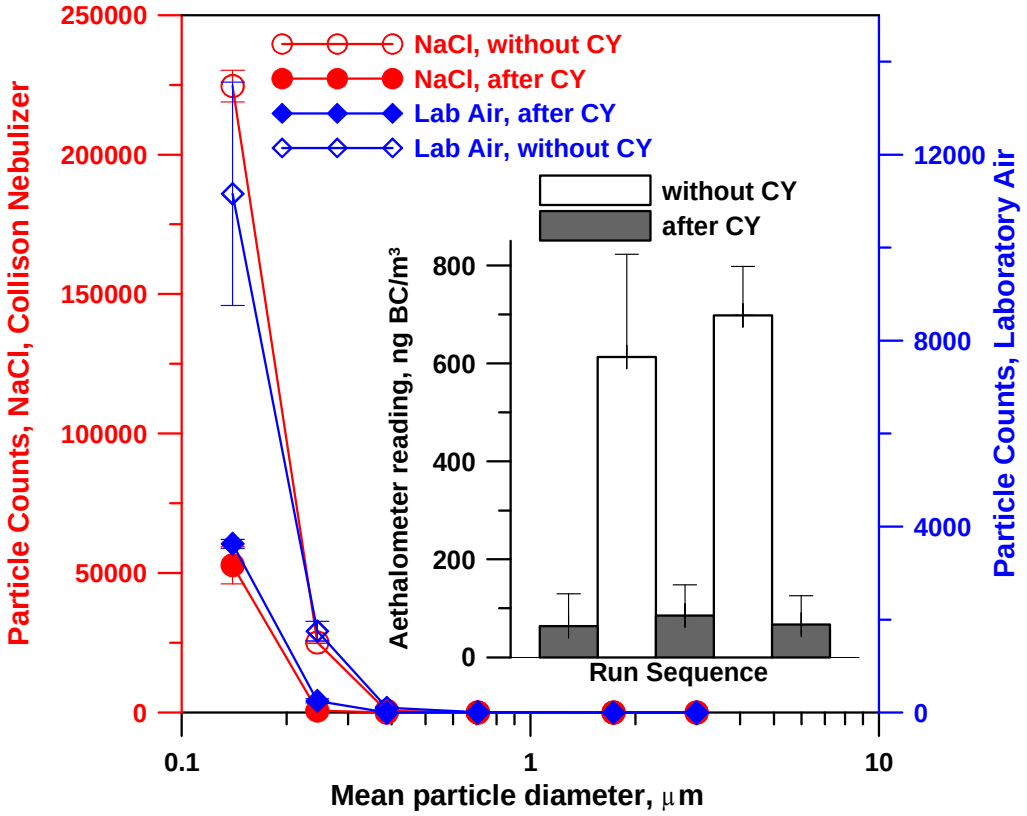

Figure 3.3 Laser based optical particle counter readings of NaCl aerosol generated by a Collison Nebulizer (circles, left ordinate) and of room air (diamonds, right ordinate) before (open symbols) and after (filled symbols) passage through the URG2000 cyclone at 30.5 L/min. The nebulizer (BGI USA Inc.) was fed with 1 mM NaCl. The count bins correspond to 0.1-0.2, 0.2-0.3, 0.3-0.5, 0.5-1.0, 1.0-3.0 and >3.0 µm, and are plotted respectively at the geometric mean of the interval bounds, except the largest size bin is plotted at 3 µm.

3.3, experimental arrangement can be seen in Appendix Figure B.5) with an optical particle counter (OPC). The geometric mean of the OPC smallest size bin was 0.14 µm; 67-77% of the particles in this size class were removed from room air and the generated NaCl aerosol, respectively, suggesting a D_{50} size cutoff below 0.14 µm. A further similar experiment was conducted where an aethalometer sampled ambient air either directly or after the cyclone, the results of the apparent BC concentration thus measured are shown in Figure 3.3 inset; 88±2% is removed by the cyclone. Considering some of the BC is known to occur in the ultrafine range, this result is in accord with the OPC data as well.

In the water evaporative loss experiment, no significant loss of water from the bottom of the cyclone was observable in 30 min operation. Over this period, air entered at 22.0±0.2 °C at 52.6±0.3% RH and exited at 21.8±0.1 °C at 52.5±0.1% RH suggesting that there is minimal interaction of the sample air with the water. This is consistent with known aerodynamics of a cyclone design, else deposited particles will tend to resuspend. Unlike samplers using filters, this instrument should be free from VOC-adsorption interference.

3.4.4 System response behavior and carryover

Figure 3.4 shows calibration behavior for the LDS with different amounts of carbon. The inset shows response from a low level sample (1 µM KHP, 360 ng C) from the SDS. Based on the standard deviation of 6 consecutive filtered air blanks and direct addition of acid persulfate, we estimate an S/N=3 LOD of 140 ng C for OC based on the KHP response. If IC is separately determined by an acid-only step, the LOD is significantly better but this approach was not pursued in the present work.

Obviously, we cannot assure that all of the particles collected in the cyclone are removed by the liquid withdrawal; particles can also adhere to the holding loop walls. The measured carryover is <12% without washing (the data can be seen in Appendix Figure B.6); with the two wash steps incorporated, the carryover was too small to measure.

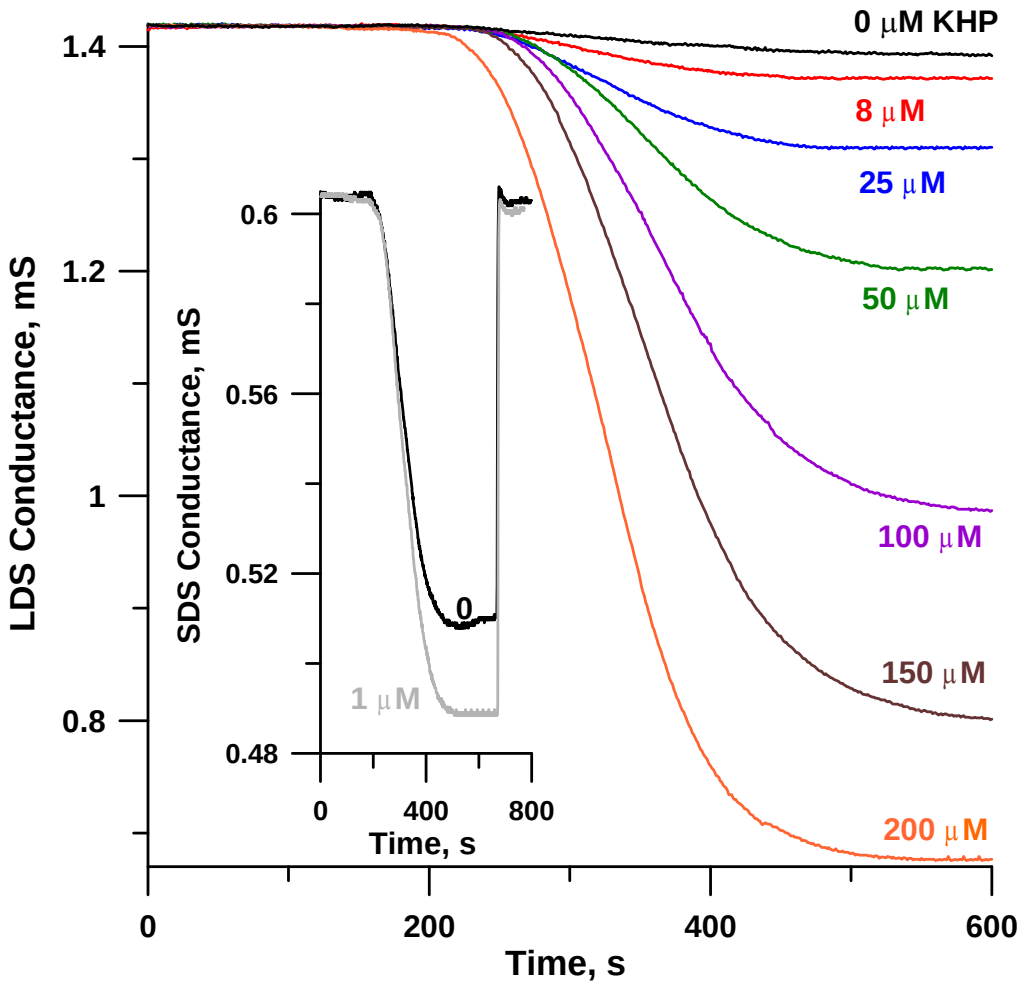

Figure 3.4 Calibration behavior with KHP standards of indicated concentrations in µM (3.8 mL taken) with the long sensor output. The inset shows the difference between a blank and a standard (365 ng C as KHP) for the short sensor.

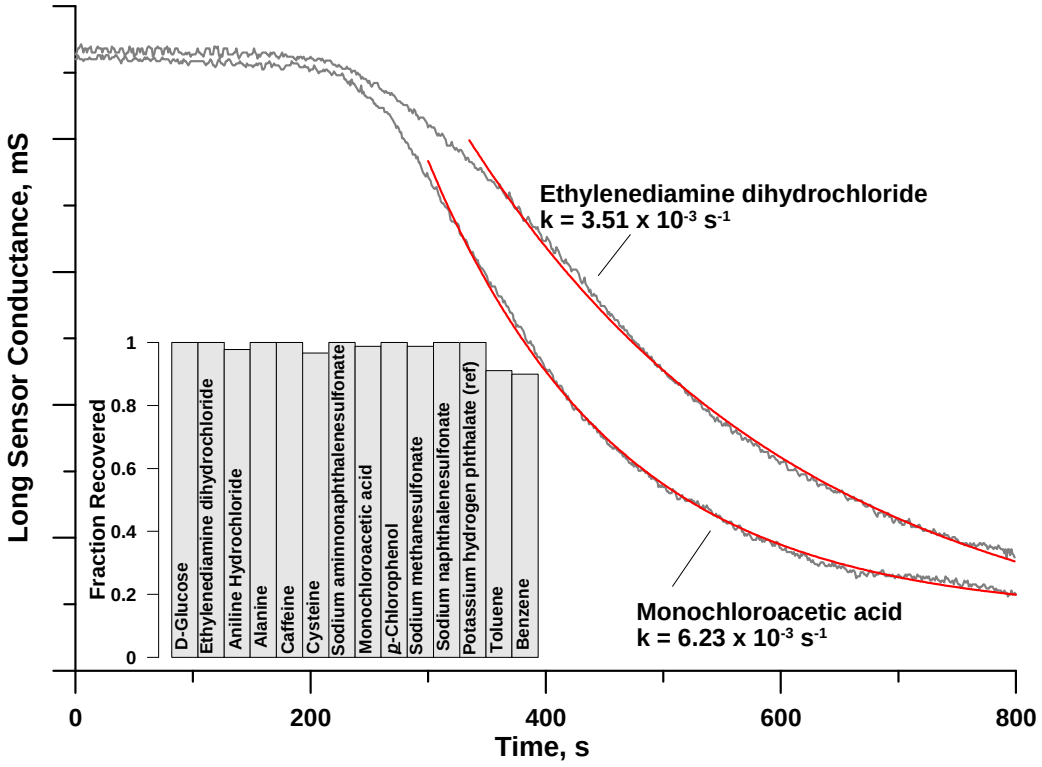

Figure 3.5 Profile of CO_2 evolution for the first 800 s for monochloroacetic acid and ethylenediamine dihydrochloride, each aliquot containing 4.1 µg C. The best first order fit for the data between 300-500 s is shown as a solid line, in both cases r^2 for the fit is >0.99. The inset shows the relative response of a number of different compounds; with the exception of benzene and toluene, all respond quantitatively.

3.4.5 Uniform carbon response to various organic compounds: Differences in kinetics

We looked at test compounds that variously contained CH, CHO, CHN, CHNCl, CHNO, CHOCl, CHSO and CHNSO in addition to Na in some cases (a list is given in Appendix Table B.2). The recovered signal from the indicated compounds, taken as an aliquot containing 4.10 µg C, was 4.04 ± 0.04 µg C, based on KHP as the standard (see Figure 3.5 inset). Only benzene and toluene showed lower recovery (3.69 ± 0.04 µg C), possibly because of volatilization losses. These findings were anticipated since TOC determination by persulfate oxidation is acknowledged to be generally applicable. For the water soluble portion of atmospheric particulate OC, it has already been shown that measured TOC compares well with the same measured by the T/O approach.[99] Even among the relatively small molecules tested, there are differences in the individual rates of oxidation, as illustrated in Figure 3.5 (numerical first order rate constants for the oxidation of the compounds tested are presented in Appendix Table B.3).

3.4.6 No response from elemental carbon

We tested activated charcoal, graphite, hexane soot, C_{60} fullerene, and carbon black as archetypal examples of elemental/graphitic/ soot//black carbon. The solids were suspended in water by ultrasonication; an aliquot representing 75 µg C was directly introduced into the reactor. No perceptible formation of CO_2 above that of the blank water (from dissolved CO_2 and persulfate reagent blank) was seen for any of the samples in many repeat experiments (Representative data are in Appendix Figure B.7). This approach therefore does *not* measure what is traditionally regarded as EC.

3.4.7 Illustrative ambient aerosol data

Figures 3.6 and 3.7 (inset) show the results of one week of ambient monitoring outside our laboratory (15 m above ground level), located in a highly urban center. The BC data was aethalometrically obtained at 880 nm (model AE22, www.mageesci.com) with the manufacturer suggested conversion factor. The data (note especially Figure 3.7 inset, depicting BC vs. OC) clearly indicate that BC and OC must come from *at least* two sources. High OC levels have little

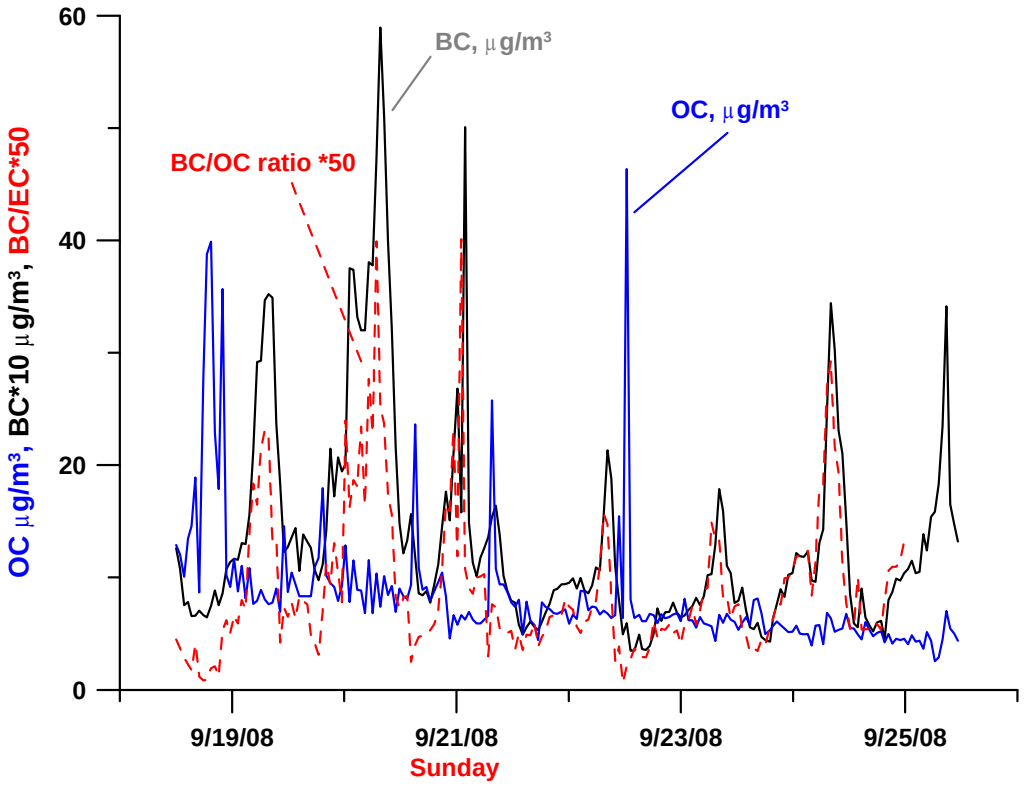

Figure 3.6 Ambient organic carbon (OC) measured by the present approach, aethalometrically measured black carbon at 880 nm (BC) and the BC/OC ratio at Arlington, TX (32.731° Lat., -97.112° Long.), in the center of a metropolitan area of ~6 million people.

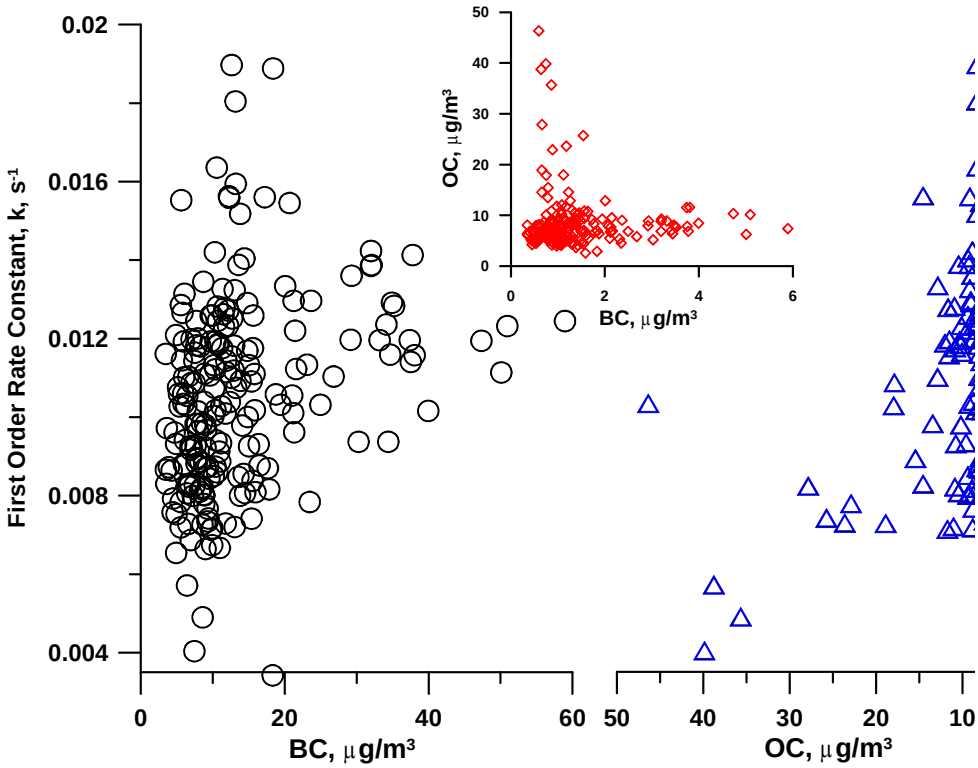

Figure 3.7 Rates of oxidation of the collected OC as a function of BC (left) and OC (right) for the measurements in Figure 3.6. Note the inverted OC abscissa scaling in the right plot. The inset shows a plot of OC vs. BC.

associated BC and no relationship with BC while there is likely an additional BC source with a low OC/BC slope but for which, nevertheless, the OC is correlated to BC. The BC peaks generally occur when OC is relatively low and invariant so the BC/OC ratio closely mimics the BC profile (Figure 3.6). The ease of oxidation data (first order oxidation rate constants) are freely available in these measurements and provide an additional tool to characterize the source and possibly the nature of the carbon. This tool will become more valuable when individual carbon aerosol emission source types are characterized by this technique to allow source apportionment. Presently, the observed oxidation rate constants for each of the OC measurements were ascertained and are plotted against both BC and OC in Figure 3.7. Note first that the OC in most of our ambient samples exhibit a substantially faster rate of oxidation (higher k) than the test compounds. If some of the OC is associated with BC, the photoassisted oxidation may be promoted by better absorption of UV. This hypothesis is supported by the fact that the lowest k values (slowest oxidation) occur only when BC is low. The data in the left panel of Figure 3.7 suggests the presence of a class of samples where oxidation rate increases with the BC content whereas no relationship is observed with the rate of OC oxidation with the OC content (right panel).

Detailed ambient data analysis is beyond the scope of the present chapter; but we note that back trajectory analyses (which can be seen in Appendix Figure B.12 and B.13) show that the origins of the air mass in OC excursion vs. low-OC periods are consistently in different geographic regions.

3.5 Conclusions

We have described a practical automated device that is sufficiently sensitive for the measurement of OC and that unambiguously does not measure EC. No filter is used; filter-induced artifacts are thus avoided. The instrument is assembled at a relatively low cost. As such, an affordable duplex instrument for complete time coverage will be possible. The present sensor(s) collect only a fraction of the evolved CO_2, it may be possible to improve further on the sensitivity provided by the sensors. The instrument is capable of long unattended operation. The

general approach of collection into a collector liquid in a cyclone should be applicable to other cases.

CHAPTER 4

CONCLUSIONS AND FUTURE WORK

This thesis research work dealt with the fabrication of a particle spectrometer, which could be used to provide semi-quantitative information regarding the size distribution and spectral absorption characteristics of sampled atmospheric aerosol particles. At the time this device was fabricated, there was very limited availability of UV LEDs, this has since expanded greatly. A particle spectrometer with a light source containing a greater number of elements that extends the wavelength range, especially deeper into the UV will extend its applicability greatly.

The objective of this research was to develop SSL source based analytical instrumentation to determine the size-dependent optical absorption of particles present in ambient atmosphere. Also, since carbonaceous aerosols are prevalent in atmosphere, part of my efforts went to the development of a fully automated instrument to measure organic carbon in ambient carbonaceous aerosols. In particular, the collection efficiencies of different cyclone-based particle collection systems that functioned as the front end to the OC analyzer was determined at high flow rates.

While various instruments are commercially available to either measure the particle size of ambient aerosol or optical absorption of aerosols without regard to size. Even instruments that provided optical absorption characteristics (without regard to size), do so at a very limited number of wavelengths. There have been no instruments that can provide size-dependent optical absorption characteristics of aerosols. The instrument described in this thesis fills that gap. The device could successfully differentiate between multi-colored as well as multi-sized particles and was used for determining color and particle size of ambient aerosol particles. Although repeated sampling can be made on the same filter segment, when light attenuation reaches a high enough level, the filter must be replaced. As presently implemented, this is a manual operation. It would

be a relatively simple matter to modify the design where a quartz fiber filter tape will automatically advance through the device at preset intervals to introduce a fresh portion of the tape.

The particle spectrometer is non-destructive and the size dependent collection of samples on a relatively inert substrate also leaves the sample freely available for subsequent analysis, e.g., by spatially resolved analysis techniques like laser ablation induction coupled plasma mass spectrometry or matrix assisted laser desorption ionization mass spectrometry.

APPENDIX A

MULTIWAVELENGTH SIZE DISCRIMINATING PARTICLE SPECTROMETER: A NEW TOOL FOR CHARACTERIZING ATMOSPHERIC PARTICULATE MATTER

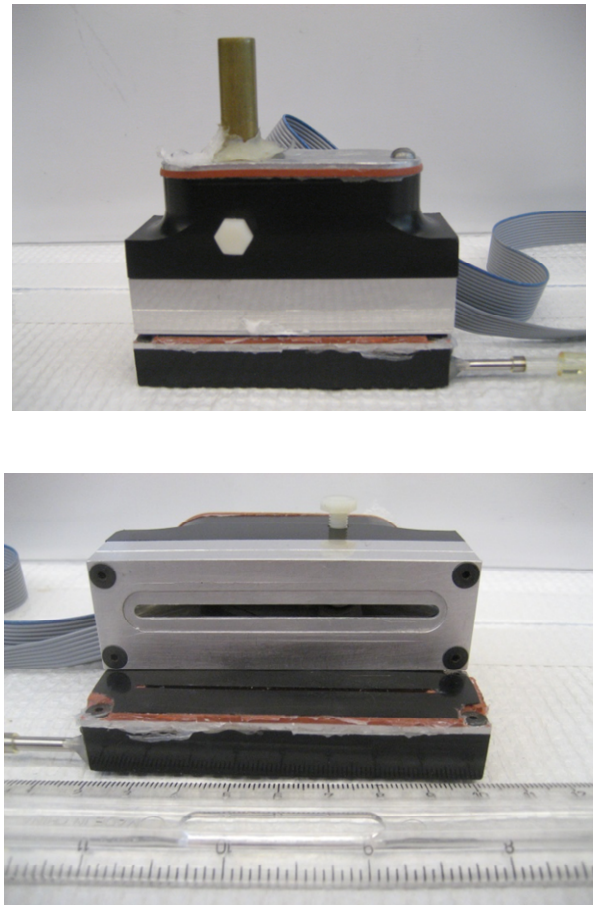

Figure A.1 Photographs of particle spectrometer: Front view (top), instrument opened view (bottom).

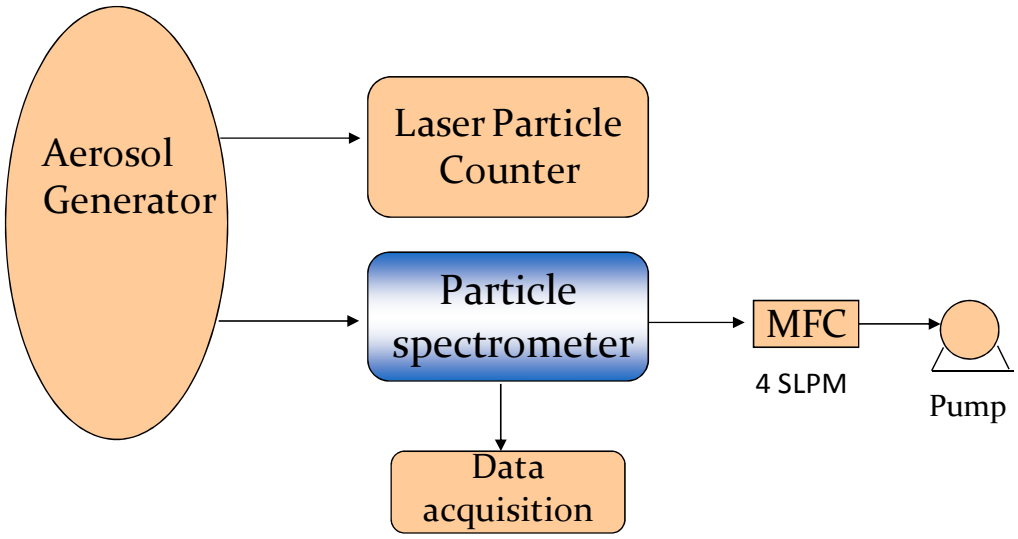

Figure A.2 Schematic diagram of aerosol generation and collection of particles using particle spectrometer.

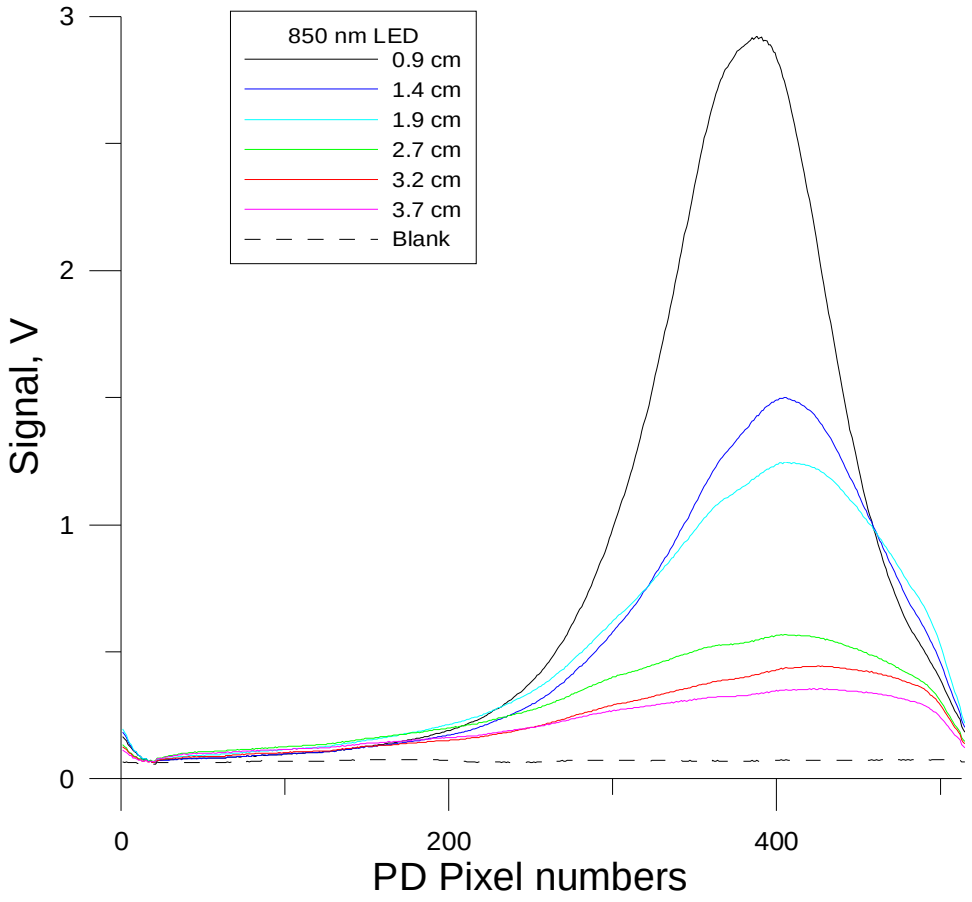

Figure A.3 Same size particle distribution pattern of black ink particles as observed by 850 nm LED when the distance between the quartz filter and LED was varied.

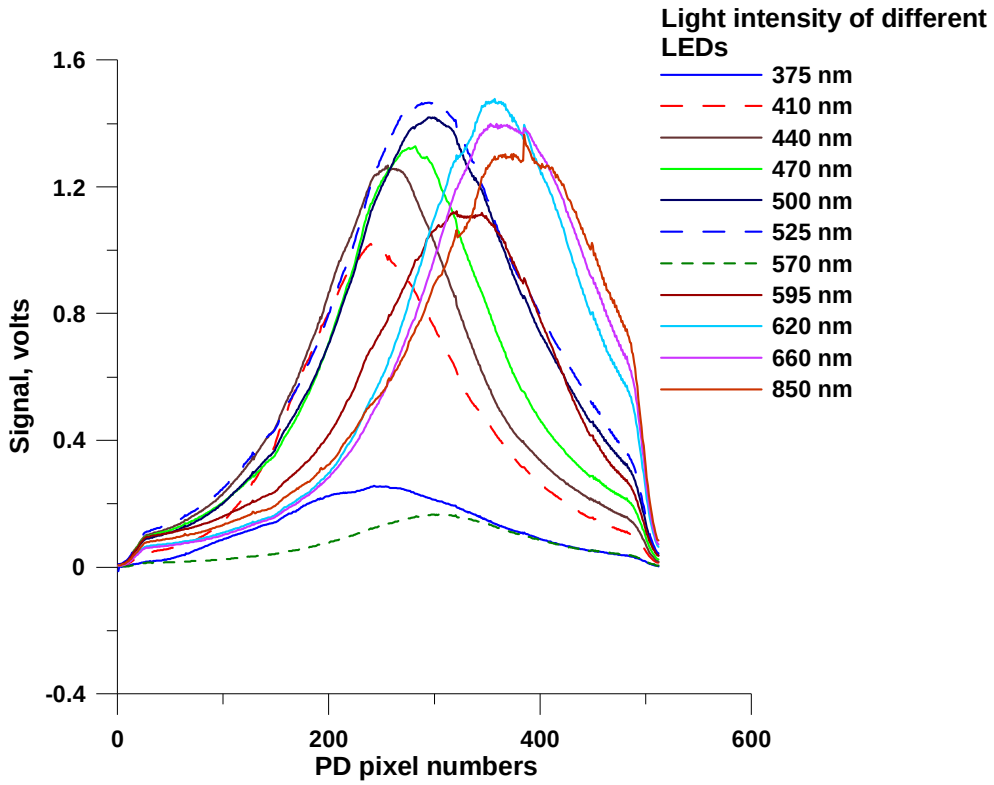

Figure A.4 Particle spectrometer blank response light intensity absorbance spectra (without any particle deposition on the quartz filter) with LED to quartz filter distance of 2.7 cm.

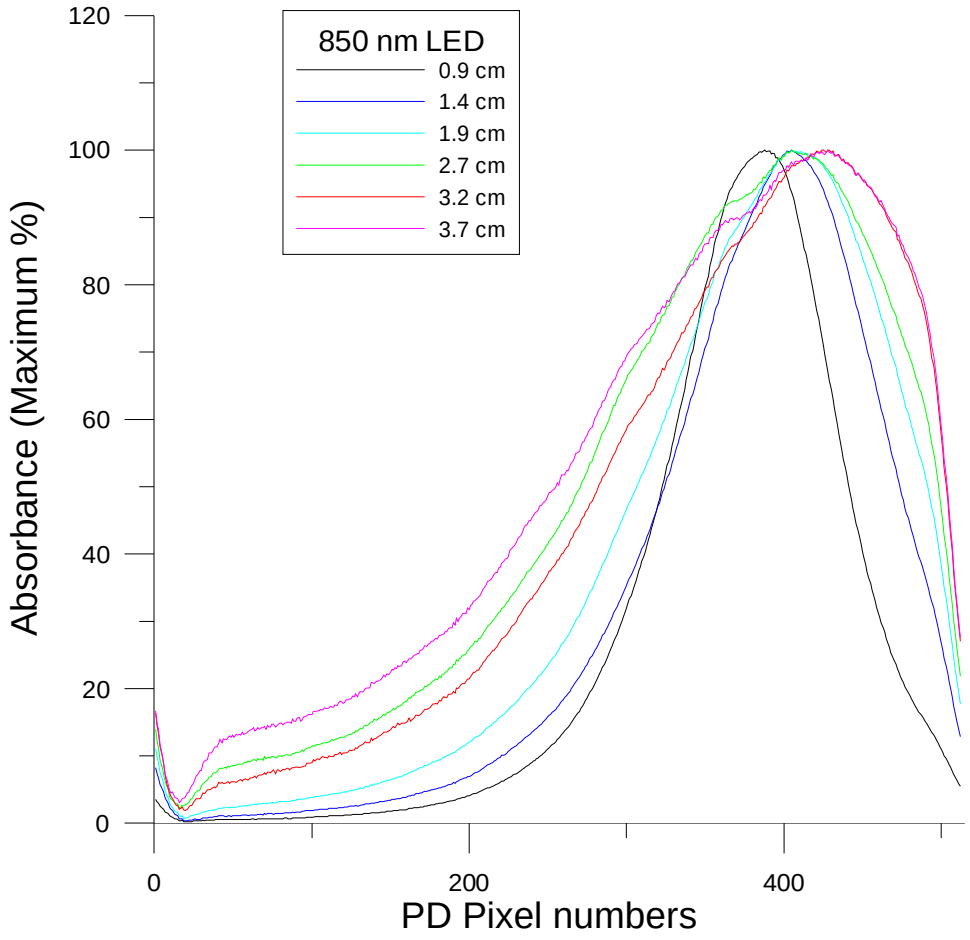

Figure A.5 Percentage maximum light intensity of 850 nm across quartz filter at different LED to quartz filter distance.

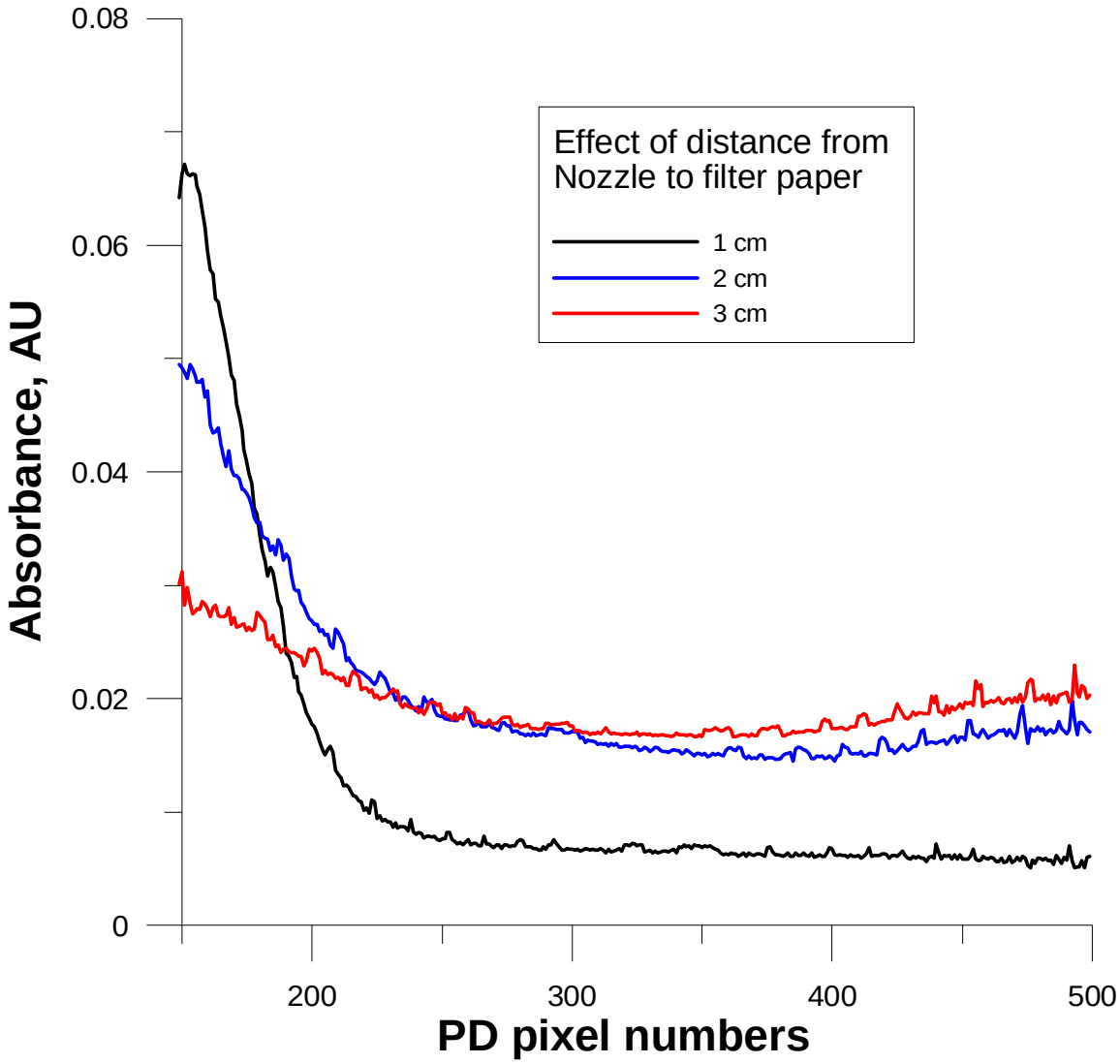

Figure A.6 Effect of nozzle-to-filter distance on the particle distribution pattern (0.73 µm particle size, 3 SLPM sampling flow rate).

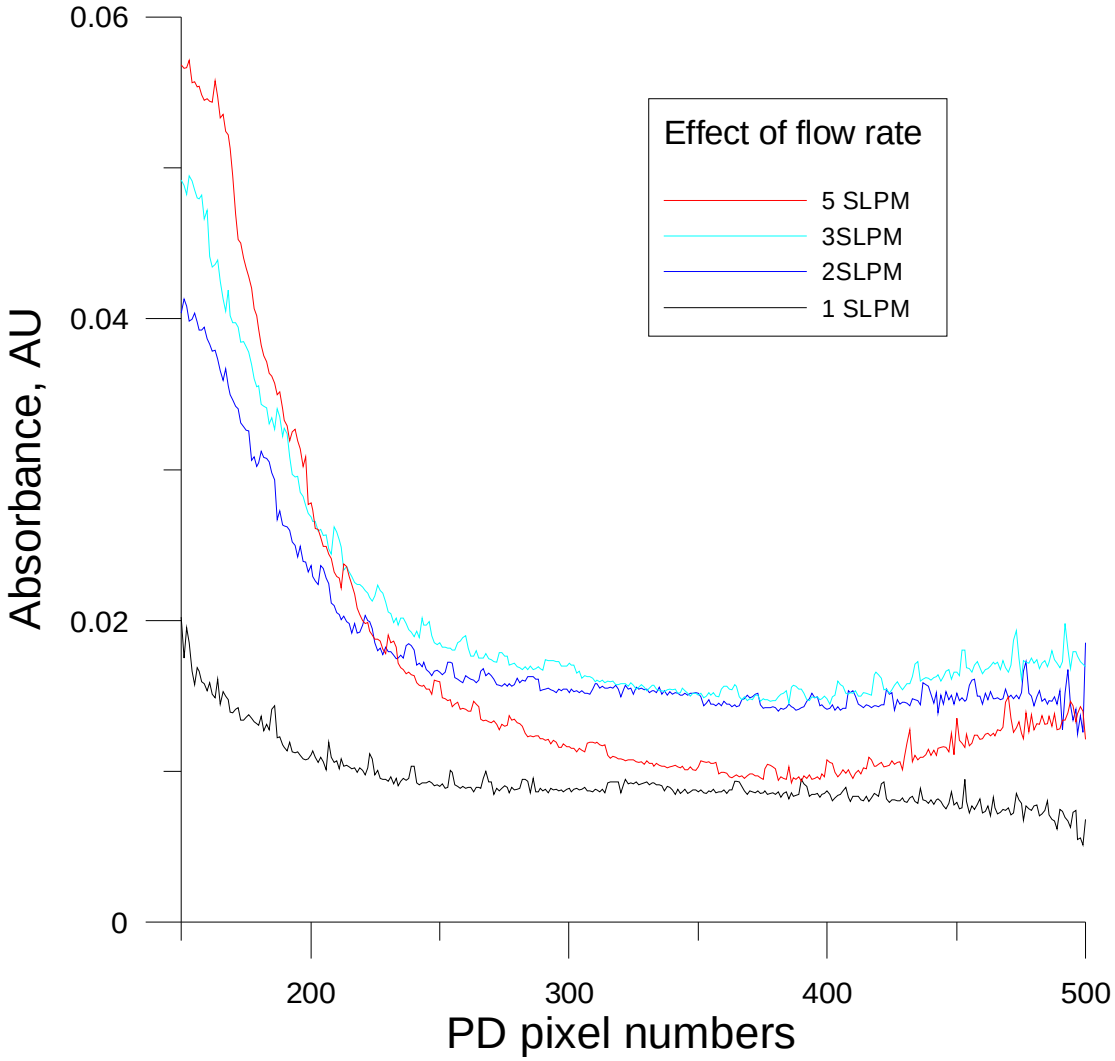

Figure A.7 Effect of air sampling flow rate on the particle distribution pattern when 0.73 micrometer particle was sampled at different flow rates (0.73 µm particle at 595 nm LED data).

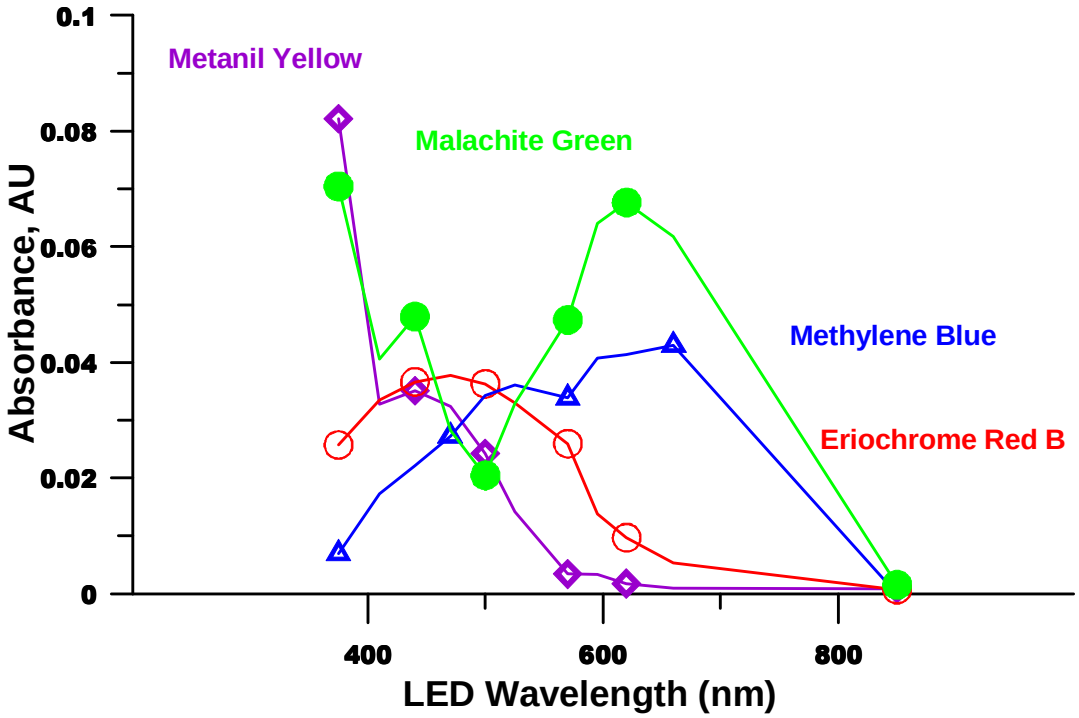

Figure A.8 Absorbance spectra of four different dye particles as obtained from particle spectrometer.

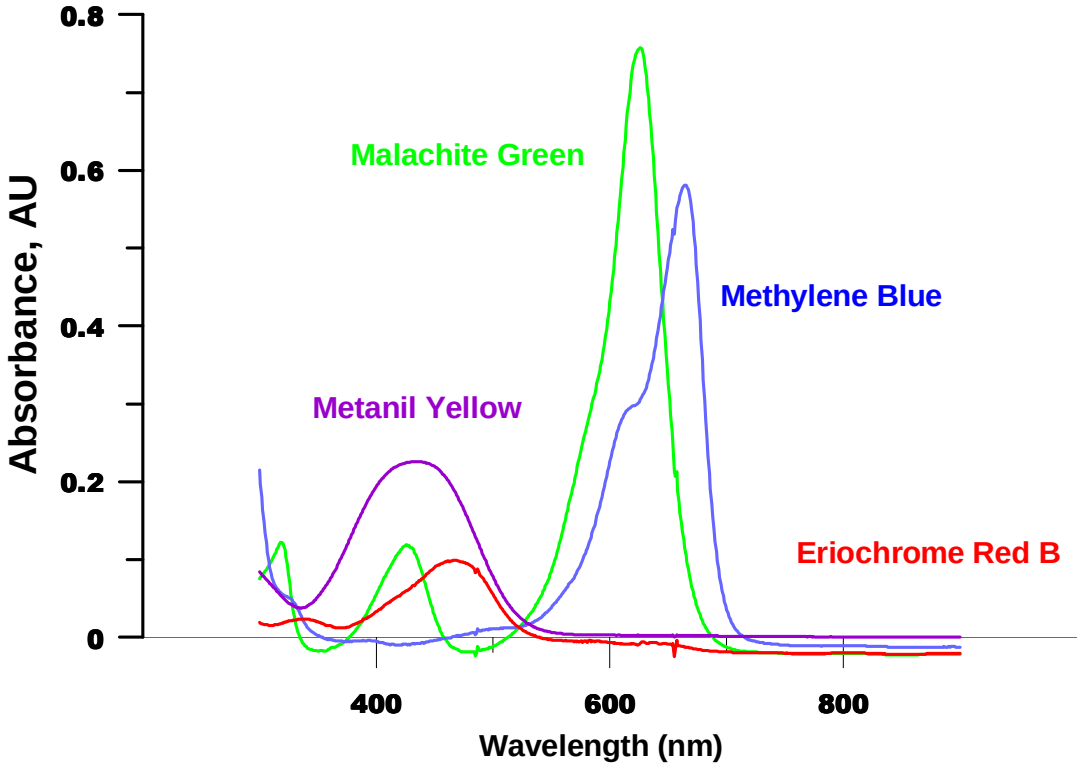

Figure A.9 Solution spectra of four dyes from spectrophotometer.

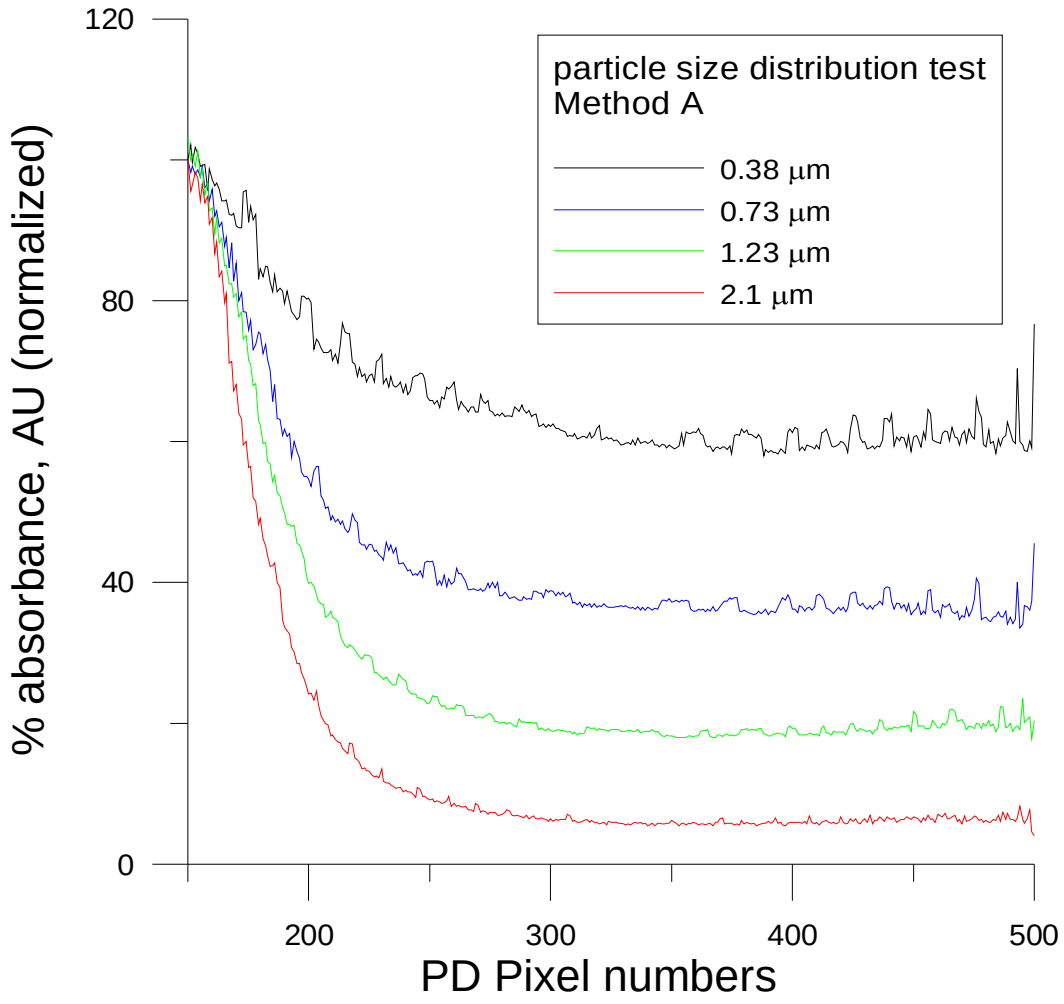

Figure A.10 Normalized absorbance (Percent of Max absorbance on each pixles) for different size particles wherein particle size was calculated by Method A. LED-Filter distance: 2.7 cm, Nozzle -Filter distance 2.0 cm, Sampling rate at 4 SLPM.

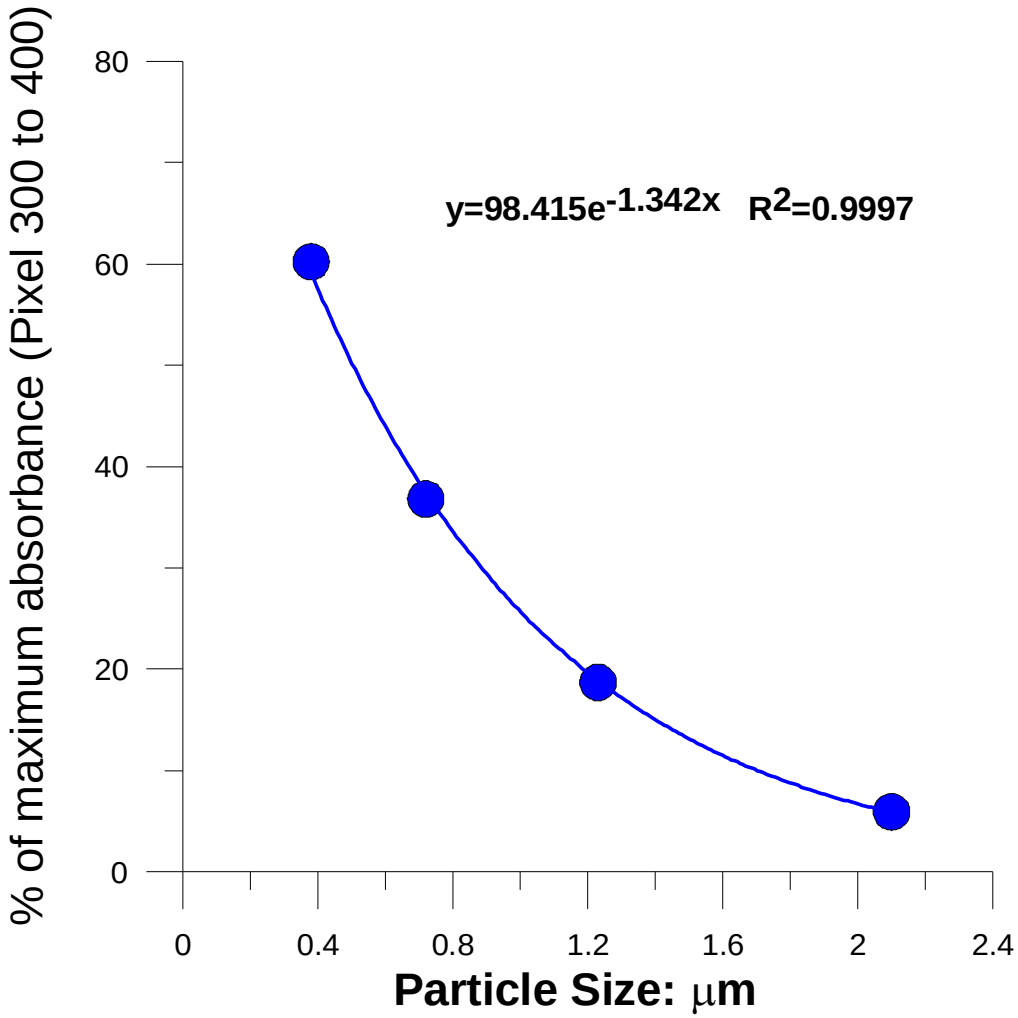

Figure A.11 Particle Size determination using Method A: Best fit curve representing average value of percentage of maximum absorbance on pixel numbers 300-400 for different particle sizes.

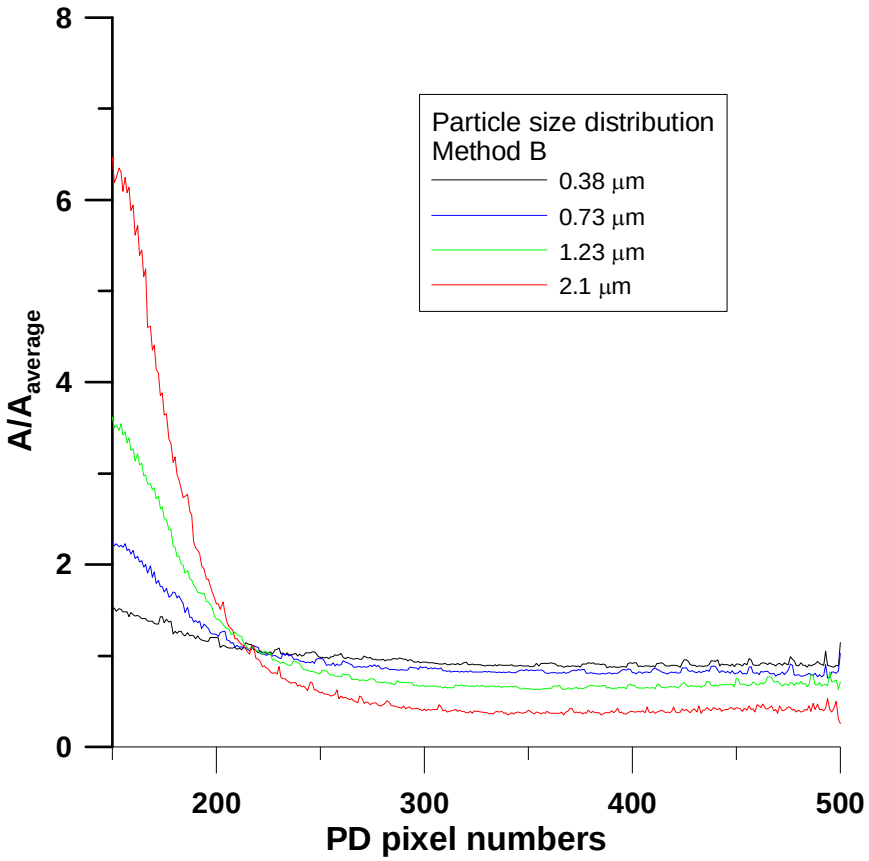

Figure A.12 Ratio of absorbance at each pixel to that of average absorbance from pixels 150 to 500 for different particle sizes (calculated by Method B). Particles were sampled at 4 SLPM while LED-to-filter and nozzle-to-filter distances were 2.7 cm and 2.0 cm respectively.

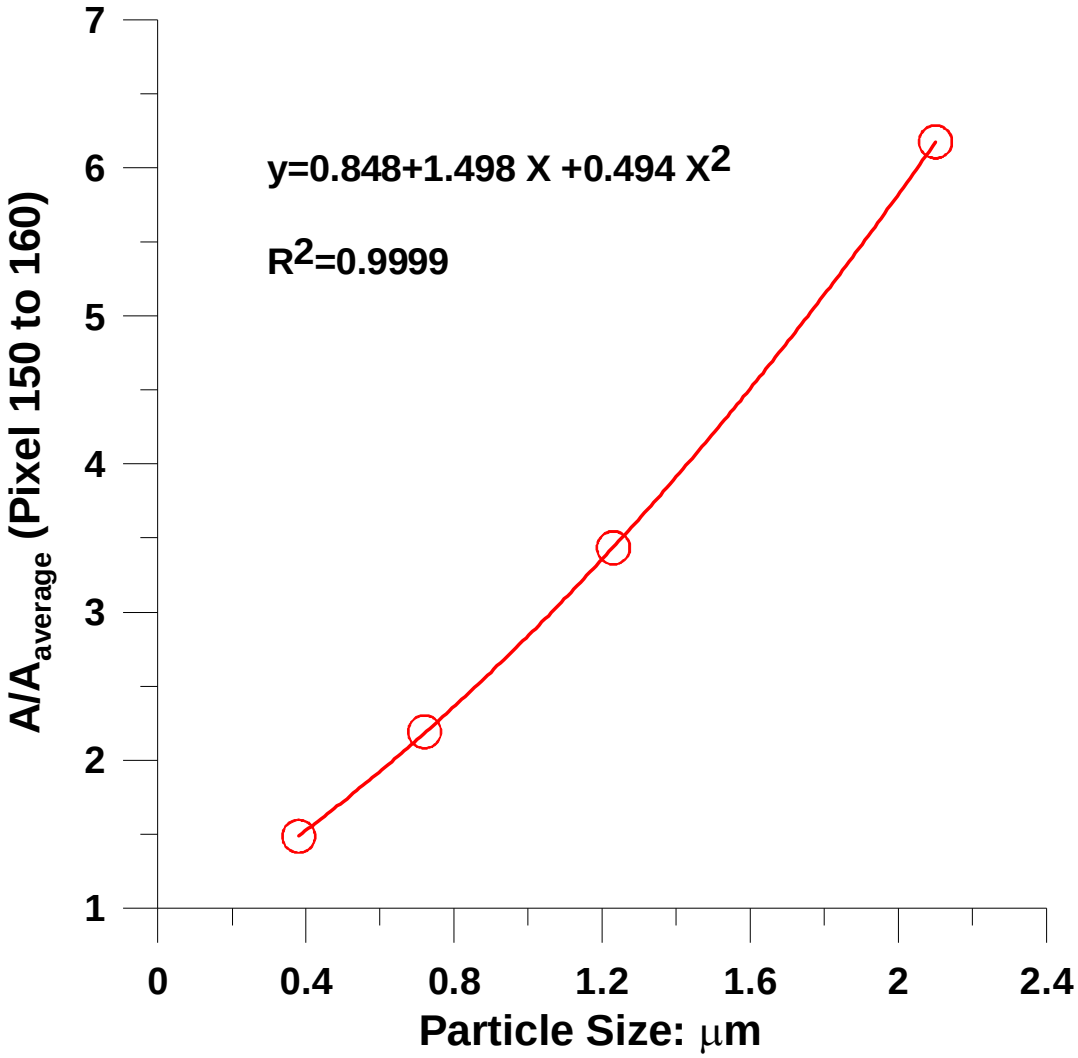

Figure A.13 Method B for the calculation of particle size using the best-fit curve of the ratio of absorbance to average absorbance (470 nm channel data, 5 minute time resolution) from pixel 150 to 160 versus the particle size.

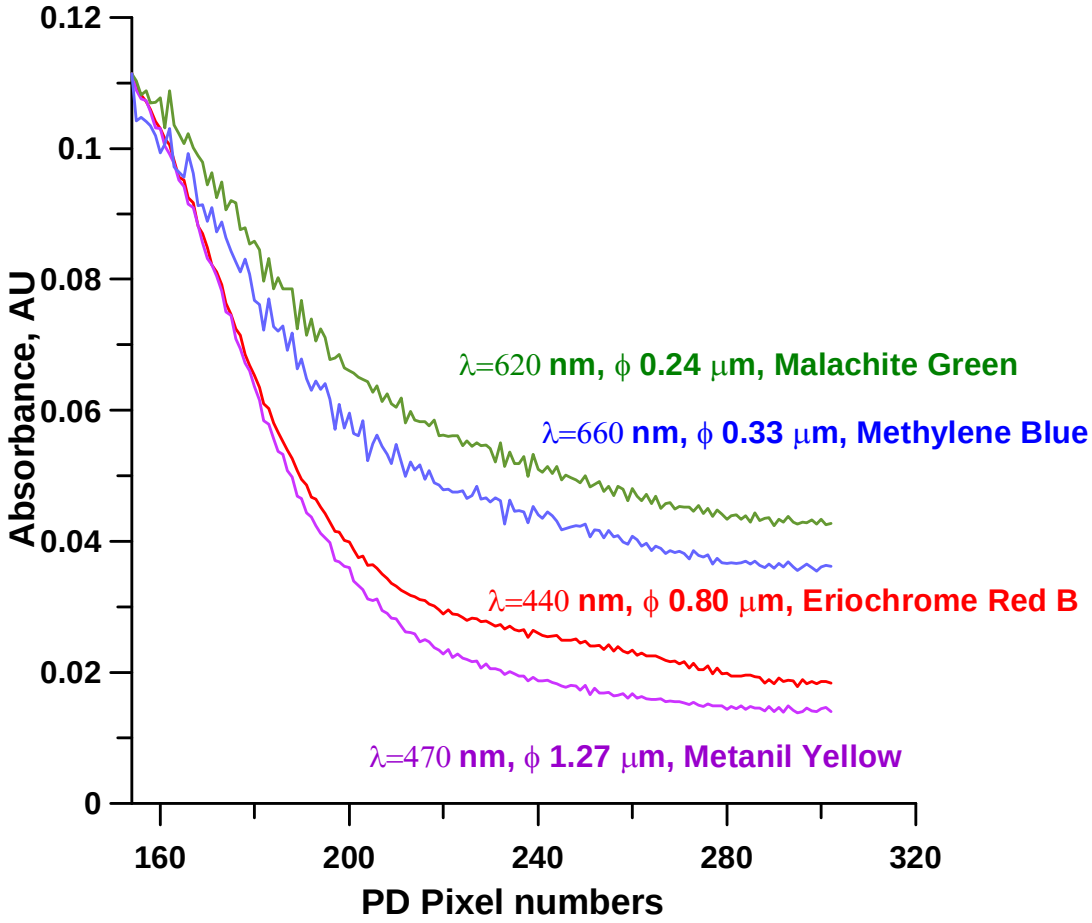

Figure A.14 Dye particle discrimination on the basis of their size and color at the wavelength of maximum absorption using particle spectrometer (when four different dye particles were deposited on a single quartz filter tape sequentially).

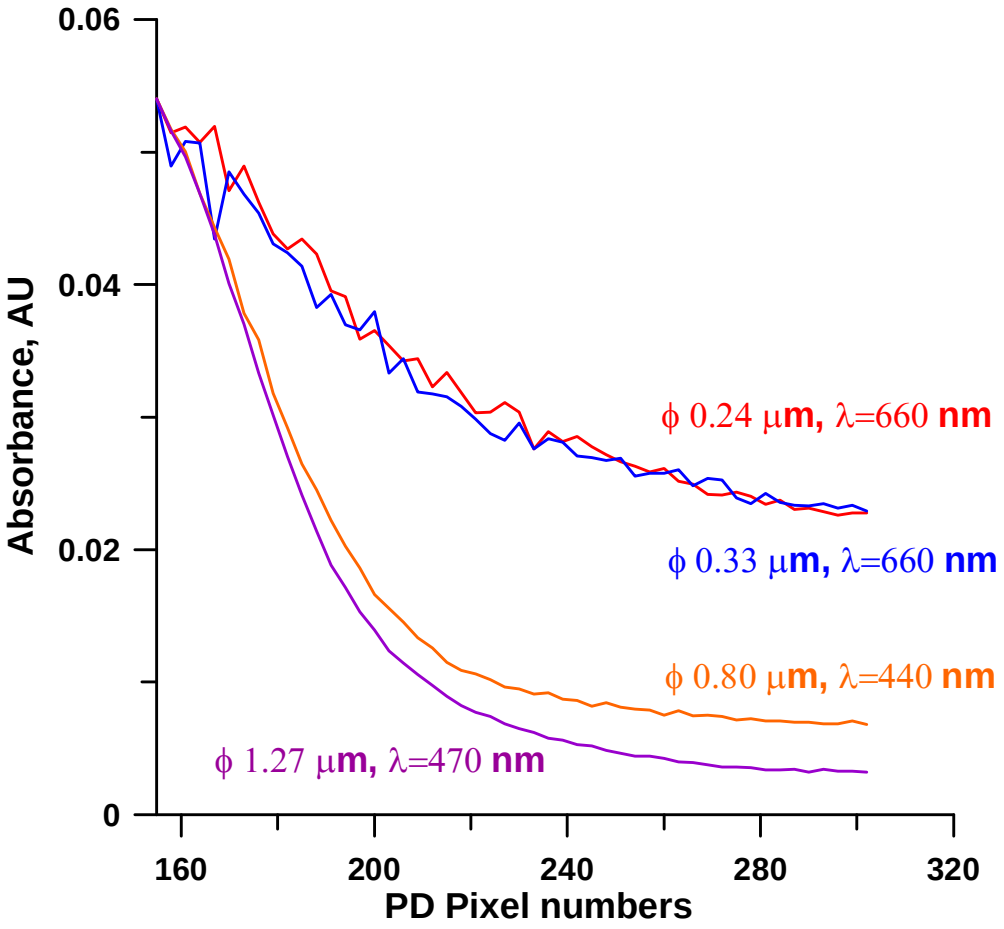

Figure A.15 Dye particle discrimination on the basis of their size and color at the wavelength of maximum absorption using particle spectrometer (when four different dye particles were deposited on different quartz filter tapes).

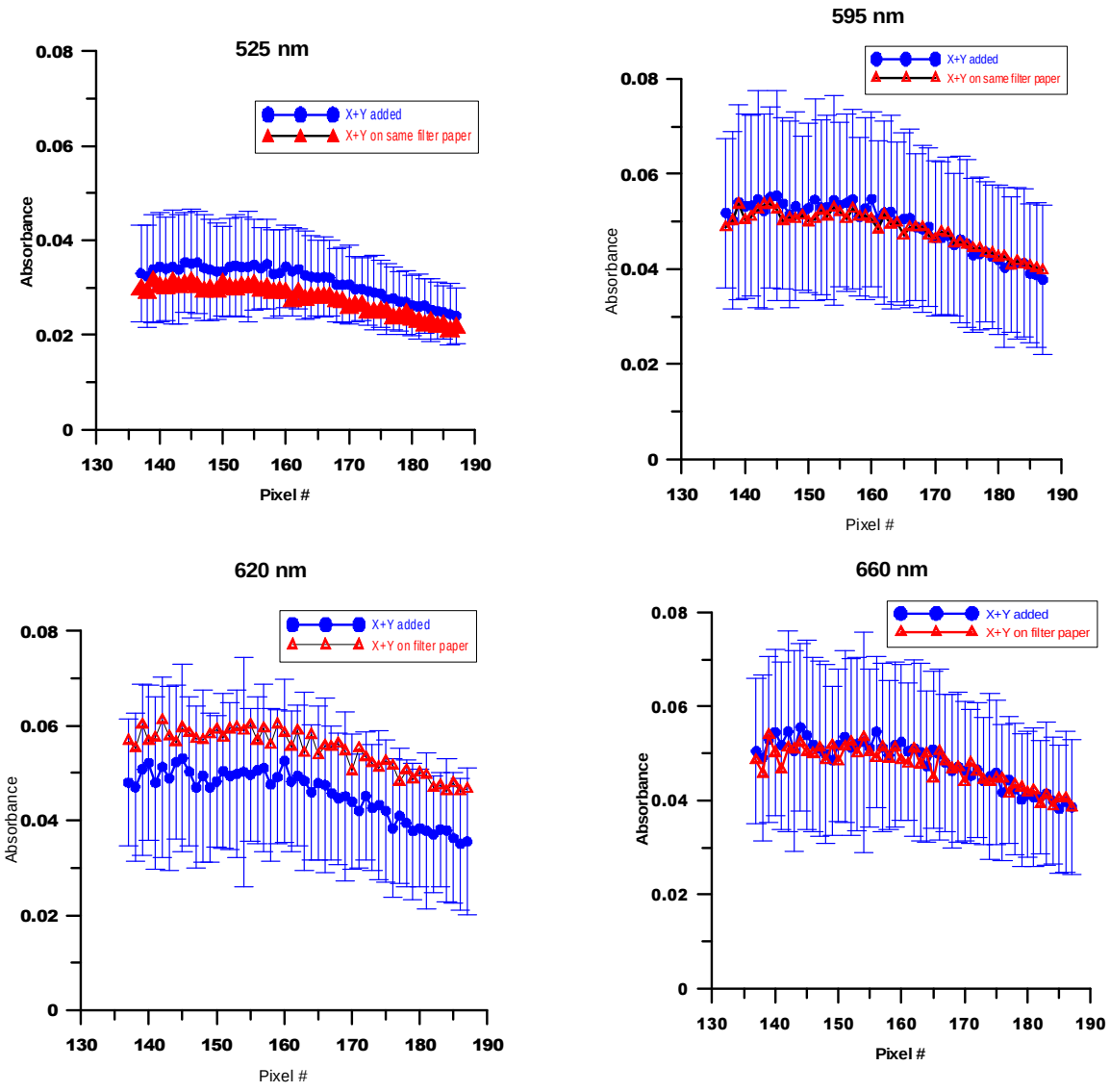

Figure A.16 Standard deviation graphs: X (0.01mM MG) and Y (0.01mM MB+0.1 mM NaCl) taken on different filter papers and {X (0.01mM MG) + Y (0.01mM MB+0.1 mM NaCl)} taken on the same filter paper.

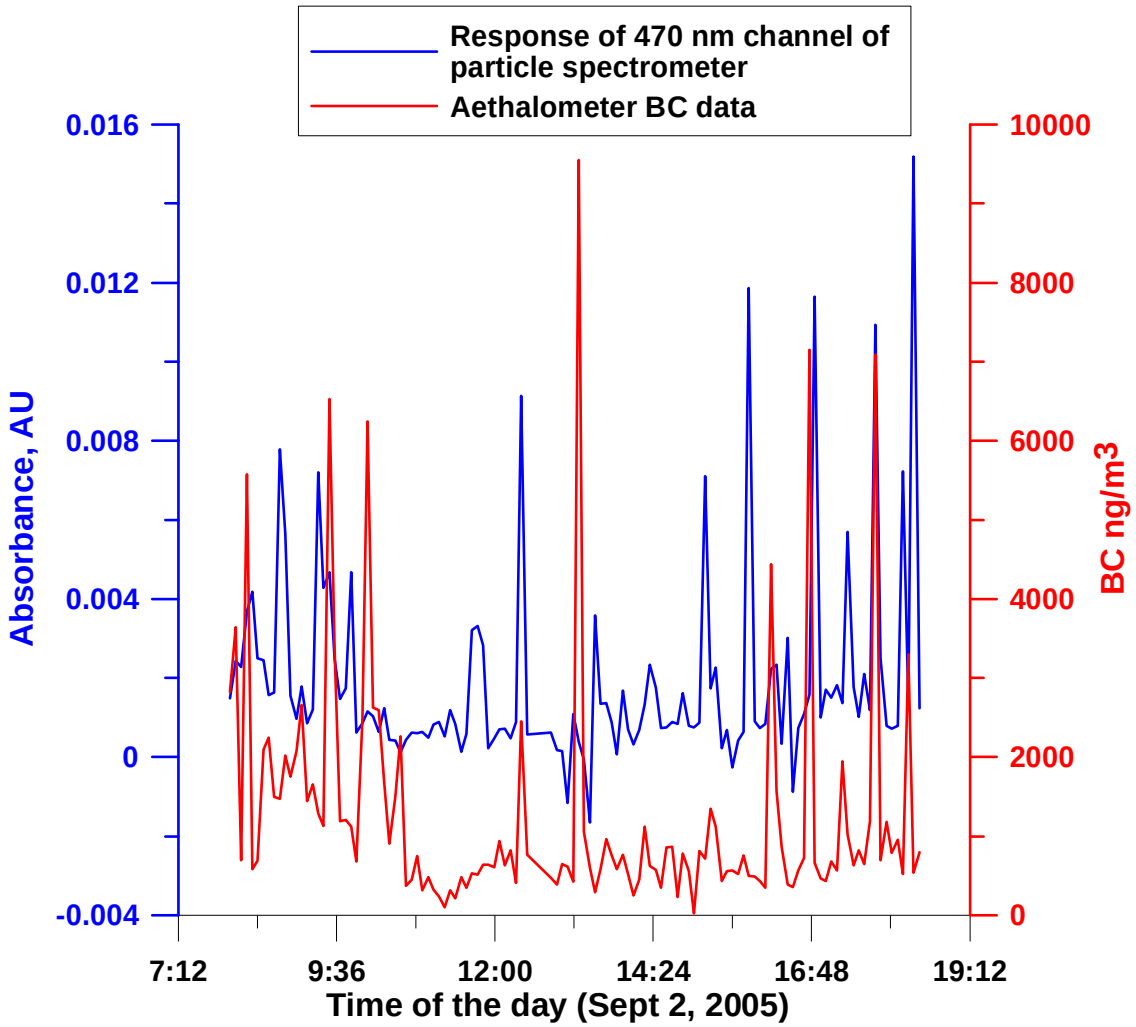

Figure A.17 Ambient BC measurement data (September 2, 2005, Lubbock downtown city bus station, Lubbock, Texas) as observed with particle spectrometer (blue trace) vis-à-vis commercial aethalometer (red trace).

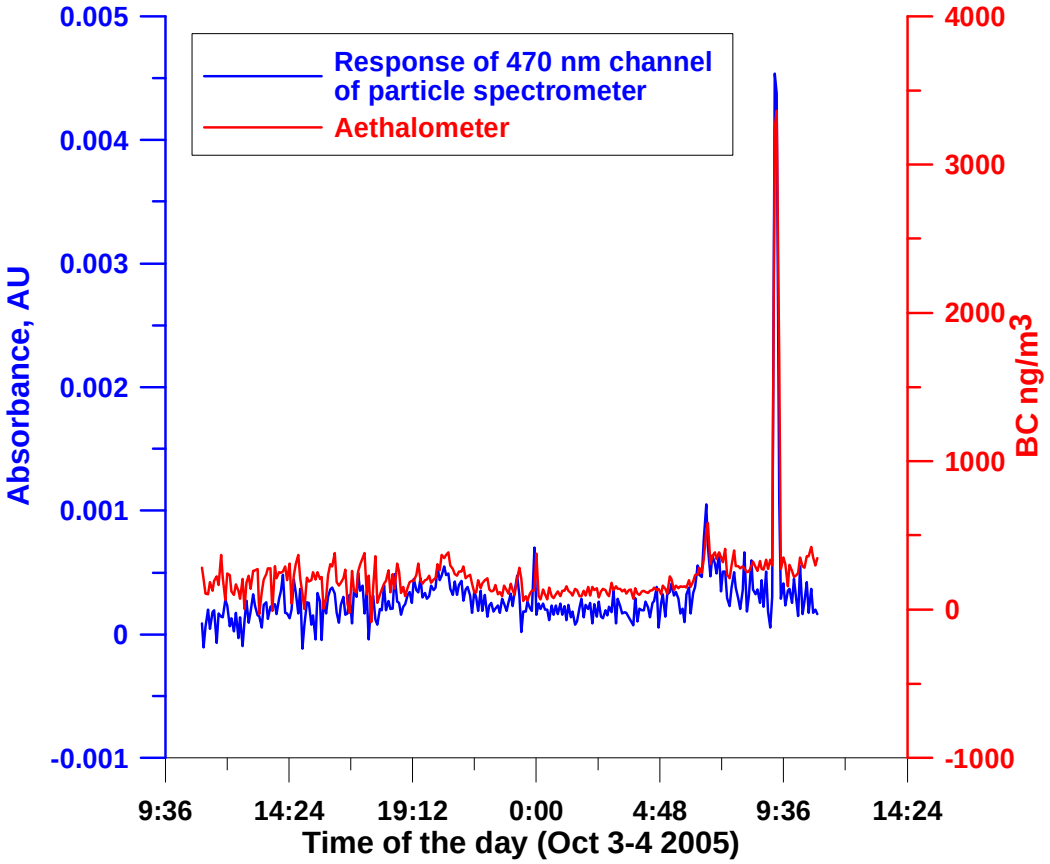

Figure A.18 24 hours ambient BC measurement data (October 3-4, 2005, Texas Tech University Chemistry Department Building, Lubbock, Texas; 5 minute resolution, 470 nm channel data) as observed with particle spectrometer (blue trace) vis-à-vis commercial aethalometer (red trace).

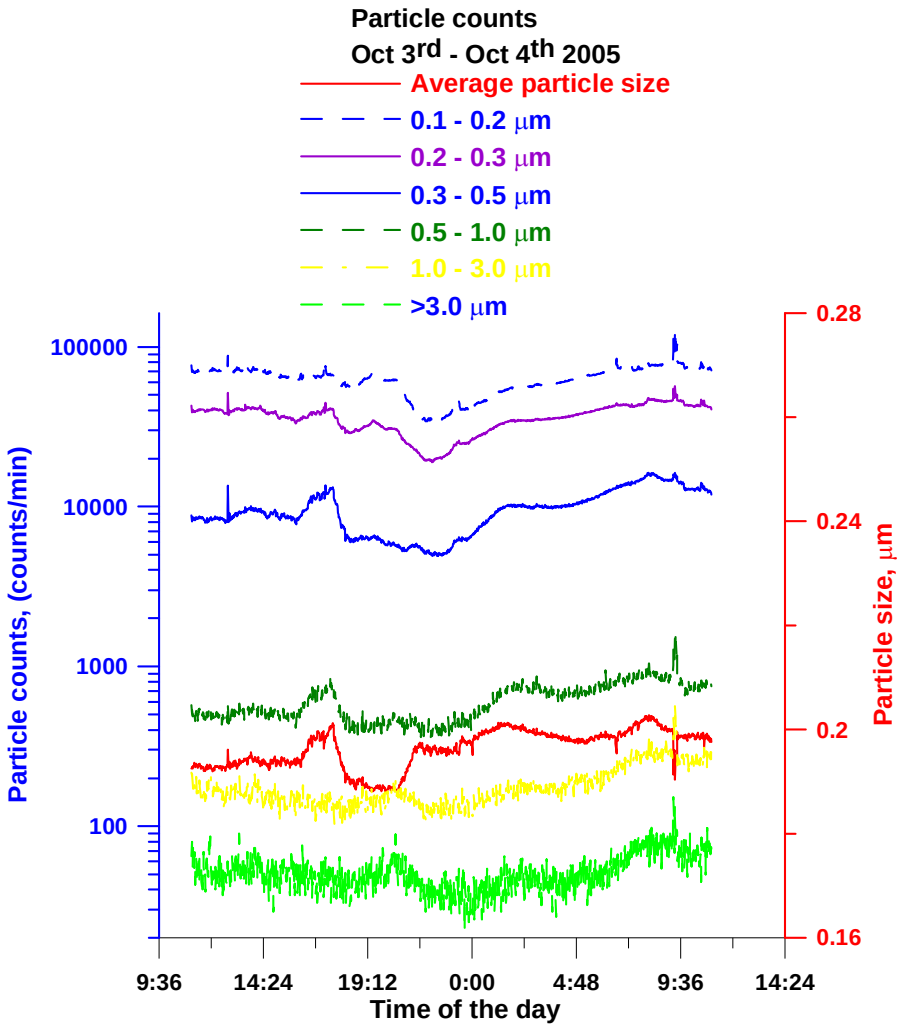

Figure A.19 Laser particle counter data from Oct 3-4, 2005 and average particle size data.

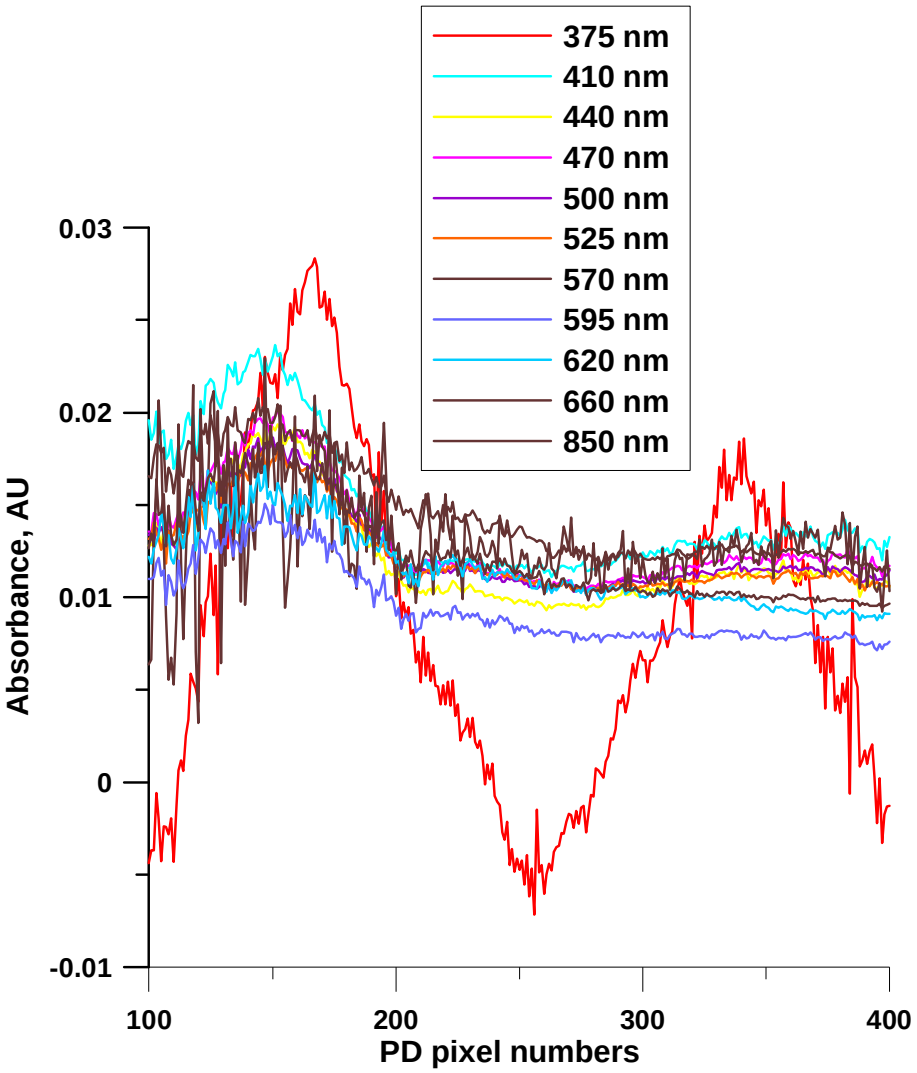

Figure A.20 Absorbance spectra from particle spectrometer (after 3 hours of particle collection on its filter tape).

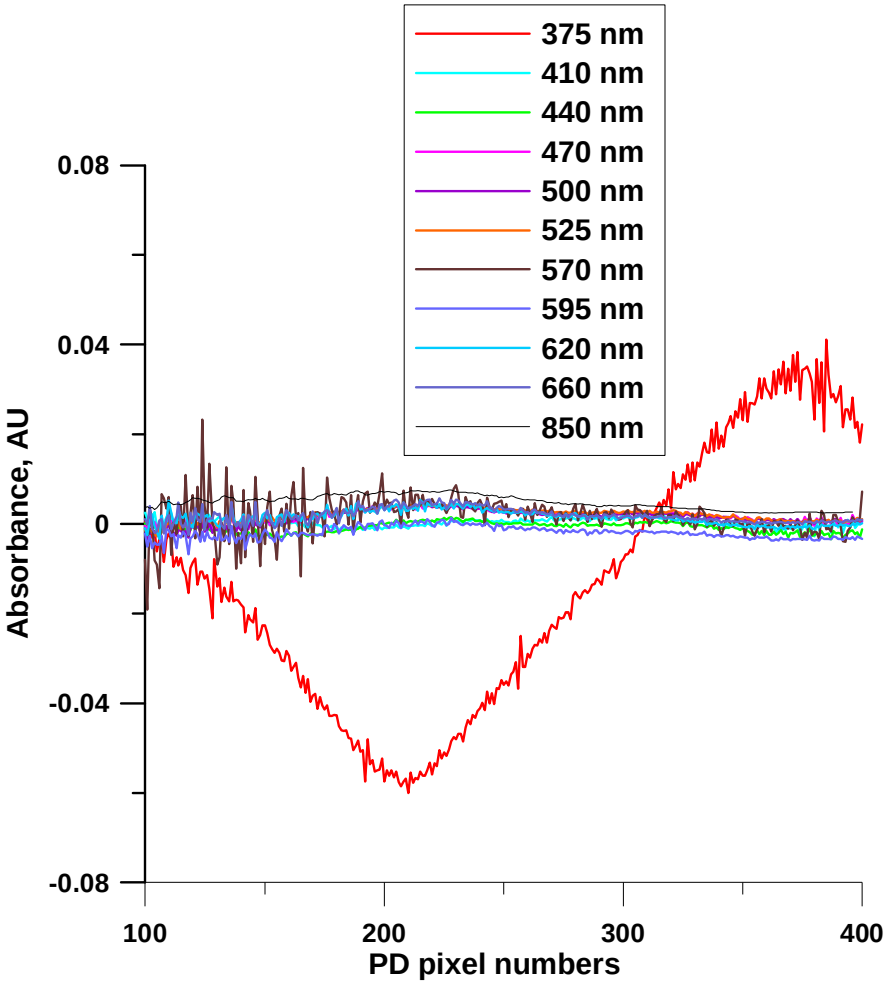

Figure A.21 Absorbance spectra from particle spectrometer when quartz filter tape was placed before particle spectrometer. (After 3 hours of particle collection just before the particle spectrometer).

APPENDIX B

SEMI-CONTINUOUS AUTOMATED MEASUREMENT OF ORGANIC CARBON IN ATMOSPHERIC AEROSOL SAMPLES

Table B.1 Manufacturer's characterization data for N231 Carbon Black (www.sidrich.com)

BET Nitrogen Surface Area	114.6 m^2/g
Iodine No.	127
Volatiles	0.6%
Moisture	0.9%
pH of slurry	9.8
%C	97.61
%S	1.61
%O	0.667
%N	0.102
%H	0.02
N2SA	114.6

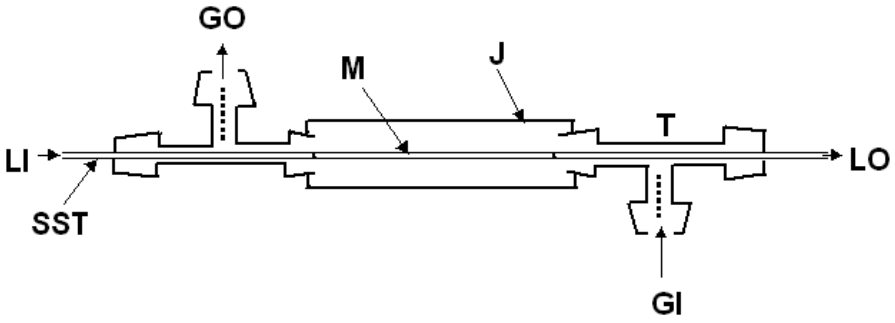

Figure B.1 Conductivity-based CO_2 sensor.

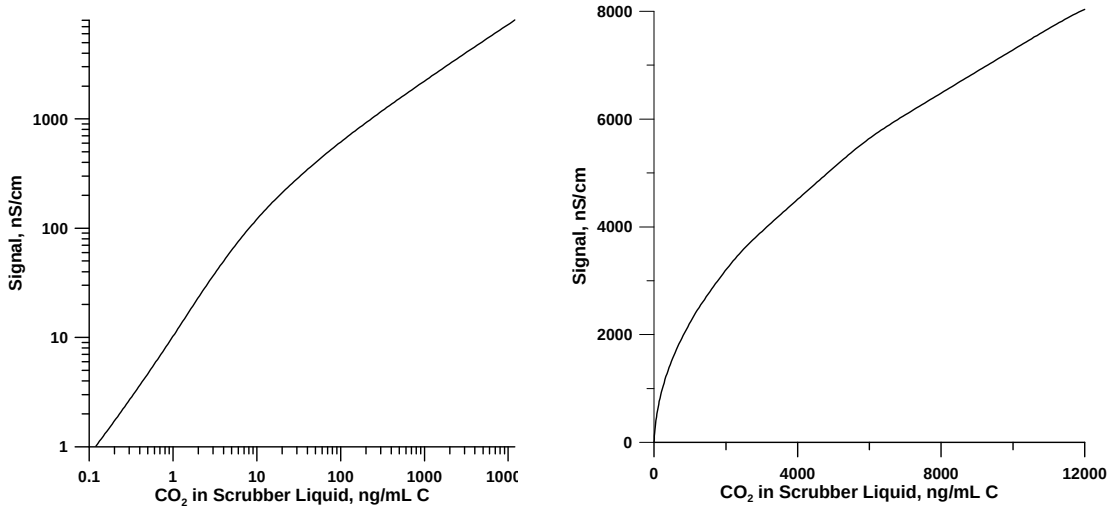

Figure B.2 Conductivity increase as CO_2 concentration in a pure water absorber is increased from 0.01 to 1000 µM C. The left plot has logarithmic abscissa and ordinate that shows how the slope over a large range changes; the right plot in linear scaling more clearly shows how the slope changes rather dramatically in the very beginning.

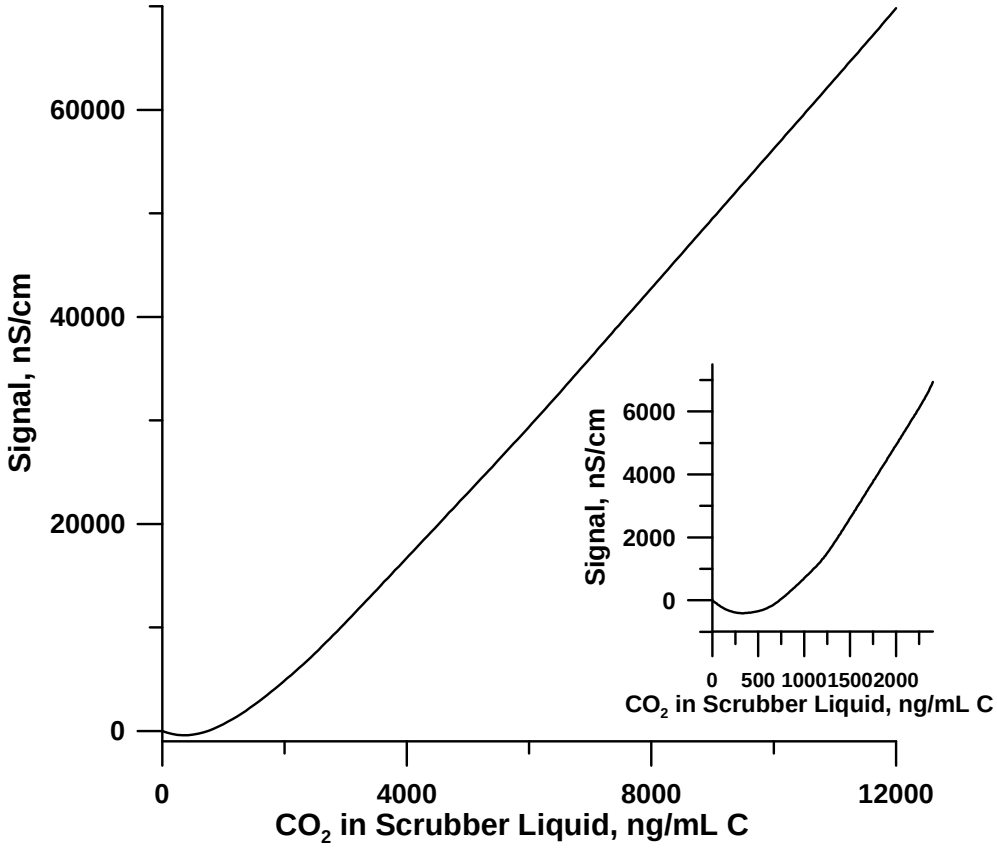

Figure B.3 Conductivity increase as CO_2 concentration in a 5 mM Tris absorber is increased from 0.01 to 1000 µM C. The main plot indicates that while the slope is linear and invariant after ca. 1500 ng/mL C as CO_2 has dissolved, the inset shows that in the very beginning the signal is actually negative and over a concentration range of ca. 0-750 ng/mL C as CO_2, the signal is not a single valued function of the dissolved CO_2 concentration.

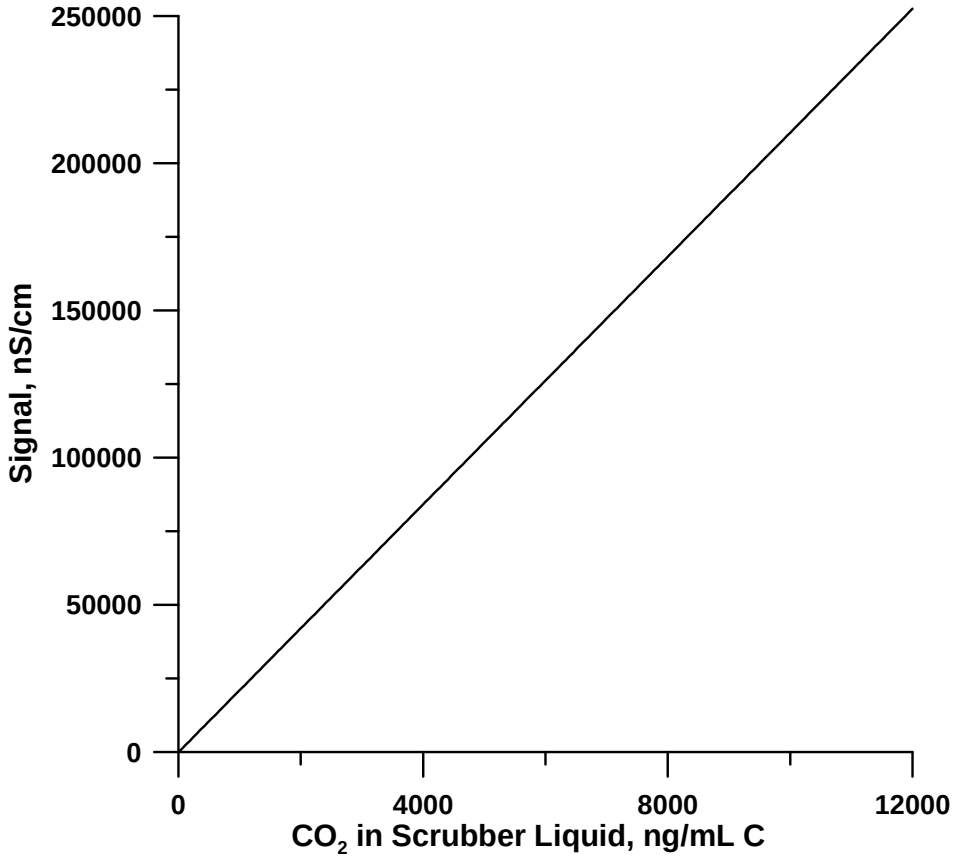

Figure B.4 The signal in an alkali hydroxide absorber is negative (shown here with sign inversion) and highly linear over an extended rage. Calculations were carried out for a 5 mM LiOH solution but the conductivity change (signal) will be the same for any strong base asthe signal is essentially proportional to ($\lambda_{Carbonate}$ - $\lambda_{Hydroxide}$) where λ_i is the equivalent conductance of ion *i*, 72 and 198.6 µS/cm / eq/L, respectively.

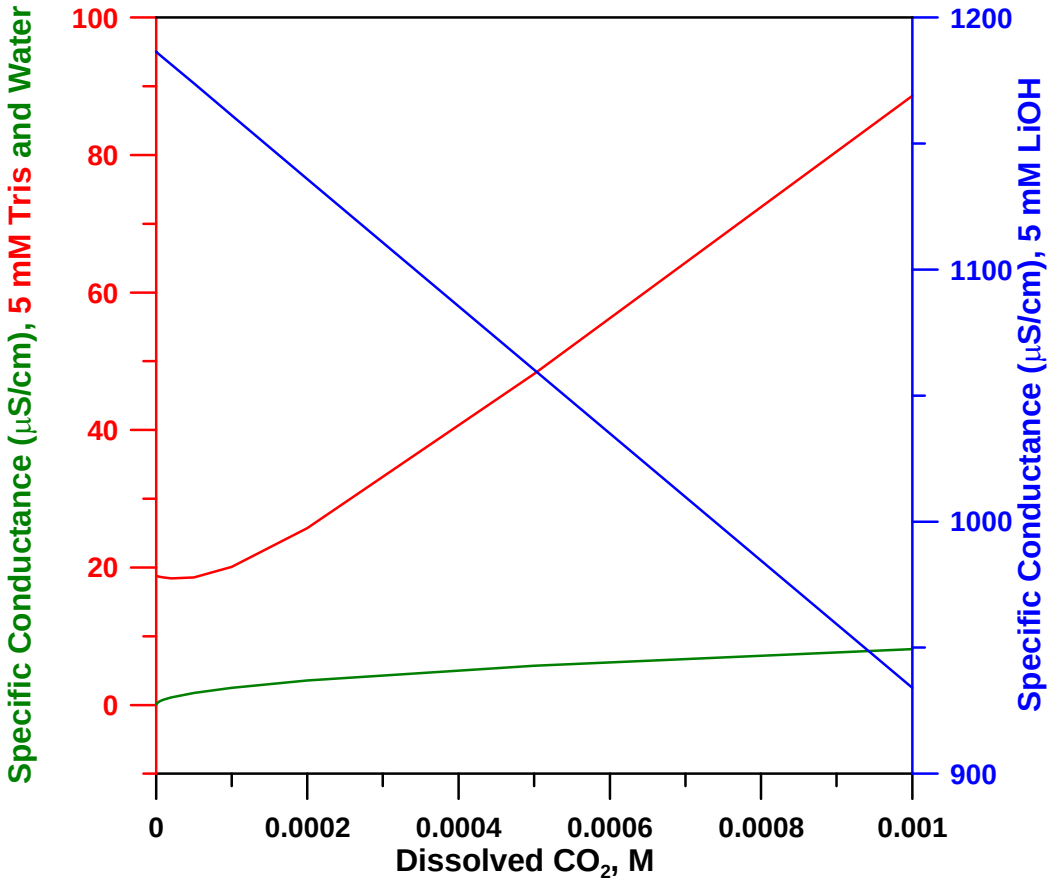

Figure B.5 Composite picture of relative change in signal with three different absorbers.

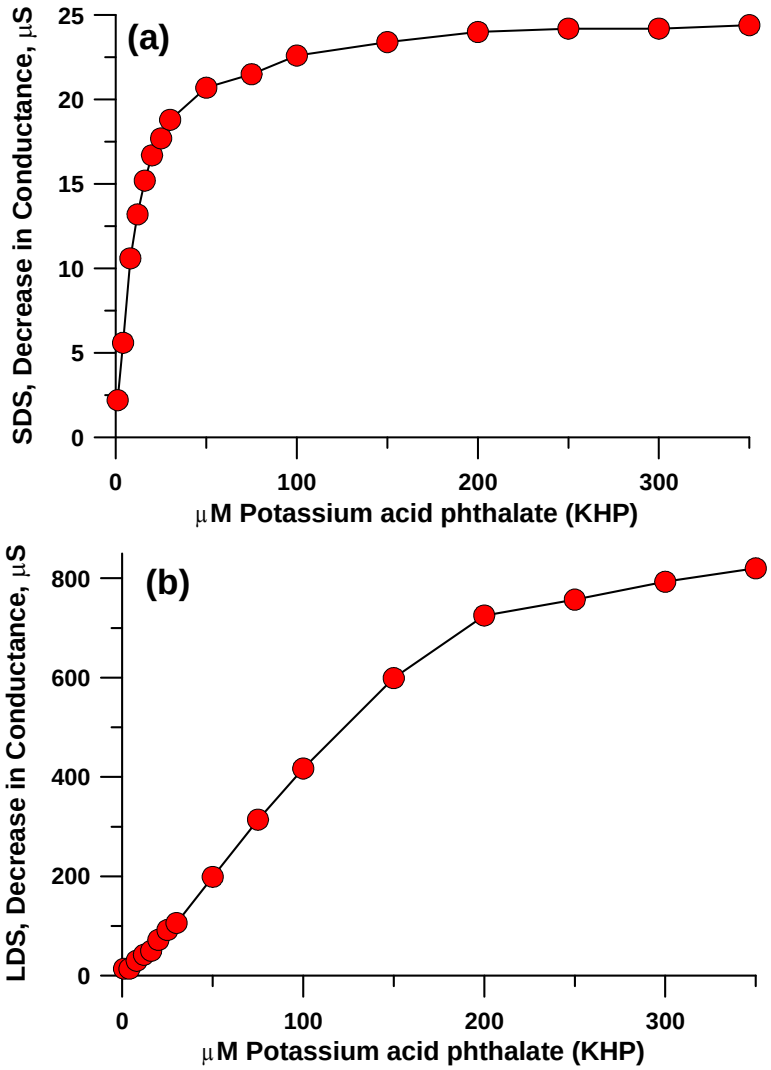

Figure B.6 (a) Short sensor calibration behavior (b) The long sensor contains 150 mM LiOH and is 20 mm long and 0.6 mm in i.d. The active zone thus contains ~0.85 µmole LiOH. The sample volume is 3.8 mL, The maximum linear range is about 200 µM KHP or 1.6 mM C that translates to ~6 µmol C.

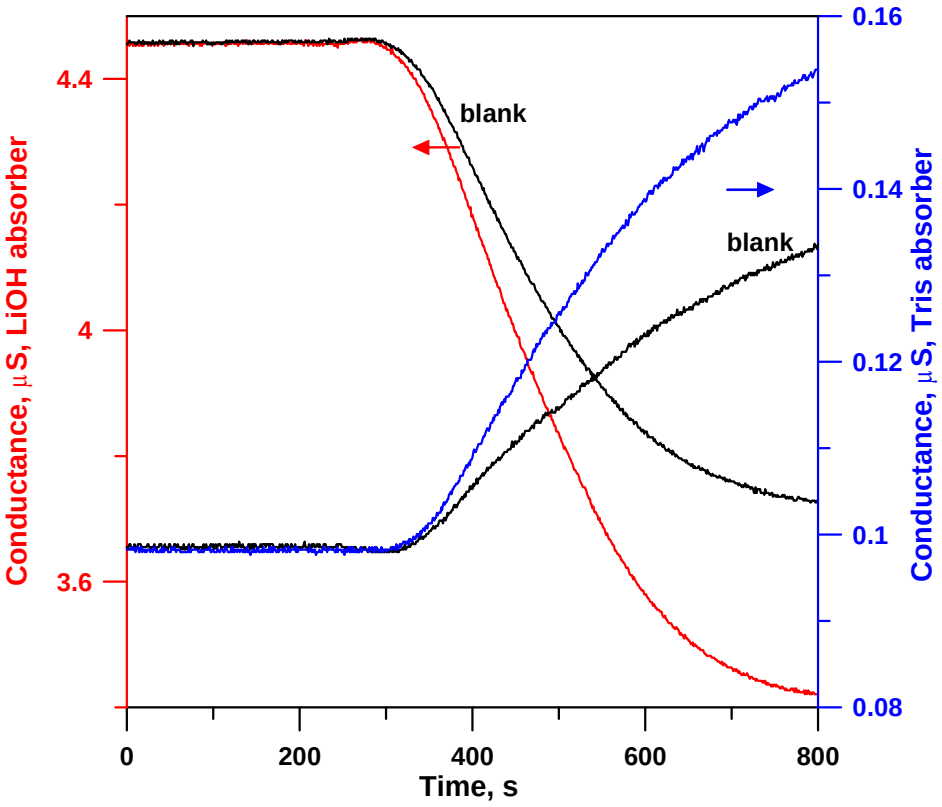

Figure B.7 Experimental response to blank and a 3 µM KHP sample (total 1.1 µg C) is shown both for a 5 mM LiOH absorber and a 5 mM Tris absorber for the SDS. .

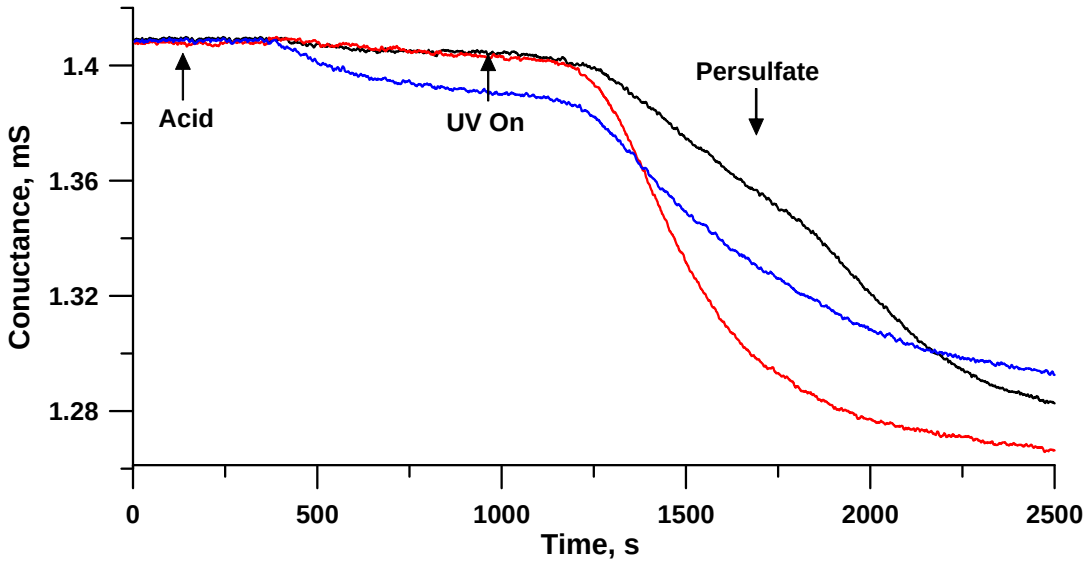

Figure B.8 Illustrative multi-step CO_2 evolution. Acid is first added to liberate CO_2 from inorganic carbonates, then the UV lamp is turned on in the presence of oxygen and finally persulfate is added. The oxidation is not completed in the timeframe shown.

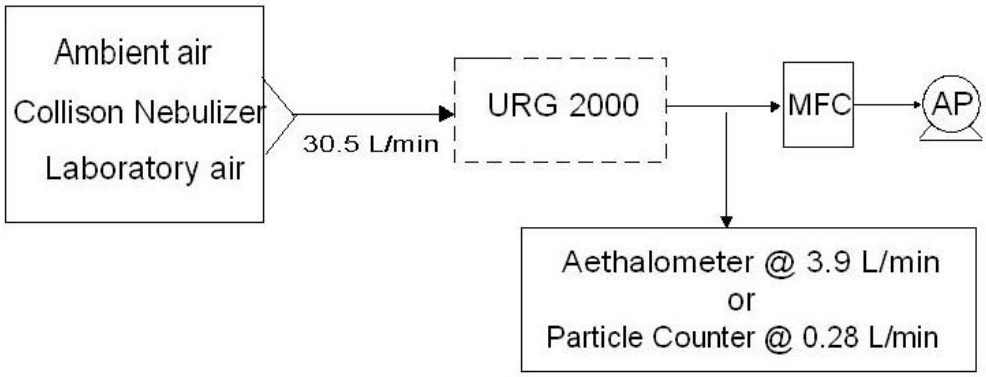

Figure B.9 Test arrangement for URG 2000 cyclone removal efficiency. Ambient air, laboratory air or diluted Collison nebulizer output is sampled at a total flow rate of 30.5 L/min directly or via the cyclone by air pump AP via mass flow controller MFC. With the URG 2000 in place, the post cyclone stream is sampled at 3.9 L/min.

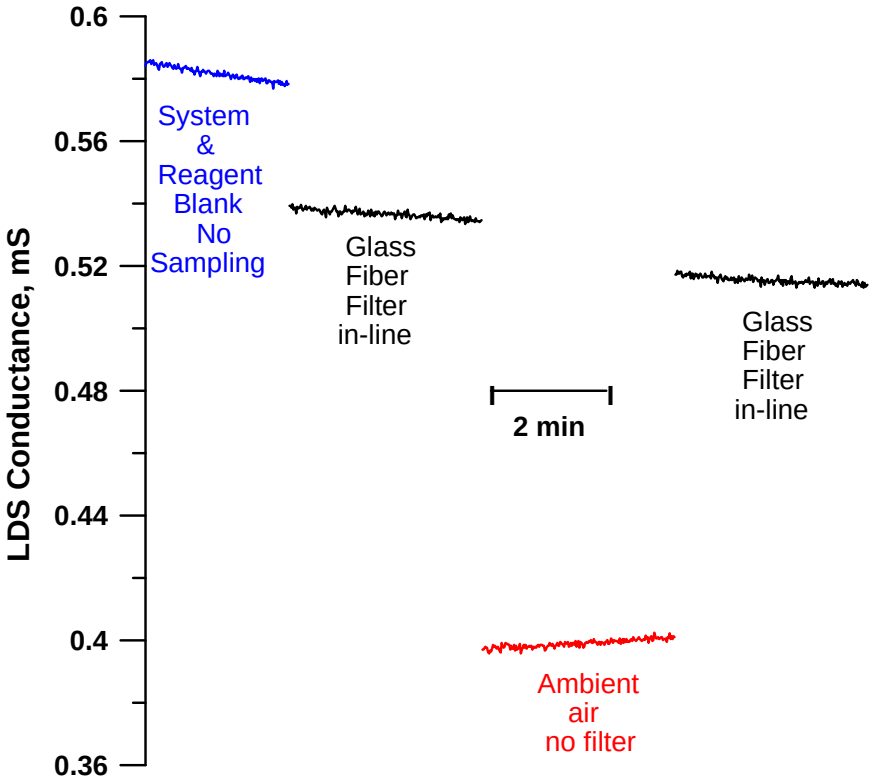

Figure B.10 The last few minutes of the 20 min oxidation/measurement run is shown in four sequential experiments with a freshly cleaned system (1) reagent and system blank, (2) Tissuquartz filter in line, responding to gaseous C, mostly CO_2, (3) Ambient air without filter (4) filter put back on line.

Table B.2 Compounds tested for response

1	(Mallinckrodt)
2	Ethylenediamine dihydrochloride (Acros)
3	Aniline hydrochloride (J. T. Baker)
4	Alanine (Aldrich)
5	Caffeine (Aldrich)
6	Cysteine (Acros)
7	4-Amino-1-naphthalenesulfonic sodium salt (Aldrich)
8	Monochloroacetic acid(Aldrich)
9	*p*-chlorophenol (Eastman)
10	Sodium methanesulfonate (Aldrich)
11	Sodium naphthalenesulfonate (Aldrich)
12	Potassium hydrogen phthalate (KHP, Matheson Coleman and Bell)
13	Sodium acetate (Fisher)
14	Tartaric acid (Mallinckrodt)
15	Citric acid (Fluka)
16	Phenol (J. T. Baker)
17	Levoglucosan (Aldrich)
18	Benzene (Aldrich)
19	Toluene (Aldrich)

All were reagent grade or better and used without further purification.

Table B.3 Oxidation rates of various test compounds*

Compounds	Rate constants
KHP	5.54×10^{-3} s^{-1}
4-Chlorophenol	5.68×10^{-3} s^{-1}
Alanine	5.78×10^{-3} s^{-1}
4-Amino-1-naphthalenesulfonic acid sodium salt	3.33×10^{-3} s^{-1}
Aniline hydrochloride	5.07×10^{-3} s^{-1}
Caffeine	3.48×10^{-3} s^{-1}
Chloroacetic acid	6.22×10^{-3} s^{-1}
Cysteine	4.99×10^{-3} s^{-1}
Ethylenediamine dihydrochloride	3.51×10^{-3} s^{-1}
Glucose	5.56×10^{-3} s^{-1}
Methanesulfonic acid, sodium salt	5.16×10^{-3} s^{-1}
1-Naphthalenesulfonic acid, sodium salt	5.25×10^{-3} s^{-1}

*All follow a first order rate between 300-500 s as in Figure 3.2. The rate constants were calculated beginning at t = 300 s. In all cases, r^2 for the first order fit exceeded 0.99.

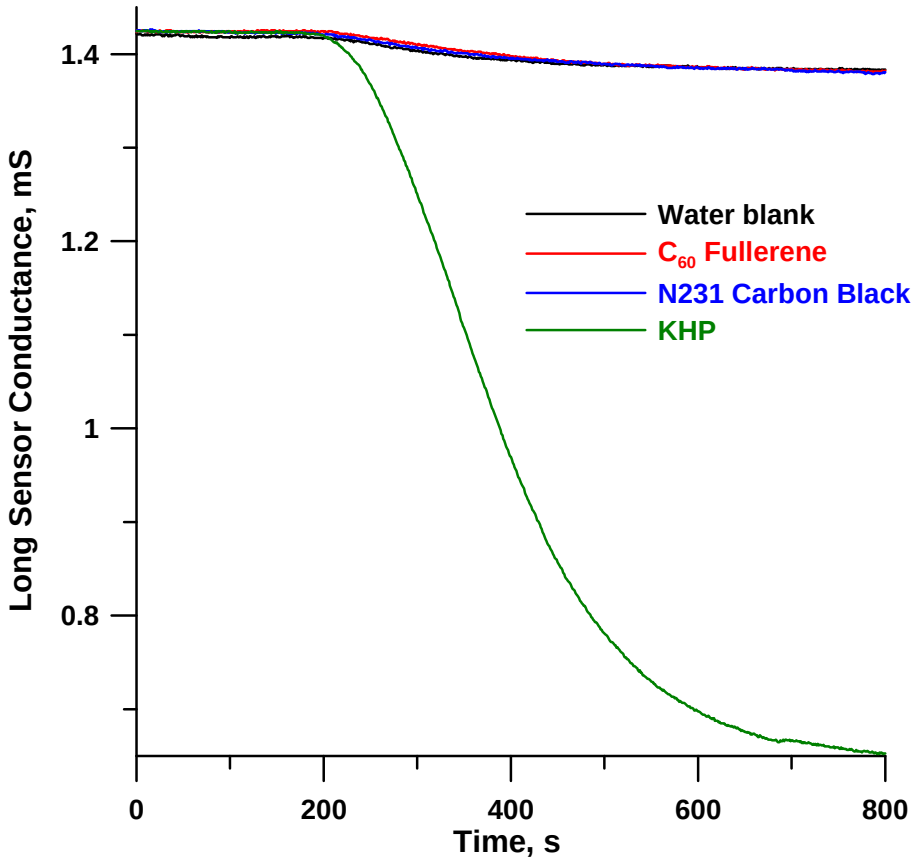

Figure B.11 The solids were prepared as slurries (1 mg/mL) in water by ultrasonication. A 75 µL aliquot was directly introduced into the reactor immediately after ultrasonication by momentarily removing the CO_2 exit line.

Back Trajectories for periods of OC Excursion

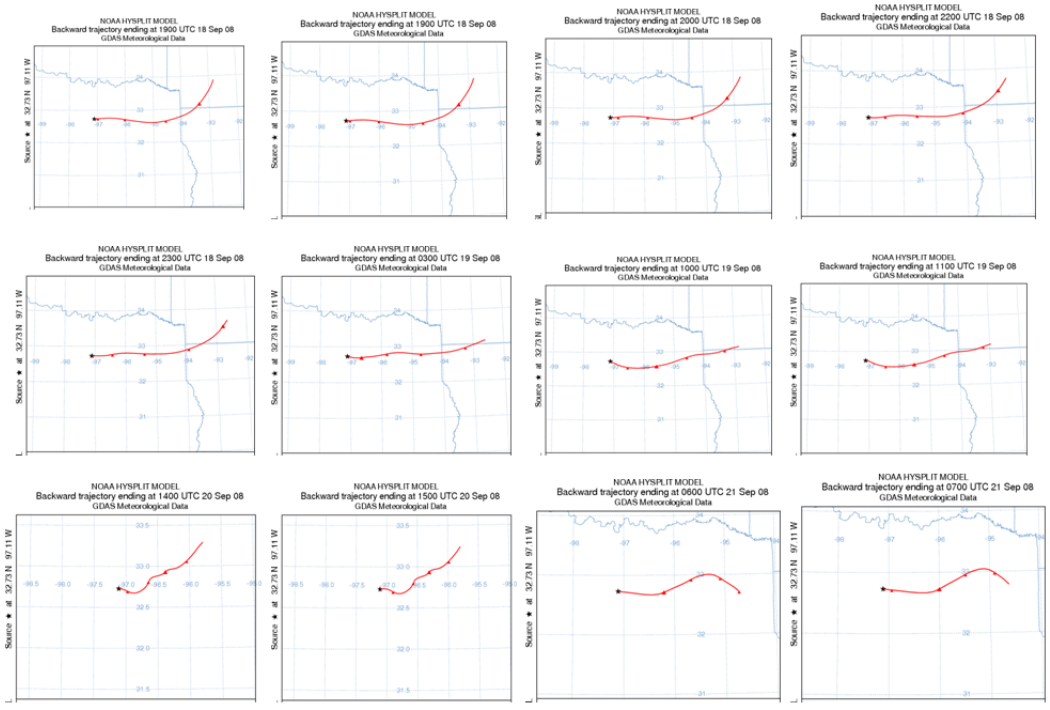

Figure B.12 24-hour Back trajectories for periods of high OC excursion from the NOAA HYSPLIT model (www.arl.noaa.gov/HYSPLIT.php).

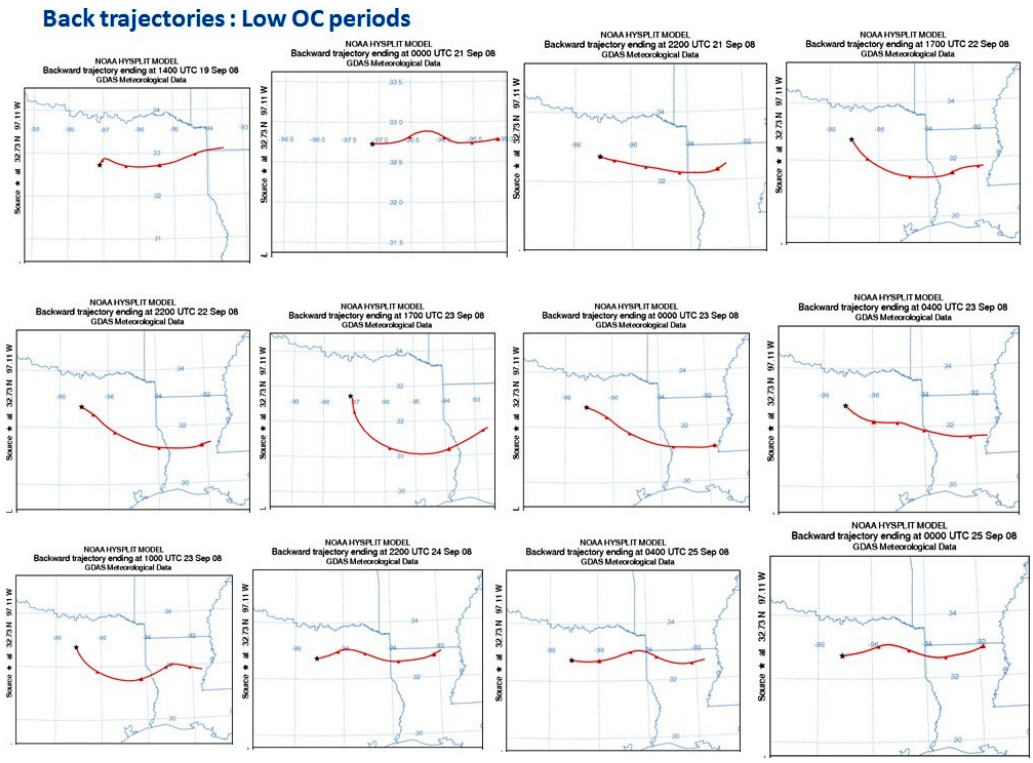

Figure B.13 24-hour Back trajectories for a sampling of periods of low OC from the NOAA HYSPLIT model (www.arl.noaa.gov/HYSPLIT.php).

REFERENCES

1. Orton, J. *The Story of Semiconductors*, 2nd Edition, Oxford University Press. 2006; pp 22.
2. Arpad, B.; Craford, G.; Duggal, A.; Haitz, R. *Phys. Today* **2001**, *54*, 42-47.
3. Schubert, E.; Kim, J. *Science*, **2005**, *308*, 1274-1278.
4. U.S. Environmental Protection Agency. *Particulate Matter*. http://www.epa.gov/air/particlepollution/ (accessed October 4, 2011).
5. Flaschka, H.; McKeithan, C.; Barnes, R. *Anal. Lett*. **1973**, *6*, 585-594.
6. Dasgupta, P.K.; Eom, I.; Morris, K.J.; Li, J. *Anal. Chim. Acta* **2003***, 500*, 337–364.
7. Li, J.; Dasgupta, P. K. *Anal. Chem*. **2000**, *72*, 5338-5447.
8. Li, J.; Dasgupta, P. K.; Zhang, G.; Hutterli, M. A. *Field Anal. Chem. Technol.* **2001**, *5*, 2-11.
9. Hinds, W.C. *Aerosol Technology*, 2nd Edition, Wiley-Interscience, 1982; pp 1-9.
10. Colbeck. I. *Environmental Chemistry of Aerosols,* 1st Edition, Blackwell Publishing, 2008, pp 1.
11. Lewis, E. R.; Schwartz, S. E. *Sea Salt Aerosol Production: Mechanisms, Methods, Measurements and Models – A Critical Review*, Geophysical Monograph Series, 2004, 152, 1, pp 1-7.
12. Levin, Z.; Cottobn, W. R. *Aerosol Pollution Impact on Precipitation: A Scientific Review*, 1st Edition, Springer, 2008, pp 52-53.
13. Katrinak, K. A.; Rez, P.; Buseck, P. R. *Environ. Sci. Technol.* **1992**, *26*, 1967–1976.
14. Schauer, J. J.; Mader, B. T.; DeMinter, J. T.; Heidmann, G.; Bae, M. S.; Seinfeld, J. H.; Flagan, R. C.; Cary, R. A.; Smith, D.; Huebert, B. J.; Bertram, T; Howell S.; Kilen, J. T.;

Qinn, P.; Bates, T.; Turpin, B.; Lim, H. J.; Yu, J. Z.; Yang, H.; Keywood, M. D. *Environ. Sci. Technol.*, **2003**, *37*, 993-1001.

15. Yu, X-Y. Measurements of Carbonaceous Aerosols Using Semi-Continuous Thermo-Optical Method; Integrated Waste Management; Volume 1 http://www.intechopen.com/source/pdfs/17453/InTech-Measurements_of_carbonaceous_aerosols_using_semi_continuous_thermal_optical_method.pdf (accessed October 4, 2011).
16. Grieshop, A. P.; Logue, J. M.; Donahue, N. M.; Robinson, A. L. *Atmos. Chem. Phys*. **2009**, *9*, 1263–1277
17. Levin, Z.; Cotton, W. *Aerosol Pollution Impact on Precipitation: A Scientific Review*, 1st Edition, Springer, 2008, pp 53-55.
18. Mikel, D. K. Nano particle/Ultrafine Monitoring State of the Science; NAAMC Nov. 3-5, 2009. United States Environmental Protection Agency OAQPS http://www.epa.gov/ttnamti1/files/2009conference/MikelNanoparticle.pdf (accessed October 4, 2011).
19. Hinds, W.C. *Aerosol Technology*, 2nd Edition, Wiley-Interscience, 1982, pp 49-51.
20. United States Environmental Protection Agency; Research; Clean Air Research Program; Particulate Matter (PM) Research. http://www.epa.gov/airscience/quick-finder/particulate-matter.htm#3 (accessed October 4, 2011).
21. Ultrafine Particles. Characterization of ultrafine particles. University of Minnesota; Fall Semester 2003; PUBH 5103: Exposure to Environmental Hazards. http://web.archive.org/web/20070624021138/http://enhs.umn.edu/5103/particles/character.html (accessed October 4, 2011).
22. Whitby, K. T.; Svendrup, G. M. *Env. Health Persp*. **1980**, *10*, 477-517.
23. Geller, M. D.; Kim, S.; Misra, C.; Sioutas, C, Olson, B. A.; Marple, V. A. *Aerosol Sci. Technol.* **2002**, *36*, 748-762.

24. United States Environmental protection Agency. Region 4. Lab and Field Operations. PM 2.5 Lab. Objectives and History. http://www.epa.gov/region4/sesd/pm25/p2.html (accessed on October 4, 2011).

25. Lave, L. B.; Seskin, E. P. *J. Am. Stat Assoc.* **1973**, *68*, 284-290.

26. Pope, C. A.; Burnett, R. T.; Thun, M. J.; Calle, E. E.; Krewski, D.; Ito, K.; Thurston, G. D. *J. Amer. Med. Assoc.* **2002**, *287*, 1132–1141.

27. Nawrot, T. S.; Perez, L.; Kunzil, N.; Munters, E.; Nemery, B. *Lancet*, **2011**, *377*, 732 - 740.

28. United States Environmental Protection Agency. How Air Pollution Affects the View http://www.epa.gov/visibility/pdfs/haze_brochure_20060426.pdf (accessed October 4, 2011).

29. Wang, W.; Liu, H.; Yue, X.; Li, H.; Chen, J.; Ren, L.; Tang, D.; Hatakeyama, S.; Takami, A. *J. Geophys. Res.*, **2006**, *111*, D18207.

30. Mendelsohn, R.; Shea, B. G. A Case Study of Effects of Acidic Air Pollutants on Crop Yields. United States Environmental Protection Agency. http://yosemite.epa.gov/ee/epa/eerm.nsf/vwAN/EE-0160-01.pdf/$file/EE-0160-01.pdf (accessed October 4, 2011).

31. Yu, H.; Kaufman, Y. J.; Chin, M.; Feingold, G.; Remer, L. A.; Anderson, T. L.; Balkanski, Y.; Bellouin, N.; Boucher, O.; Christopher, S.; DeCola, P.; Kahn, R.; Koch, D.; Loeb, N.; Reddy, M. S.; Schulz, M.; Takemura, T.; Zhou, M. *Atmos. Chem. Phys.* **2006,** *6*, 613-666.

32. Prodi, V.; Giacomelli, G. M.; Morigi, M. P.; Volta, C.; Marani, F. D.; Kenny, L. *Physica Medica*, **1993,** *9*, 129-131.

33. Prodi, V.; Melandri, C.; Tarroni, G.; Dezaiacomo, T.; Formignani, M. *J. Aerosol Sci.* **1979,** *10*, 411-419.

34. Belosi, F.; Prodi, V. *J. Aerosol Sci.* **1984,** *15*, 382-385.

35. Leslie, A. C. D.; Kaufmann, H. C.; Prodi, V. *Nucl. Instrum. Meth. B,* **1984,** *3*, 436-440.

36. Prodi, V.; Belosi, F.; Mularoni, A.; Lucialli, P. *Am. Ind. Hyg. Assoc. J.* **1988,** *49*, 75-80.

37. McMurry, P. H. *Atmos. Environ.* **2000,** *34*,1959-1999.

38. Hansen, A. D. A.; Rosen, H.; Novakov, T. *Sci. Total Environ.* **1984,** *36*, 191-196.

39. Andreae, M. O.; Gelencser, A. *Atmos. Chem. Phys.* **2006,** *6*, 3131-3148.

40. Lawless, P. A.; Rodes, C. E.; Ensor, D. S. *Atmos. Environ.* **2004,** *38*, 3373-3383.

41. Bahner, M. A.; Weitz, K. A.; Zapata, A. RTI International; DeAngelo, B. United States Environmental Protection Agency. Use of Black Carbon and Organic Carbon Inventories for Projections and Mitigation Analysis. http://www.epa.gov/ttnchie1/conference/ei16/session3/k.weitz.pdf (accessed on October 4, 2011).

42. Rao, V.; Somers, J. H. United State Environmental Protection Agency. Black Carbon as a Short-Lived Climate Forcer: A Profile of Emission Sources and Co-Emitted Pollutants. http://www.epa.gov/ttnchie1/conference/ei19/session5/rao.pdf (accessed on October 4, 2011).

43. Gong, H.; Linn, W. S.; Clark, K. W.; Anderson, K. R.; Sioutas, C.; Alexis, N. E.; Cascio, W. E.; Devlin, R. B. *Inhalation Toxicol.* **2008,** *20* (6), 533-545.

44. Smith, J. T. *BMC Public Health,* **2007,** *7,* 49.

45. Billet, S.; Garcon, G.; Dagher, Z.; Verdin, A.; Ledoux, F.; Cazier, F.; Courcot, D.; Aboukais, A.; Shirali, P. *Environ. Res.* **2007,** *105*, 212-223.

46. Kenny, L. C.; Aitken, R.; Chalmers, C.; Fabries, J. F.; GonzalezFernandez, E.; Kromhout, H.; Liden, G.; Mark, D.; Riediger, G.; Prodi, V. *Ann. Occup. Hyg.* **1997,** *41*, 135-153.

47. Arimoto, R.; Balsam, W.; Schloesslin, C. *Atmos. Environ.* **2002,** *36*, 89-96.

48. Rossel, R. A. V.; Chen, C. *Remote Sens. Environ.* **2011,** *115*, 1443-1455.

49. Fialho, P.; Hansen, A. D. A.; Honrath, R. E. *J. Aerosol Sci.* **2005,** *36*, 267-282.

50. Particle Instruments. Model 3450 Vibrating Orifice Aerosol Generator, TSI, P/N 1930086 Rev. A.

http://www.tsi.com/uploadedFiles/Product_Information/Literature/Spec_Sheets/3450VibOr1930086RevA.pdf (accessed on October 4, 2011)

51. Environmental Impact Analysis: Gas vs. Diesel in Light-duty Highway Applications in the U.S. Marz, L. C. October 2007, Revised December 2010 http://webpages.charter.net/lmarz/Diesel.pdf (accessed on October 4, 2011)
52. Weingartner, E.; Saathoff, H.; Schnaiter, M.; Streit, N.; Bitnar, B.; Baltensperger, U. *J. Aerosol Sci.* **2003,** *34*, 1445-1463.
53. Shah, J. J.; Johnson, R. L.; Heyerdahl, E. K.; Huntzicker, J. J. *J. Air Poll. Contr. Assoc.* **1986,** *36*, 254- 257.
54. Gray, H. A.; Cass, G. R.; Huntzicker, J. J.; Heyerdahl, E. K.; Rau, J. A. *Environ. Sci. Technol.* **1986,** *20*, 580-589.
55. Offenberg, J. H.; Baker, J. E. *Atmos. Environ.* **2000,** *34*, 1509-1517.
56. Molnár, A.; Mészáros, E.; Hansson, H. C.; Karlsson, H.; Gelencsér, A.; Kiss, G.Y.; Krivácsy, Z. *Atmos. Environ.* **1999,** *33*, 2745-2750.
57. Chow, J. C.; Watson, J. G.; Doraiswamy, P.; Chen, L-W. A.; Sodeman, D. A.; Lowenthal, D. H.; Park, K.; Arnott, W. P.; Motallebi, N. *Atmos. Res.* **2009,** *93*, 874-887.
58. Prather, K. A.; Hatch, C. D.; Grassian, V. H. *Annu. Rev. Anal. Chem.* **2008**, *1,* 485-514.
59. Williams, B. J.; Goldstein, A. H.; Kreisberg, N. M.; Hering, S. V. *Aerosol Sci. Technol.* **2006,** *40*, 627-638.
60. Tanner, R. L.; Gaffney, J. S.; Phillips, M. F. *Anal. Chem.* **1982,** *54*, 1627-1630.
61. Turpin, B. J.; Cary, R. A.; Huntzicker, J. J. *Aerosol Sci. Technol.* **1990,** *12*, 161-171.
62. Turpin, B. J.; Huntzicker, J. J.; Adams, K. M. *Atmos. Environ.* **1990,** *24A*, 1831-1836.
63. Kim, Y. J.; Kim, M. J.; Lee, K. H.; Park, S. S. *Atmos. Environ.* **2006,** *40,* 4064-4075.
64. Saathoff, H.; Naumann, K. H.; Schnaiter, M.; Schöck, W., Weingartner, E.; Baltensperger, U.; Krämer, L.; Bozoki, Z.; Pöschl, U.; Niessner, R.; Schurath, U. J. *Aerosol Sci.* **2003,** *34*, 1399-1420.

65. National Institute of Occupational Safety and Health. NIOSH Method 5040. Elemental Carbon (Diesel Particulate) NIOSH Manual of Analytical Methods, 4th ed., 1996. http://www.cdc.gov/niosh/nmam/pdfs/5040f3.pdf (accessed October 4, 2011).

66. Yang, H.; Yu, J. Z. *Environ. Sci. Technol.* **2002**, *36*, 5199-5204.

67. Cheng, Y.; He, K. B.; Duan, F. K.; Zheng, M.; Ma, Y. L.; Tan, J. H. *Environ. Int.* **2009,** *35,* 674-681.

68. Jones, A. M.; Harrison, R. M. *Atmos. Environ.* **2005,** *39,* 7114-7126.

69. Ten Brink, H.; Hoek, G.; Khlystov, A. *Atmos. Environ.* **2005,** *39,* 6255-6259.

70. United States Environmental Protection Agency. EPA Method 415.3. Determination of Total Organic Carbon and Specific UV Absorbance at 254 nm in Source Water and Drinking Water. Revision 1.1. February, 2005. http://www.epa.gov/nerlcwww/m_415_3Rev1_1.pdf (accessed October 4, 2011).

71. Bisutti, I.; Hilke, I.; Raessler, M. *Trends Anal. Chem.*, **2004**, 23, 716-726.

72. Visco, G.; Campanella, L.; Nobili, V. *Microchem. J.* **2005,** *79*, 185–191.

73. Tian, K.; Dasgupta, P. K. *Anal. Chim. Acta*, **2009,** *652,* 245-250.

74. American Public Health Association. Standard Methods for the Examination of Water and Wastewater. 2006. Total Organic Carbon. Method 5310C. http://www.standardmethods.org/store/ProductView.cfm?ProductID=38 (last accessed August 20, 2009).

75. Wallace, B.; Purcell, M.; Furlong, J. *J. Environ. Monit.* **2002**, *4*, 35-42.

76. Liang, C. J.; Lin, Y. T.; Shin, W. H. *J. Haz. Mater.* **2009,** *168,* 187-192.

77. Schmidt, M. W. I.; Skjemstad, J. O.; Czimezik, C. I.; Glaser, B.; Prentice, K. M.; Gelinas, Y.; Kuhlbushc, T. A. J. *Global Biogeochem. Cycles* **2001**, *15*, 163-167.

78. Ju, D.; Young, T. M. *Water Res.* **2005,** *39,* 2599–2610.

79. Han, Y. M.; Cao, J. J.; Chow, J. C.; Watson, J. G.; An, Z. S.; Jin, Z. D.; Fung, K.; Liu, S. X. *Chemosphere* **2007,** *69,* 569-574.

80. Arhami, M.; Kuhn, T.; Fine, P. M.; Delfino, R. J.; Sioutas, C. *Environ. Sci. Technol.* **2006**, *40*, 945-954.

81. Olson, D. A.; Norris, G. A. *Atmos. Environ.* **2005,** *39*, 5437-5445.

82. Dasgupta, P. K.; Poruthoor, S. K. *Compr. Anal. Chem. Ser.*, **2002,** *37*, 161-276.

83. Kuban, V.; Dasgupta, P. K. *Talanta*, **1993,** *40,* 831-840.

84. Toda, K.; Yoshioka, K.-I.; Ohira, S.-I.; Li, J. Z.; Dasgupta, P. K. *Anal. Chem*. **2003**, *75*, 4050-4056.

85. Dasgupta, P. K.; Genfa, Z.; Poruthoor, S. K.; Caldwell, S.; Dong, S.; Liu, S.-Y. *Anal. Chem*. **1998,** *70*, 4661-4669.

86. Bender D.; C. Bevilacqua, A. C. Portable Continuous TOC Monitoring in a Semiconductor Water System. http://www.cemag.us/wps/White%20Paper-Portable%20Continuous%20TOC%20Monitoring%20in%20a%20Semiconductor%20Water%20System.pdf (last accessed October 4, 2011).

87. Aubin, D. G.; Abbatt, J. P. D. *J. Phys. Chem. A,* **2007,** *111*, 6263-6273.

88. Samanta, G.; Zhang, S.; Dasgupta, P. K. *PDA J. Pharm. Sci. Technol.* **2003**, *57*, 12-24.

89. Aprile, E.; Curioni, A.; Giboni, K.-L.; Kobayashi, M.; Ni, K.; Oberlack, U. G. *IEEE Trans. Nucl. Sci.* **2003,** *50*, 1303-1308.

90. Dasgupta, P. K. *Comp. Anal. Chem. Ser.* **2002,** *37*, 97-160.

91. Kuban, P.; Berg, J. M. Dasgupta, P. K. *Anal. Chem.* **2004,** *76*, 2561-2567.

92. Li, J. Z.; Li, Q. Y.; Dyke, J. V.; Dasgupta, P. K. *Talanta,* **2008,** *74*, 958-964.

93. Toda, K.; Ohira, S.-I.; Tanaka, T.; Nishimura, T.; Dasgupta, P. K. *Environ. Sci. Technol.* **2004,** *38*, 1529-1536.

94. Glaze, W. H.; Kang, J. W.; Chapin, D. H. *Ozone Sci. Eng.* **1987,** *9*, 335-352.

95. Boring, C. B.; Al-Horr, R.; Genfa, Z.; Dasgupta, P. K.; Martin, M. W.; Smith, W. F. *Anal. Chem.* **2002,** *74,* 1256-1268.

96. Karlsson, A.; Irgum, K.; Hansson, H. C. *J. Aerosol Sci.* **1997**, *28*, 1539-1551.

97. King, M. D.; Thien, B. F.; Tiirikainen, S.; McFarland, A. R. *Aerobiologia,* **2009,** *25*, 239-247.

98. http://www.bgiusa.com/aam/pm25scc.htm (accessed October 4, 2011).

99. Yang, H.; Li, Q. F.; Yu, J. Z. *Atmos. Environ.* **2003,** *37,* 865-870.

BIOGRAPHICAL INFORMATION

The author of this thesis, Shilpa Rashinkar, has obtained her K-12 education at V. G. Vaze College, Mumbai, India. She has been academically oriented student since beginning and participated with full vigor and won awards in various co-curricular and extracurricular activities like dance, drama, fashion shows, athletics and sports. She received her Bachelor of Chemical Technology-Textile Technology (equivalent to Chemical Engineering with specialization in Textile Technology) from Mumbai University Institute of Chemical Technology (MUICT), formerly known as University Department of Chemical Technology (UDCT), the prestigious engineering college in India. She gained her first industrial experience and developed interest for analytical chemistry while working as an intern for Texanlab, a highly recognized textile and analytical laboratory in Thane, India. During her final undergraduate year, she received the award for best oral presentation at national level symposium. She followed her passion for analytical chemistry while working as technical executive trainee and later as an executive in testing and analyzing dyes for its desired application at Clariant India Ltd. She also got managerial experience of handling various facets of research and development lab while working as the manager of products lab at Lanxess India Private Ltd. She later realized the importance of graduate study in professional career and joined the University of Texas at Arlington for her graduate studies. There she conducted research in the development of solid-state light sources based analytical instrumentation for analysis of atmospheric aerosols.